Highly Productive Ester Crosslinkable Composite Hollow Fiber Membranes for Aggressive Natural Gas Separations

A Dissertation
Presented to
The Academic Faculty

by

Canghai Ma

In Partial Fulfillment
of the Requirements for the Degree
Doctor of Philosophy in the
School of Chemical & Biomolecular Engineering

Georgia Institute of Technology
December, 2012

Highly Productive Ester Crosslinkable Composite Hollow Fiber Membranes for Aggressive Natural Gas Separations

Approved by:

Dr. William Koros, Advisor
School of Chemical &
Biomolecular Engineering
Georgia Institute of Technology

Dr. Anselm Griffin
School of Materials Science &
Engineering
Georgia Institute of Technology

Dr. Yulin Deng
School of Chemical &
Biomolecular Engineering
Georgia Institute of Technology

Dr. Stephen Miller
Chevron Fellow
Chevron Energy Technology Company

Dr. Krista Walton
School of Chemical &
Biomolecular Engineering
Georgia Institute of Technology

Date Approved: October 16, 2012

Dedicated To
My Family

ACKNOWLEDGEMENTS

First and foremost, I am especially indebted to Dr. Koros. His exceptional leadership, determined enthusiasm, relentless energy, abundant knowledge, unbelievable sense of humor and unblemished reputation makes him the most extraordinary mentor I have ever met. I consider myself extremely fortunate to work with him and be one of the friends in the "tree" rooted in him. His unwearied guidance and unequaled support allows me to cross every hurdle over the years. As he says, keep smiling, and I am sure I will. I deeply cherish the past four years and treat it as the most unforgettable and invaluable memory forever.

My appreciation expands to all my committee members: Dr. Deng, Dr. Walton, Dr. Griffin and Dr. Miller for their guidance and insightful suggestions. Special gratitude goes to my collaborators: Dr. Hussain, Dr. Wind, Dr. Chin, and Dr. Okeowo from Chevron, Dr. Jason Ward, Dr. Chien-Chiang Chen and Danny from Georgia Tech for their helpful discussions and technical feedbacks. The financial supports from Chevron and KAUST are also appreciated.

I would like to acknowledge all the Koros group members, past and present. Special thanks are credited to: Dr. Junqiang Liu for the membrane formation, Dr. Wulin Qiu for the polymer synthesis, Dr. Ryan Lively for the spinneret and spinning issues, Dr. Omo. Esekhile for gas permeation, Dr. Naoki Bessho for module fabrication and English practice, Dr. JR. Johnson for almost everything in the lab and Dr. Imona Omole for constant email feedbacks. I acknowledge Fuyue (Stephanie) for her time and help in the proof-reading. I also appreciate the valuable discussions with past and present group members: Dr. Cheng Chen, Dr. Oguz Karvan, Dr. Surrendar Venna, Dr. Rachana Singh, Dr. Shouliang Yi, Dr Ying Labreche, Dr. Kuang

Zhang, Fuyue, Vinod, Justin, Nitesh, Brian, Carine, Lu, Dr. Jong Lee, Neha, Chen, Xue, Steve, Andrew and et al. Michelle Martin, our group administrative assistant, makes things beyond research possible.

I would also like to thank my previous advisors, Dr. Liao, Dr. Liu and Dr. Shi, for continuous communication and guidance. Friends at Georgia Tech, who make my life so enjoyable, deserve my gratitude. I like traveling with Delong, Na, Hanjun, and Wei. Xiaohui and Yi are the most kind-hearted couple I have ever met and gave me unlimited help. I am also happy to play games with Hao, Wenchao, Juan, Liang and Siwei during weekends and holidays. I also appreciate my classmates, especially Dun-Yen, Wei-Ming, Liren, Linda, Bobby, Praveen, for their help in coursework during the "heaviest" first semester. Special thanks are also given to senior students: Qiong, Fangyu, Yanhui, Pei Yoong, Shantanu, and Lingbo. It is also my great pleasure to communicate with my friends outside of Georgia Tech: Yongliang, Niancai, Jiang, Fengzhi, Peng, Zhengxin, and Haifeng.

Lastly but not least, my great appreciation is attributed to all my family for their unconditional supports. They are all unsung heroes. I am incredibly grateful to my dearest wife, Hongjuan Cui. I sincerely appreciate her unmatched care during the darkest night and kind "quenching" during the brightest day. She also cooks the most delicious food in the world. Perhaps the biggest achievement during the past years is having my son, Ryan Ma, who makes me more joyful than ever.

TABLE OF CONTENTS

LIST OF TABLES

LIST OF FIGURES

SUMMARY

Natural gas feed often contains a high level of carbon dioxide (CO_2), which must be removed to a level below 2% to meet U. S. pipeline delivery specifications. Compared to traditional separation technologies (including amine adsorption and cryogenic distillation) to remove CO_2 from natural gas, membrane separation technology is less expensive, energy efficient and more environmentally friendly.

Despite intrinsically high separation performance, conventional polymeric membranes suffer from CO_2 induced plasticization, which reduces CO_2/CH_4 separation efficiency significantly. Covalent ester-crosslinking can improve the plasticization resistance by controlling the segmental chain mobility in the polymer; however, only relatively thick selective skin layers and lower separation productivity have been reported to date. On the other hand, the high cost of crosslinkable polymers makes the approach challenging, especially for large-scale gas separations which require large membrane areas with high feed pressures. Dual-layer hollow fiber spinning can be used to reduce the cost of membrane production by integrating a low-cost supporting core polymer with the expensive crosslinkable sheath polymer. However, the complexity of interfacial interaction between the sheath/core layers and subsequent crosslinking required can delaminate the sheath/core layers and collapse the core layer polymer. This can reduce mechanical strength and the permeance (separation productivity) significantly.

This work, therefore, aimed to develop thin-skinned high-performing ester-crosslinked hollow fiber membranes with improved CO_2 plasticization resistance. The skin layer thickness of hollow fibers was first optimized by simultaneous optimization of the polymer solution and spinning process variables. Moreover, this study also addresses the solutions of challenging in transitioning the *monolithic* hollow fiber to *composite* hollow fiber format. The *ester-crosslinked* hollow fibers were subjected to high feed pressures and high-level contaminants to probe their CO_2 plasticization and hydrocarbon antiplasticization resistance, respectively.

The resultant ester-crosslinked *monolithic* hollow fibers show significantly reduced skin layer thickness and improved separation productivity under extremely challenging operation conditions. They also demonstrate strong stability under high feed pressures and reversibility after contaminant exposure. Moreover, this study presents a newly discovered core layer material, Torlon®, which demonstrates excellent compatibility with the crosslinkable polymer and superior thermal stability during crosslinking without sheath/core layer delamination or collapse. The characterization under aggressive feed conditions clearly suggests that ester-crosslinked composite hollow fibers can achieve high separation performance and reduce membrane cost simultaneously. This provides a significant advance in state of the art for natural gas separations under realistic operation environments.

CHAPTER 1

INTRODUCTION

1.1 Natural gas background

Energy availability has become a challenge faced for mankind as world population keeps expanding and demands more energy. As one of the key energy resources, natural gas provides about 24% of energy for the world in 2011, as shown in Figure 1.1.

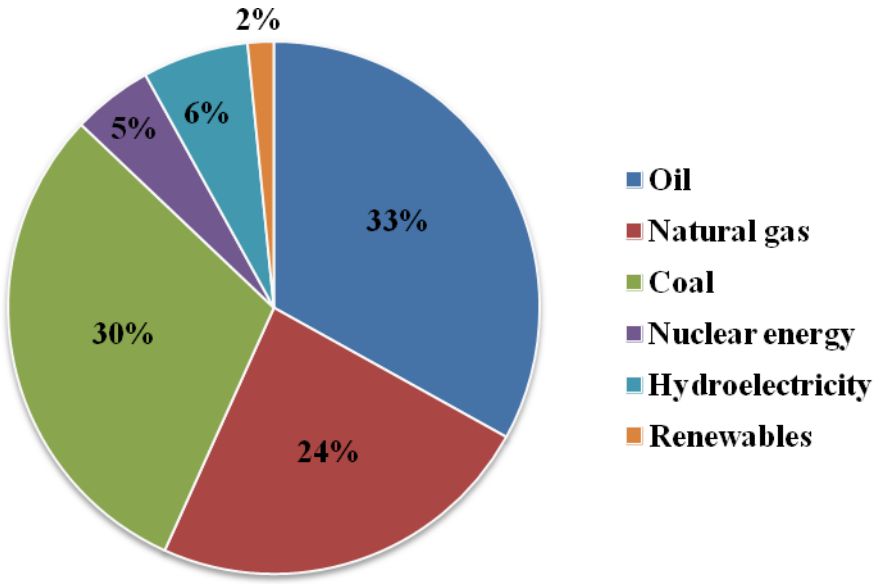

Figure 1.1: World consumption of energy in 2011 [1].

In the last decade, the U.S. consumed around 22~23 trillion SCF/yr of natural gas but produced only 19~21 trillion SCF/yr ("SCF" represents Standard Cubic Feet) [2]. The US natural gas consumption shows an increasing trend over the last half century, as depicted in Figure 1.2.

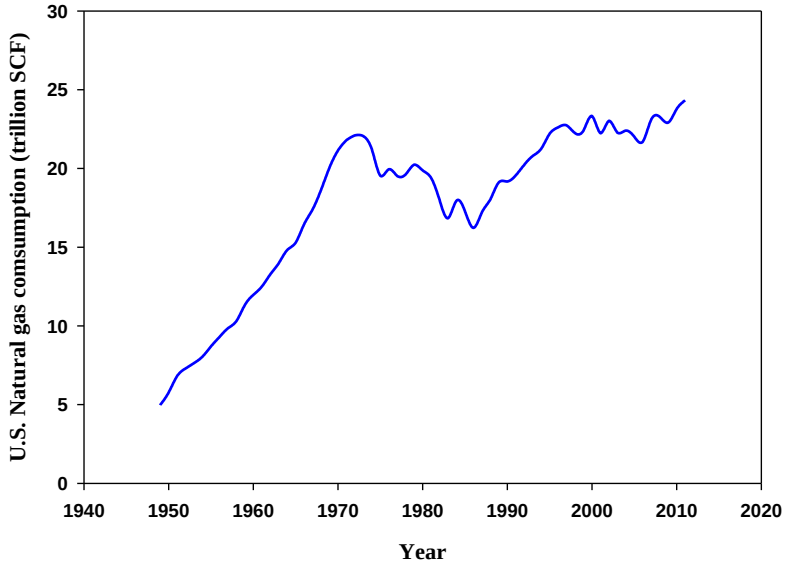

Figure 1.2: U.S natural gas total consumption [3].

Despite its importance as an important energy source, raw natural gas often contains an undesirable level of carbon dioxide (CO_2). Removal of the CO_2 to a level <2% (mol) is required to meet the U.S. pipeline specifications, primarily due to CO_2 induced pipeline corrosion, reduction of heating value and additional compression cost [4]. Other impurities like hydrogen sulfide (H_2S), water, and C_3+ hydrocarbon must also be removed to meet pipeline delivery specifications, as shown in Table 1.1.

Table 1.1: Natural gas composition specifications for pipeline delivery in the U.S. [4].

Component	Specification
CO_2	<2%
H_2S	<4ppm
H_2O	<120ppm
C_3+ hydrocarbon	950~1050 BTU/SCF; T_{dew}<-20^oC

1.2 Membrane separation technology

The main technologies currently used to remove CO_2 from natural gas include amine absorption, membrane separation and cryogenic distillation [4-6]. Amine absorption technology has been widely used as the standard for natural gas separations. Although amine absorption removes CO_2 almost completely, high capital cost, complex operation, expensive maintenance and corrosion makes this approach problematic [6]. Moreover, for high CO_2 levels, system sizes are very large. High-maintenance also hinders the application of amine absorption in remote locations. Cryogenic distillation is highly energy intensive because gases must be cooled down to realize the separation [7]. Membrane separation technology described in this dissertation can overcome the key challenges associated with amine absorption processes and cryogenic distillation [8-9].

Materials used to produce membranes include polymers, ceramics, zeolites and carbon molecular sieves [6, 10]; however, polymers are the dominant membrane materials used for natural gas separations. Polymeric membranes are produced as plate-and-frame, spiral-wound or hollow fibers modules; however, the hollow fiber module is an industrially preferred configuration as it provides higher surface area to volume ratio over 10,000 ft^2/ft^3 due to its cylindrical morphology [11]. The small dimension of hollow fibers allows the membrane to withstand a high feeding pressure up to 1000 psi [12]. A typical hollow fiber module for natural gas separations is shown in Figure 1.3.

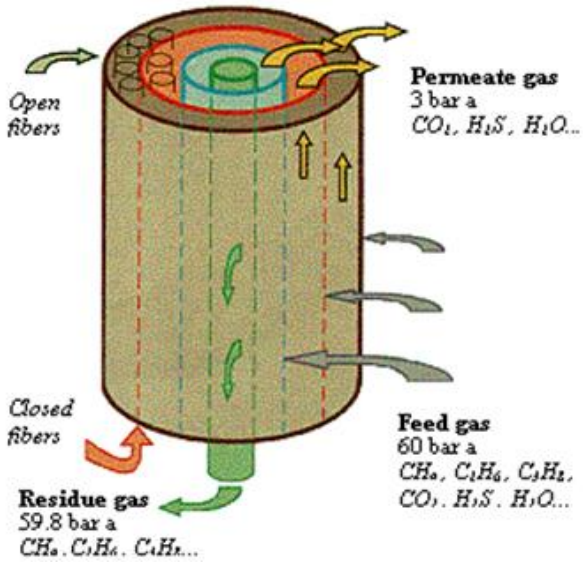

Figure 1.3: Hollow fiber modules for natural separations [figure courtesy of Medal.inc.].

Hollow fiber membrane modules for gas separations were developed as an alternative to flat sheet or spiral wound membrane and were first commercialized by Monsanto in 1977 [13]. Since then, membrane separation technology has become a competitive technology and grown into a $150 million/yr business [5]. Membrane gas separation technology does not require a phase change, and the consumption of energy is significantly reduced, compared to thermally-

driven processes. Moreover, membrane separation systems are suitable for use in remote locations due to its easy operation [6].

Despite its excellent separation performance, plasticization induced by high CO_2 partial pressure tends to cause polymeric membranes to show lower CO_2/CH_4 separation efficacy and loss of CH_4 into the permeate. To mitigate this problem, ester-crosslinking has been investigated and shown to stabilize polymeric membranes against plasticization by suppressing the degree of swelling and segmental chain mobility in the polymer [11,14-16]; however, only relatively thick selective skin layers and lower CO_2 permeance (productivity) have been reported to date. On the other hand, notwithstanding the high separation performance and CO_2 plasticization resistance, the high cost of crosslinkable polymers limits their applications. To reduce the cost of membrane formation, composite hollow fiber spinning has been developed to reduce the use of expensive polymer by integrating a low-cost supporting polymer with the expensive polymer; however, the complexity of interfacial interaction between the core layer and sheath layer makes this approach challenging. Furthermore, ester-crosslinking may cause a serious delamination of sheath/core layers and even a collapse of core layer, which significantly reduces the mechanical strength and the permeance (productivity) of hollow fibers.

This study focuses on extending the success of ester-crosslinking to developing hollow fibers with significantly improved separation performance and composite hollow fibers on a robust supporting polymer. A significantly improved defect-free ester-crosslinkable hollow fiber membrane will be first developed through simultaneous optimization of the spinning solution and dry-jet/wet-quench spinning process variables. Upon the success of single-layer hollow fiber development, crosslinked composite hollow fibers by integrating a low-cost supporting core

layer with the expensive crosslinkable sheath layer will be pursued to significantly reduce the cost of membrane formation.

1.3 Research objectives

The primary objectives of this research are shown below:

1. **Develop asymmetric hollow fibers with significantly reduced skin layer thickness and improved separation productivity**

Asymmetric crosslinked hollow fibers have been developed to achieve high CO_2 plasticization resistance under aggressive feeding conditions [13, 14-16]; however, the relatively thicker skin layer and lower CO_2 permeance reported somehow hinder the application of crosslinked hollow fiber membranes for natural gas separations. Reducing the skin layer thickness through simultaneous optimization of the spinning solution, spinning process variables and crosslinking conditions to further improve the CO_2 permeance of hollow fibers will be addressed in this objective.

2. **Demonstrate the separation efficacy of crosslinked hollow fibers under extremely challenging and realistic feed conditions**

The separation performance of crosslinked hollow fibers will be characterized under realistic operation conditions, including high CO_2 feed pressure and high-level hydrocarbon contaminants. Effects of high CO_2 partial pressures and operating temperatures will be studied with a clean CO_2/CH_4 mixed gas. Physical aging and active CO_2 feed crosslinked hollow fibers will also be studied. Effects of high-level hydrocarbon contaminants, such as aliphatic and aromatic impurities, will be explored to simulate realistic feed conditions.

3. **Create defect-free and delamination-free crosslinked composite hollow fibers by using a robust supporting polymer**

The selection of a supporting polymer for the composite hollow fiber spinning will be performed by screening polymer candidates with different structures and thermal stabilities. Effects of crosslinking on the interface of layers and the supporting core layer will be studied on composite hollow fibers. The separation performance of composite hollow fibers will be characterized by using mixed gas and contaminants in the feed. The challenges to achieve the desirable open porous morphology, compatibility of sheath/core layers and core layer thermal stability during ester-crosslinking will be addressed in this objective.

1.4 Dissertation overview

Chapter 1 contains introductory materials, including background on natural gas and membrane separation technology. Research objectives and dissertation organization are also described.

Chapter 2 relates the technical background for this research. This includes membrane separation fundamentals, effect of feed conditions on membrane separation properties, hollow fiber formation process and spinning techniques.

Chapter 3 presents materials and experimental methods. Dense film membranes and hollow fiber membranes are introduced, followed by characterization methods of membranes and ester-crosslinking.

Chapter 4 describes the work and results on the reduction of effective skin layer thickness of *uncrosslinked* hollow fibers to produce most productive crosslinked hollow fibers, which mainly includes dope reformulation and spinning process optimization.

Chapter 5 discusses the work and results on the development and characterization of improved performance *crosslinked* hollow fibers with significantly reduced skin layer thickness, which mainly involves the hollow fiber spinning, high CO_2 feed pressure, operating temperatures, and physical aging.

Chapter 6 describes the separation performance of crosslinked asymmetric hollow fibers under high-level contaminants, including toluene, heptane and water impurities.

Chapter 7 focuses on the creation and characterization of crosslinked composite hollow fibers without skin defects or delamination of sheath/core layers.

Chapter 8 provides a summary of conclusions of this study and recommends paths for future work and investigation.

The appendix contains a detailed description of polymer monoesterification reaction procedures.

1.5 Reference

[1] BP Statistical Review of World Energy, bp.com/statisticalreview.

[2] U.S. Energy Information Administration: Independent Statistical Analyses. *International Energy Outlook 2009*. http://www.eia.doe.gov/oiaf/ieo/graphic_data_natgas.html.

[3] U.S. Energy Information Administration: Independent Statistical Analyses, http://www.eia.gov/dnav/ng/hist_xls/N9140US2a.xls

[4] Baker, R.W., and Lokhandwala, K., *Natural Gas Processing with Membranes: An Overview.* Ind. Eng. Chem. Res. 47 (2008) 2109-2121.

[5] Baker, R.W., *Future Directions of Membrane Gas Separation Technology.* Eng. Chem. Res. 41 (2002) 1393-1411.

[6] Bernardo, P., et al., *Membrane Gas Separation: A review/State of the Art*. Ind. Eng. Chem. Res. 48 (2009) 4638-4663.

[7] Olajire, A., *CO_2 capture and separation technologies for end-of-pipe applications-A review*. Energy 35 (2010) 2610-2628.

[8] Koros, W.J., G.K.F., *Membrane-based gas separation.* J Membrane Sci 83 **(**1993) 1-80.

[9] Mulder, M., *Basic Principles of Membrane Technology. Second Edition*. 1996. 564 pp.

[10] Bird, A.J. and Trimm, D.L., *Carbon molecular sieves used in gas separation membranes*, Carbon 21 (1983) 177-80.

[11] Wallace, D.W., *Crosslinked Hollow Fiber Membranes for Natural Gas Purification and Their Manufacture from Novel Polymers*, in *Chemical Engineering*. 2004, The University of Texas at Austin: Austin, Texas. p. 202.

[12] Baker, R.W., *Membrane Technology and Applications*. 2nd ed. 2004: John Wiley & Sons, Ltd. 538 pp.

[13] Colin A. Scholes, Sandra E. Kentish, Geoff W. *Stevens, Carbon Dioxide Separation through Polymeric Membrane Systems for Flue Gas Applications*, Recent Patents on Chemical Engineering 1 (2008) 52-66.

[14] Hillock, A.M.W., *Crosslinkable polyimide mixed matrix membranes for natural gas purification*, in *Chemical Engineering. 2005*., Georgia Institute of Technology: Atlanta, Georgia. p. 199.

[15] Wind, J.D., *Improving Polyimide Membrane Resistance to Carbon Dioxide Plasticization in Natural Gas Separations*, in *Chemical Engineering*. 2002, The University of Texas at Austin: Austin, Texas. p. 215.

[16] Omole, I. C., Crosslinked Polyimide Hollow Fiber Membranes for Aggressive Natural Gas Feed Streams in *Chemical Engineering. 2008*., Georgia Institute of Technology: Atlanta, Georgia. p. 199.

CHAPTER 2

BACKGROUND AND THEORY

2.1 Overview

This chapter provides background and theory related to the research on ester-crosslinked hollow fiber membranes for natural gas separation. Section 2.2 covers the gas transport mechanism in polymeric membranes. Section 2.3 discusses effects of feed conditions on the membrane separation performance. Section 2.4 describes the hollow fiber formation mechanism. Section 2.5 focuses on hollow fiber spinning process.

2.2 Gas transport in membranes

2.2.1 Transport mechanism in membranes

Generally, membrane separations are based on one of the three general gas transport mechanisms: Knudsen-diffusion, sorption-diffusion and molecular sieving [1-4]. For polymeric membrane separations, only two of these mechanisms are studied: Knudsen-diffusion and sorption-diffusion process. Knudsen-diffusion occurs when the membrane pore size is smaller than the gas molecular mean free path in the bulk. The Knudsen-diffusion selectivity is equal to the inverse square root ratio of the molecular weights of the gas molecules [3]. The low selectivity achieved in Knudsen-diffusion is inadequate to meet most practical gas separation requirements and will be not discussed further in this work.

The sorption-diffusion model was first qualitatively described by Graham in 1833 and most widely accepted as the description of gas transport in polymeric membranes without continuous pores [1, 5]. In this model, the permeants sorb in the upstream of membrane and then diffuse through the membrane under a pressure or fugacity difference. The penetrants will desorb

from the downstream at a lower pressure. The differences in the amount of permeants dissolved in the membrane and the diffusion rate through the membrane cause the gas mixture to be separated as they permeate across the membrane. In this case, the permeability coefficient, *P*, of a polymeric membrane can be described by the product of the diffusion coefficient, *D*, and sorption coefficients, *S*, as shown in Equation 2.1 [1].

$$P=D\cdot S \tag{2.1}$$

Assuming the selective layer of the membrane is isotropic and the permeants can move equally in any of the six coordinate directions, the diffusion coefficient, *D*, can be determined by the average jumps length, λ, and average jumping frequency, *f*, as shown in Equation 2.2 [1].

$$D=f\cdot \lambda^2/6 \tag{2.2}$$

In a glassy polymer membrane, the sorption coefficient, *S*, is most commonly described by the dual-mode sorption model, shown in Equation 2.3 [6].

$$\frac{C_A}{p_A} = S_A = k_{Di} + \frac{C'_{Hi} b_i}{1 + b_A p_A + b_B p_B} \tag{2.3}$$

In Equation 2.3, k_{Di} is the Henry's law constant; C'_{Hi} and b_i represent the Langmuir capacity constant and Langmuir affinity constant, respectively. p_i is the local effective partial pressure of component *i*, which measures the local chemical potential for component *i*.

In dual-mode sorption model, Langmuir sorption describes the sorption of penetrants in the intersegmental packing defects, called "microvoids", while Henry's Law sorption describes the sorption in more or less well packed environments in the glassy polymer. At lower pressures, Langmuir sorption dominates the gas sorption in the membrane as microvoids offer low energy

sorption sites in the glassy matrix. At elevated pressures, the Langmuir sites become saturated due to penetrant sorption and Henry's Law becomes the dominant mechanism of gas transport in the membrane [7].

2.2.2 Membrane characterization

To characterize the separation performance of a polymeric membrane, two key factors are commonly studied: permeability and selectivity. The permeability describes the intrinsic productivity of a membrane and is defined by the flux of penetrant *i*, normalized by the membrane thickness and the partial pressure or fugacity difference across the membrane, as shown in Equation 2.4 [1].

$$P_i = \frac{n_i \cdot l}{\Delta p_i} \tag{2.4}$$

In Equation 2.4, n_i represents the flux of penetrant *i* through the membrane; *l* refers the membrane thickness; Δp represents the partial pressure or fugacity difference of penetrant *i* across the membrane. The common unit of permeability is the Barrer, as shown in Equation 2.5.

$$1 \text{ Barrer} = 10^{-10}\left(\frac{\text{cc(STP)}}{\text{cm}^2 \cdot \text{s}}\right) \cdot \frac{\text{cm}}{\text{cmHg}} \tag{2.5}$$

In an asymmetric hollow fiber membrane, the actual membrane thickness, *l*, is difficult to define unambiguously. Therefore, the productivity of a hollow fiber membrane is usually determined by the permeance, P_i/l, which is the flux of penetrant *i* normalized by partial pressure or fugacity difference, as shown in Equation 2.6.

$$\frac{P_i}{l} = \frac{n_i}{\Delta p_i} \tag{2.6}$$

The common unit of permeance is the GPU [8], defined as Equation 2.7.

$$1\ \text{GPU} = 10^{-6}\left(\frac{\text{cc(STP)}}{\text{cm}^2 \cdot \text{s} \cdot cmHg}\right) \tag{2.7}$$

On the other hand, the selectivity measures the intrinsic membrane separation efficiency. For a given gas pair, if the total upstream pressure is much larger than the total downstream pressure, the ideal selectivity, α_{ij}, is determined by the ratio of the fast gas (i) permeability or permeance to the slow gas (j), as shown in Equation 2.8.

$$\alpha_{ij} = \frac{P_i}{P_j} = \frac{P_i / l}{P_j / l} \tag{2.8}$$

For practical mixed gas permeation, complications including plasticization, non-infinite feed to permeate pressure ratio and gas molecule competition may occur. Therefore, the separation factor, $(S.F.)_{ij}$, is commonly used to characterize the separation performance, as shown in Equation 2.9 [8].

$$(S.F.)_{ij} = \frac{y_i / y_j}{x_i / x_j} \tag{2.9}$$

In Equation 2.9, x and y are the mole fraction of the penetrants in the upstream and downstream of the membrane, respectively. i and j represent the "fast" gas and "slow" gas in the mixed gases, respectively. The α_{ij} and $(S.F.)_{ij}$ equal when the ratio of upstream pressure to downstream pressure is very high (ideally infinite). Nevertheless, the relative permeability or

permeance ratio is preferred to measure the intrinsic separation performance of a membrane, since $(S.F.)_{ij}$ is affected by the ratio of feed to permeate pressure.

2.3. Effects of feed conditions on membrane separation

2.3.1 Plasticization of polymeric membranes

High CO_2 partial pressure in the feed can swell the glassy polymer and cause so-called "plasticization". CO_2 induced plasticization occurs when the permeability or permeance increases while the selectivity decreases in the presence of high CO_2 feed pressure. The penetrant-polymer interaction increases the segmental mobility of polymer chains and increases the diffusion coefficients of each penetrant; thereby increasing the permeability. However, for natural gas separation, the increase of CH_4 diffusivity is larger than that of CO_2; therefore, the CO_2/CH_4 selectivity decreases in the presence of plasticization. The plasticization effect can be illustrated by Figure 2.1 [9].

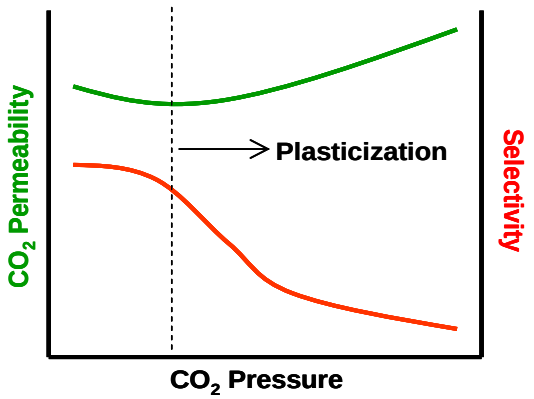

Figure 2.1: CO_2 permeability and selectivity at different CO_2 partial feed pressure. The dashed line represents the CO_2 plasticization pressure.

The plasticization pressure is defined as the pressure when the permeability starts to rise when increasing the CO_2 pressure after an initial drop of permeability, as shown in Figure 2.1. Thin dense films can be plasticized immediately without experiencing the initial permeability loss [10]. When the plasticization pressure is reached, the selectivity starts to decrease with pressure. To develop a commercial membrane with high separation performance under aggressive feed conditions, the plasticization must be suppressed so that both high permeability and selectivity can be maintained.

Different strategies can be utilized to stabilize polymeric membranes against CO_2 induced plasticization, including thermal annealing [11, 12], blending [13, 14] and crosslinking [15-19]. Covalent ester-crosslinking has been investigated in previous research and proven to be able to stabilize the polymeric membranes against CO_2 induced plasticization by suppressing the degree of swelling and segmental chain mobility in the polymer. Wind and Hillock studied ester-crosslinking and found that the covalent ester-crosslinking can effectively suppress the CO_2 plasticization of dense film membranes [16, 18, 20]. Figure 2.2 shows that the ester-crosslinking improves the CO_2 plasticization pressure up to ~40 atm [16]. Wallace and Omole focused on the development of asymmetric hollow fibers from propane diol monoesterified crosslinkable (PDMC) material and found the ester-crosslinked PDMC hollow fibers can provide high CO_2 plasticization resistance and natural gas separation performance [9, 21].

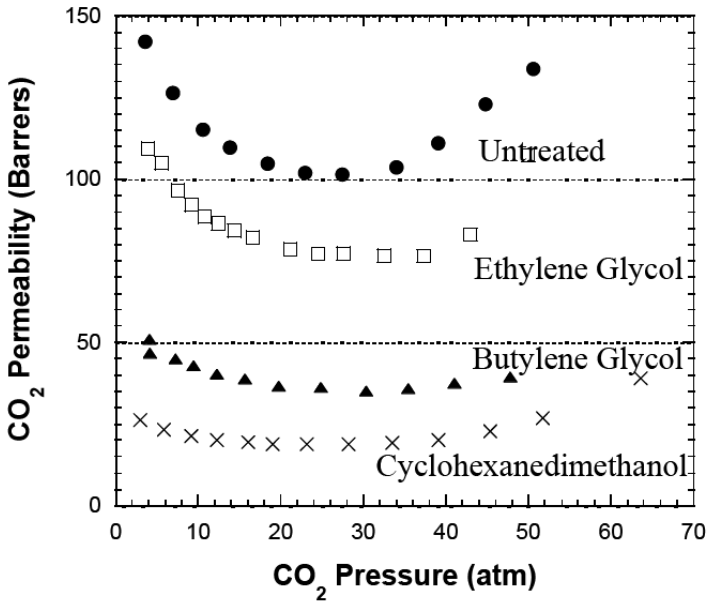

Figure 2.2**:** CO_2 permeability of 6FDA-DAM: DABA (2:1) crosslinked with ethylene glycol, butylene glycol, and 1, 4-cyclohexanedimethanol [16].

2.3.2 Antiplasticization

Antiplasticization refers to the phenomenon by which some low molecular weight additives retard the segmental motions of polymer chains, causing increase of modulus and strength, losses in elongation at break and impact resistance [22-24]. Those lower molecular weight additives are called antiplasticatizers when present below a critical level; however, above this level, they acts as plasticatizers. Antiplasticization is often associated with a decrease in permeability of permeants and may also lead to an increase or a decrease in the permselectivity for a gas mixture [23].

Extensive studies showed that most low molecular weight compounds miscible with polymers tend to cause antiplasticization to some degree at low concentrations. Maeda and Park studied the antiplasticization phenomenon with aromatic compounds at low concentrations and

showed that the CO_2/CH_4 selectivity somehow depends on the concentration of additives in poly (phenylene oxide), as shown in Figure 2.3 [23].

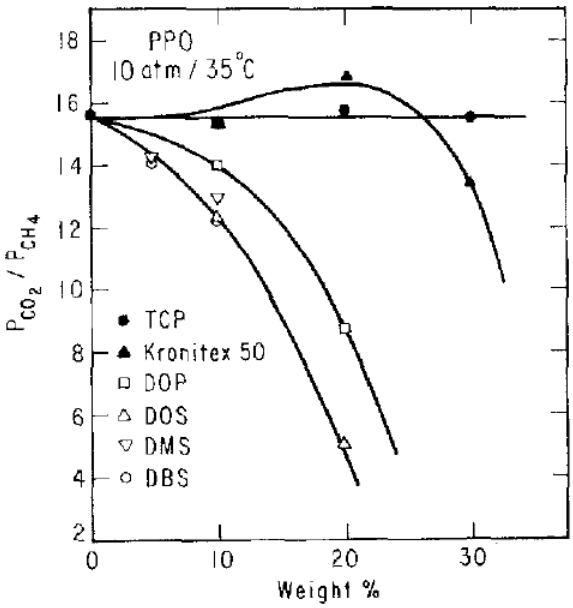

Figure 2.3**:** CO_2/CH_4 selectivity at different concentrations of additives in poly(phenylene oxide) [23].

Due to the non-equilibrium state of glassy polymer, an antiplasticizer can reduce the fractional free volume (*FFV*) and increase the stiffness by lowering the glass transition temperature, as shown in Figure 2.4 [1, 25].

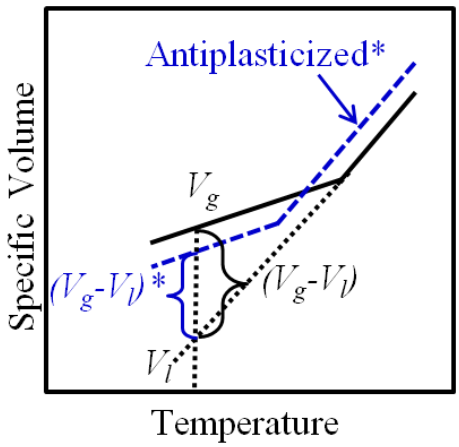

Figure 2.4: Specific volume of pure polymer (solid black line) and antiplasticized polymer mixture (blue dashed line), showing *FFV'*<*FFV* for antiplasticized vs. neat polymer.

In Figure 2.4, *FFV* and *FFV'* represent the Fractional Free Volume of neat polymer and antiplasticized polymer, respectively. As shown in Figure 2.4, antiplasticization can reduce Fractional Free Volume (*FFV*) and thereby hinder the diffusion of each penetrant and reduce permeability accordingly. More discussions regarding antiplasticization will be shown in Chapter 6.

2.3.3 Competition effects in mixed gas

The competition among penetrants in a mixed gas should be considered to study the mixed gas separation properties. According to the dual-mode sorption model (Eq. 2.3), the permeability of each penetrant is reduced due to the competitive effect between penetrants on Langmuir sorption sites [6].

For the CO_2/CH_4 gas mixture, since CO_2 is more condensable than CH_4, CO_2 penetrant can partially exclude CH_4 and dominate the sorption process [26]. As a result, CO_2 molecules out-compete CH_4 molecules as they permeate through the membrane. Since the competition effect does not occur in pure gas permeation, the CO_2/CH_4 selectivity in a mixed gas is generally

higher than that in pure gas measurements if the membrane is not plasticized [18]. However, competitive sorption can be affected by plasticization. Visser et al. studied the competition sorption and plasticization effect and showed that competitive sorption can be totally counterbalanced by the plasticization effect at a certain level of inert gas [27].

2.3.4 Non-ideal gas thermodynamics

As shown in Equation (2.4) in Section 2.2.2, the partial pressure difference across the membrane is usually considered as the driving force to determine the permeance of each permeant. However, the actual driving force is the fugacity difference of penetrants, which approximately equals to partial pressure difference at low pressures. At elevated feed pressures, the permeance can be significantly different if calculated by using the partial pressure difference instead of partial fugacity difference.

The fugacity coefficients for a gas mixture can be calculated by using the commercial process simulator Aspen. Commonly used equations to determine the fugacity coefficients include the Virial Equation of State, Peng-Robinson, and Soave-Redlich-Kong Equation [28, 29].

2.4 Asymmetric hollow fiber membranes

2.4.1 Introduction

Asymmetric hollow fiber membranes are the industrially preferred configuration to improve the separation productivity and reduce the cost of membrane fabrication. This is because the hollow fiber high surface area to volume ratio up to 10,000 m^2/m^3, which is over 30 times than spiral-wound membranes [21]. The cylindrical structure allows the hollow fibers to

withstand high transmembrane pressure difference up to 1000 psi [3]. The schematic of a typical asymmetric hollow fiber membrane is shown in Figure 2.5 [7].

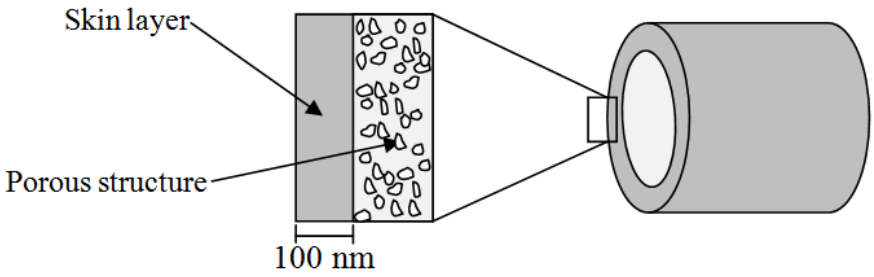

Figure 2.5: Schematic of a typical asymmetric hollow fiber showing the skin layer (~100 nm) and open porous structure [7] .

The open porous substructure of hollow fibers just underneath the outer skin layer has negligible transport resistance and provides mechanical strength for the membrane against high feed pressures. On the other hand, the selective skin layer with an ideal thickness lower than 100 nm performs the separation of a gas mixture. The study on reducing the skin layer thickness to this level will be described in Chapter 4.

2.4.2 Phase separation of hollow fibers

The asymmetric hollow fiber formation is based on the phase separation behavior of a homogenous ternary phase polymer solution (called dope), which consists of polymer, solvents and non-solvents. Non-solvent is introduced to allow rapid phase separation of the polymer solution. To understand the hollow fiber formation process, the ternary phase diagram of the dope is useful, as shown in Figure 2.6 [7].

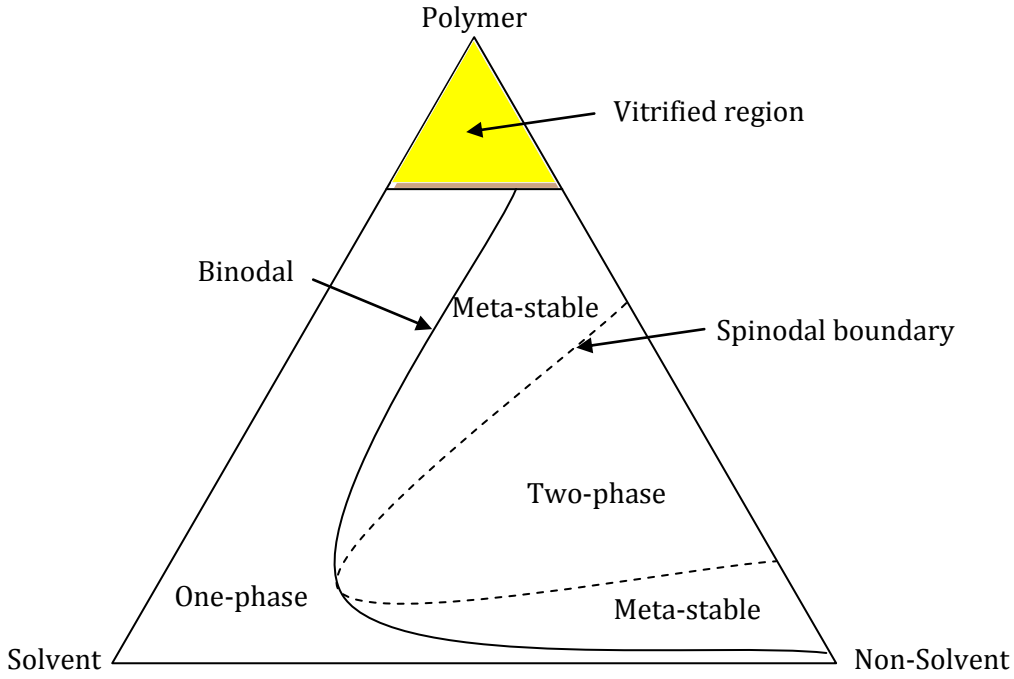

Figure 2.6: Ternary phase diagram showing important boundary lines and phase regions [7].

In the ternary phase diagram as shown in Figure 2.6, there are three regions: the stable one-phase, meta-stable phase and two-phase region. The binodal (solid line) and spinodal (dashed line) lie between the stable one-phase, meta-stable phase and two-phase region. The addition of non-solvent or the removal of solvent from the dope can move the dope composition from the one-phase region to the two-phase region, causing the phase separation of the dope to occur. The phase separation will produce an open porous substructure in the asymmetric hollow fibers, as shown in Figure 2.5.

A possible phase separation mechanism is so-called nucleation and growth [30]. In this case, the vitrification of nascent skin occurs while polymer-lean domains are nucleated and grow in the substrate region to intersect and create a low substrate resistance unless the intersection and rupture of the polymer-lean domains fails, which produces close-cell supports with

undesirably high transport resistance [7]. The formation of porous substructure is also thought sometimes to involve so-called “spinodal decomposition”, which leads to desirable naturally biscontinuous polymer-lean and polymer-rich phases with negligible substrate resistance [1, 7]. The loss of solvent and non-solvent occurs in the region underneath the vitrified skin to form an interconnected open supporting layer with a minimal substrate resistance [7].

2.4.3 Skin layer formation

The skin layer formation was studied and it is believed that the vitrification of the skin layer, caused by the evaporation of solvent and non-solvent, occurs prior to the phase separation of the dope. Figure 2.7 is a ternary phase diagram depicting the skin layer formation and phase separation [30, 31].

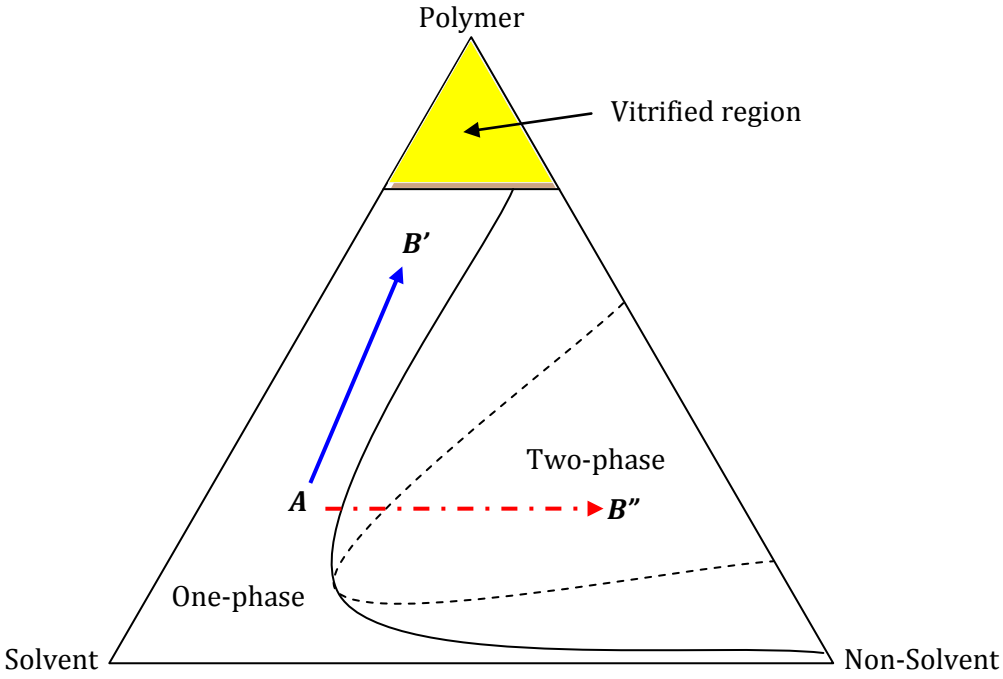

Figure 2.7: Ternary phase diagram showing the skin layer and substructure formation processes. The solid line, A→B', represents the trajectory of the skin layer formation and the dashed line, A→B'', describes the trajectory of the substructure formation.

In Figure 2.7, Point *A* represents the initial dope composition. The evaporation of solvent and non-solvent can increase the local polymer concentration in the outermost surface of the nascent fiber; thereby moving the dope composition from point A to point *B'*. The skin layer of hollow fiber is believed to be formed during this process (A→B'). On the other hand, the invasion of non-solvent to the dope will move the dope composition from one-phase region to two-phase region, as shown from A→B''. Point B" represents the lower local polymer concentration in the supporting layer of the fiber. During this process (A→B''), phase separation occurs and an open porous substructure is formed just underneath the skin layer.

2.5 Dry-jet/wet-quench hollow fiber spinning

2.5.1 Overview

The technique used in this work to produce asymmetric hollow fiber membranes is so-called dry-jet/wet-quench hollow fiber spinning. In this process, the dope initially passes through an "air gap" (dry-jet) to form the skin layer of nascent hollow fibers; then enters the aqueous quench bath (wet-quench) and phase separation occurs immediately to form an open porous substructure. The spinning process includes dope development, hollow fiber spinning, dehydration and sometimes post-spinning treatment, as will be discussed in sections below.

2.5.2 Dope development

A typical spinning dope consists of polymer, solvents, and non-solvents. In this dope, the polymer serves as the membrane framework and determines the separation performance of hollow fibers. Solvents dissolve polymer and keep the solution homogeneously in a single phase. Non-solvents in the dope can accelerate phase separation. Details of preparing a dope will be described in Chapter 3.

2.5.3 Hollow fiber spinning

Asymmetric hollow fiber membranes are spun through a dry-jet/wet-quench hollow fiber spinning system, as shown in Figure 2.8.

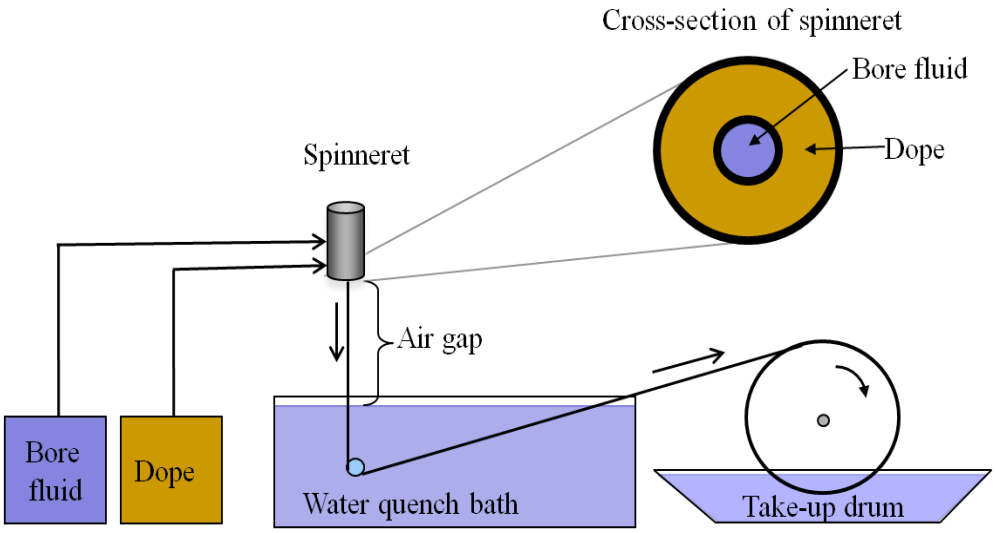

Figure 2.8: Dry-jet/wet-quench hollow spinning system to form asymmetric hollow fibers.

The dope is co-extruded with the bore fluid through an annual die, called spinneret. The bore fluid, consisting of solvents and non-solvents, can prevent the collapse of nascent fibers during spinning. Another dope (sheath dope) can be added to form dual-layer hollow fibers. This dual-layer spinning technique will be discussed in Chapter 7.

The extruded nascent fibers are exposed in the air gap. During this dry-jet step, the volatile components evaporate from the dope and increase the local polymer concentration in the outmost layer of fibers to form the skin layer. When the nascent fiber enters the quench bath, the dope demixes into polymer-rich and polymer-lean phase and phase separation occurs rapidly to form a solid and open porous structure underneath the skin layer [7]. The hollow fibers are then wound on a rotating drum.

Main spinning process variables include dope composition, dope flow rate, spinneret temperature, air gap height, quench temperature, and take-up rate, which will be discussed in Chapter 3.

2.5.4 Fiber dehydration

Solvents and non-solvents must be removed from hollow fibers to avoid subsequent fiber collapse, which is particularly important for preserving the transition layer just beneath the skin layer. The wet fibers from the quench bath should not be dried directly since the dehydration-induced capillary force in the fibers will collapse the pores or damage the fibers. Therefore, solvent exchange should be conducted as the final spinning step. Typically, alcohol (e.g. methanol or ethanol) is first used to replace water in the fibers. Then the alcohol is substituted by using a volatile non-solvent (e.g. hexane). Through solvent exchange, the fiber surface tension is greatly reduced and the fibers can be dried under vacuum and heating without collapsing the fiber inner structure.

2.5.5 Post-spinning treatment

A post-spinning treatment is needed if the hollow fibers are defective. Post-treatment aims to repair the pinholes defects in the fiber skins by caulking the fiber shell side with a highly permeable rubber polymer layer. Two post-treatment methods are commonly used for curing hollow fiber minor defects. The first one uses the high molecular weight polydimethylsiloxane (PDMS) solution in heptane. The other post treatment method, so-called reactive post-treatment, uses two solutions: diethyltoluenediamine in iso-octane and trimesoyl chloride/PDMS mixture in iso-octane. Details about post-treatment can be found in reference [21, 32]. In general, for use in aggressive feeds, post treatment caulking or "healing" of defects is questionable, since the caulking in the defects can fail and cause drastic selectivity loss.

2.6 References

[1] W.J. Koros, G.K. Fleming, Membrane-Based Gas Separation, J Membrane Sci, 83 (1993) 1-80.

[2] M. Mulder, Basic principles of membrane technology, 2nd ed., Kluwer Academic, Dordrecht ; Boston, 1996.

[3] R.W. Baker, Membrane technology and applications, 2nd ed., J. Wiley, Chichester ; New York, 2004.

[4] A.J. Bird, D.L. Trimm, Carbon Molecular-Sieves Used in Gas Separation Membranes, Carbon, 21 (1983) 177-180.

[5] T. Graham, On the Law of the Diffusion of Gases (Reprinted from the London and Edinburgh Philosophical Magazine and Journal of Science, Vol Ii, Pg 175, Pg 269, Pg 351, 1833), J Membrane Sci, 100 (1995) 17-21.

[6] W.J. Koros, R.T. Chern, V. Stannett, H.B. Hopfenberg, A Model for Permeation of Mixed Gases and Vapors in Glassy-Polymers, J Polym Sci Pol Phys, 19 (1981) 1513-1530.

[7] C. Ma, OPTIMIZATION OF ASYMMETRIC HOLLOW FIBER MEMBRANES FOR NATURAL GAS SEPARATION, MS THESIS, in: School of Chemical and Biomolecular Engineering, Georgia Institute of Technology, Atlanta, GA, 2011.

[8] I.C. Omole, R.T. Adams, S.J. Miller, W.J. Koros, Effects of CO2 on a High Performance Hollow-Fiber Membrane for Natural Gas Purification, Ind Eng Chem Res, 49 (2010) 4887-4896.

[9] I.C. Omole, Crosslinked Polyimide Hollow Fiber Membranes for Aggressive Natural Gas Feed Streams, Ph.D. Dissertation, in: Chemical and Biomolecular Engineering, Georgia Institute of Technology, Atlanta, GA, 2008.

[10] I.C. Omole, S.J. Miller, W.J. Koros, Increased molecular weight of a cross-linkable polyimide for spinning plasticization resistant hollow fiber membranes, Macromolecules, 41 (2008) 6367-6375.

[11] J.T. Vaughn, W.J. Koros, J.R. Johnson, O. Karvan, Effect of thermal annealing on a novel polyamide-imide polymer membrane for aggressive acid gas separations, J Membrane Sci, 401 (2012) 163-174.

[12] A.F. Ismail, N. Yaacob, Performance of treated and untreated asymmetric polysulfone hollow fiber membrane in series and cascade module configurations for CO2/CH4 gas separation system, J Membrane Sci, 275 (2006) 151-165.

[13] A. Bos, I.G.M. Punt, M. Wessling, H. Strathmann, Suppression of CO2-plasticization by semiinterpenetrating polymer network formation, J Polym Sci Pol Phys, 36 (1998) 1547-1556.

[14] P.C. Raymond, W.J. Koros, D.R. Paul, Comparison of Mixed and Pure Gas Permeation Characteristics for Co2 and Ch4 in Copolymers and Blends Containing Methyl-Methacrylate Units, J Membrane Sci, 77 (1993) 49-57.

[15] J.D. Wind, S.M. Sirard, D.R. Paul, P.F. Green, K.P. Johnston, W.J. Koros, Carbon dioxide-induced plasticization of polyimide membranes: Pseudo-equilibrium relationships of diffusion, sorption, and swelling, Macromolecules, 36 (2003) 6433-6441.

[16] J.D. Wind, C. Staudt-Bickel, D.R. Paul, W.J. Koros, The effects of crosslinking chemistry on CO2 plasticization of polyimide gas separation membranes, Ind Eng Chem Res, 41 (2002) 6139-6148.

[17] A. Taubert, J.D. Wind, D.R. Paul, W.J. Koros, K.I. Winey, Novel polyimide ionomers: CO2 plasticization, morphology, and ion distribution, Polymer, 44 (2003) 1881-1892.

[18] A.M.W. Hillock, W.J. Koros, Cross-linkable polyimide membrane for natural gas purification and carbon dioxide plasticization reduction, Macromolecules, 40 (2007) 583-587.

[19] A.M.W. Hillock, S.J. Miller, W.J. Koros, Crosslinked mixed matrix membranes for the purification of natural gas: Effects of sieve surface modification, J Membrane Sci, 314 (2008) 193-199.

[20] J.D. Wind, Improving Polyimide Membrane Resistance to Carbon Dioxide Plasticization in Natural Gas Separations, PhD dissertation, in: Chemical Engineering, The University of Texas at Austin, Austin, TX, 2002.

[21] D.W. Wallace, Crosslinked Hollow Fiber Membranes for Natural Gas Purification and Their Manufacture from Novel Polymers, Ph.D. Dissertation, in: Chemical Engineering, The University of Texas at Austin, Austin, TX, 2004.

[22] J.L. Duda, I.H. Romdhane, R.P. Danner, Diffusion in Glassy-Polymers - Relaxation and Antiplasticization, J Non-Cryst Solids, 172 (1994) 715-720.

[23] Y. Maeda, D.R. Paul, Effect of Antiplasticization on Selectivity and Productivity of Gas Separation Membranes, J Membrane Sci, 30 (1987) 1-9.

[24] Y. Maeda, D.R. Paul, Effect of Antiplasticization on Gas Sorption and Transport .1. Polysulfone, J Polym Sci Pol Phys, 25 (1987) 957-980.

[25] W.C. Madden, THE PERFORMANCE OF HOLLOW FIBER GAS SEPARATION MEMBRANES IN THE PRESENCE OF AN AGGRESSIVE FEED STREAM, PhD Dissertation, in: Chemical Engineering, Georgia Institute of Technology, Atlanta, GA, 2005.

[26] A.M.W. Hillock, CROSSLINKABLE POLYIMIDE MIXED MATRIX MEMBRANES FOR NATURAL GAS PURIFICATION, PhD Dissertation, in: Chemical Engineering, Georgia Institute of Technology, Atlanta, GA, 2005.

[27] T. Visser, G.H. Koops, M. Wessling, On the subtle balance between competitive sorption and plasticization effects in asymmetric hollow fiber gas separation membranes, J Membrane Sci, 252 (2005) 265-277.

[28] D. Peng, D.B. Robinson, New 2-Constant Equation of State, Ind Eng Chem Fund, 15 (1976) 59-64.

[29] A. Bertucco, M. Barolo, G. Soave, Estimation of Chemical-Equilibria in High-Pressure Gaseous Systems by a Modified Redlich-Kwong-Soave Equation of State, Ind Eng Chem Res, 34 (1995) 3159-3165.

[30] D.T. Clausi, W.J. Koros, Formation of defect-free polyimide hollow fiber membranes for gas separations, J Membrane Sci, 167 (2000) 79-89.

[31] S.B. Carruthers, Integral-skin formation in hollow fiber membranes for gas separations, Ph.D. Dissertation, in: Chemical Engineering, The University of Texas at Austin, Austin, TX, 2001.

[32] S. Husain, MIXED MATRIX DUAL LAYER HOLLOW FIBER MEMBRANES FOR NATURAL GAS SEPARATION, PhD Dissertation, in: School of Chemical & Biomolecular Engineering, Georgia Institute of Technology, Atlanta, GA, 2006.

CHAPTER 3

METERIALS AND EXPERIMENTAL METHODS

3.1 Overview

This chapter describes the materials and experimental methods. Section 3.2 presents the polymer synthesis and characterization. Section 3.3 describes dense film membrane formation. Section 3.4 focuses on hollow fiber membrane formation. Section 3.5 provides a summary of membrane characterization methods.

3.2 Materials

3.2.1 Polymer synthesis

The polymer used in this work is called PDMC, which stands for 1, 3-propane-diol monoesterified crosslinkable polyimide (3:2). The synthesis of PDMC is associated with two steps of reactions: the first step is involved the synthesis of 6FDA-DAM: DABA (3:2) polyimide. The second step is the monoesterification of 6FDA-DAM: DABA (3:2) polyimide to produce PDMC, as will be discussed in Section 3.2.2.

The 6FDA-DAM: DABA (3:2) polyimide copolymer is synthesized by a two-step polycondensation reaction and imidization from 4, 4'-(hexafluoroisopropylidene) diphthalic anhydride (6FDA), 2, 4, 6-trimethyl-1, 3-diaminobenzene (DAM) and 3, 5-diaminobenzoic acid (DABA). The 3:2 monomer ratio is chosen based on its excellent CO_2/CH_4 separation performance and high CO_2 induced plasticization resistance, as investigated in previous research [1-3].

There are mainly two types of imidization methods: chemical imidization and thermal imidization. Chemical imidization occurs at relatively lower temperatures and uses an imidization catalyst and dehydrating agent to remove the water produced during the reaction. Due to the lower temperature, the chemical imidization conditions are relatively easy to process and less cost [4]. Moreover, a final heat treatment after imidization can help close rings to achieve complete imidization and avoid possible chain scissioning during the following monoesterification reaction. Isoimidization may occur during chemical imidization, as suggested in references [5-7]; however, these isoimides can be converted to imides during the heat treatment [3]. Since the heat treatment of polymers is required, the polymer needs to be precipitated from the polymer solution and re-dissolve in NMP to react with propane-diol to form PDMC during the monoesterification, which is termed as "two-pot" method.

On the other hand, thermal imidization occurs by simply heating the polymer solution to a relatively high temperature (say 180^{o}C). Catalyst and dehydrating agents are also needed in thermal imidization to remove the water by-product. Despite a high degree of imidization, high temperature tends to form crosslinks between the polymers or oligomers; thereby affecting the solubility of polymers. Nevertheless, molecular weight build-up was found in thermal imidization [3, 8]. After thermal imidization, monoesterification can be performed immediately without polymer precipitation since heat treatment of polymer is not required, which makes this approach a "one-pot" method. Details of synthesis can be found in references [3, 4].

The carboxylic acid pendant groups of DABA units in the polymer are further monoesterified with 1, 3-propanediol and form ester bonds, which is called monoesterification reaction. This monoesterification reaction will be discussed in 3.2.2. The structures of monomers and 6FDA-DAM: DABA are shown in Figure 3.1.

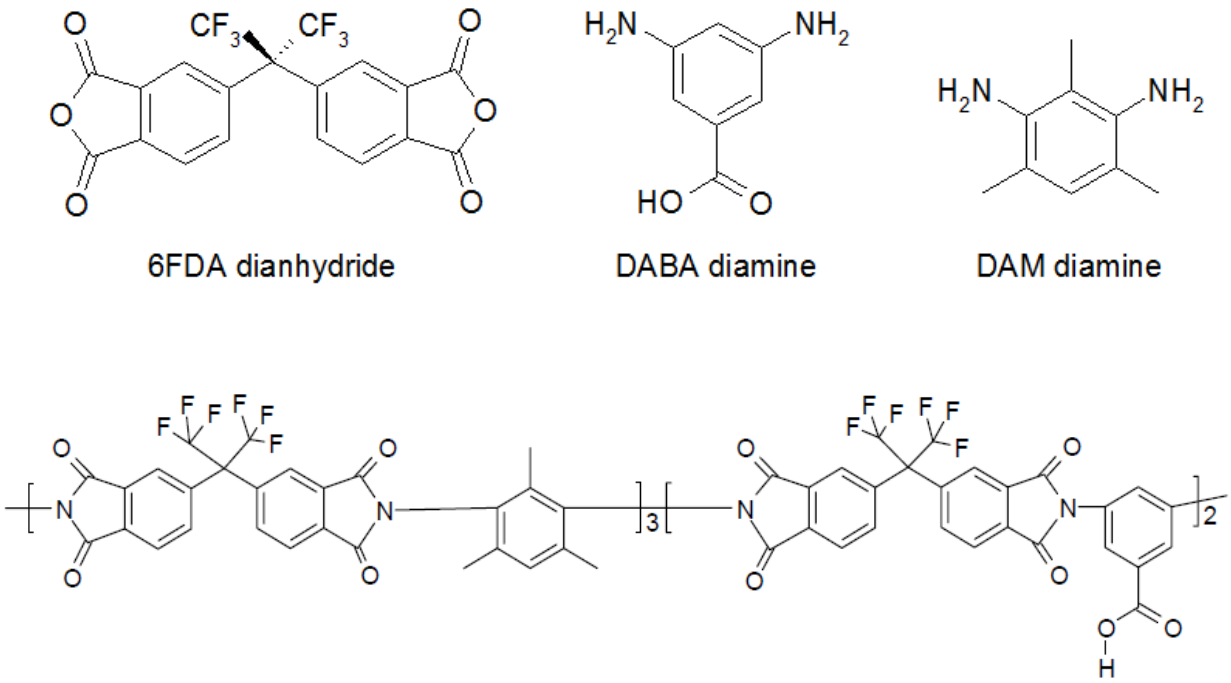

Figure 3.1: Chemical structures of monomers and 6FDA-DAM: DABA (3:2) polyimide.

3.2.2 Monoesterification

Different polyalcohols (e.g. 1,3-propane diol, ethylene glycol, butylenes glycol 1,4-benzenedimethanol and 1,4-cyclohexanedimethanol) can react with the carboxylic acid groups in DABA units of 6FDA-DAM: DABA(3:2) polymer to form covalent ester bonds [9, 10]. However, 1, 3-propane diol is chosen in this work due to its potential to produce PDMC polymer with high separation productivity and CO_2 plasticization resistance. The monoesterification reaction is demonstrated in Figure 3.2. Details about monoesterification can be found in Appendix A.

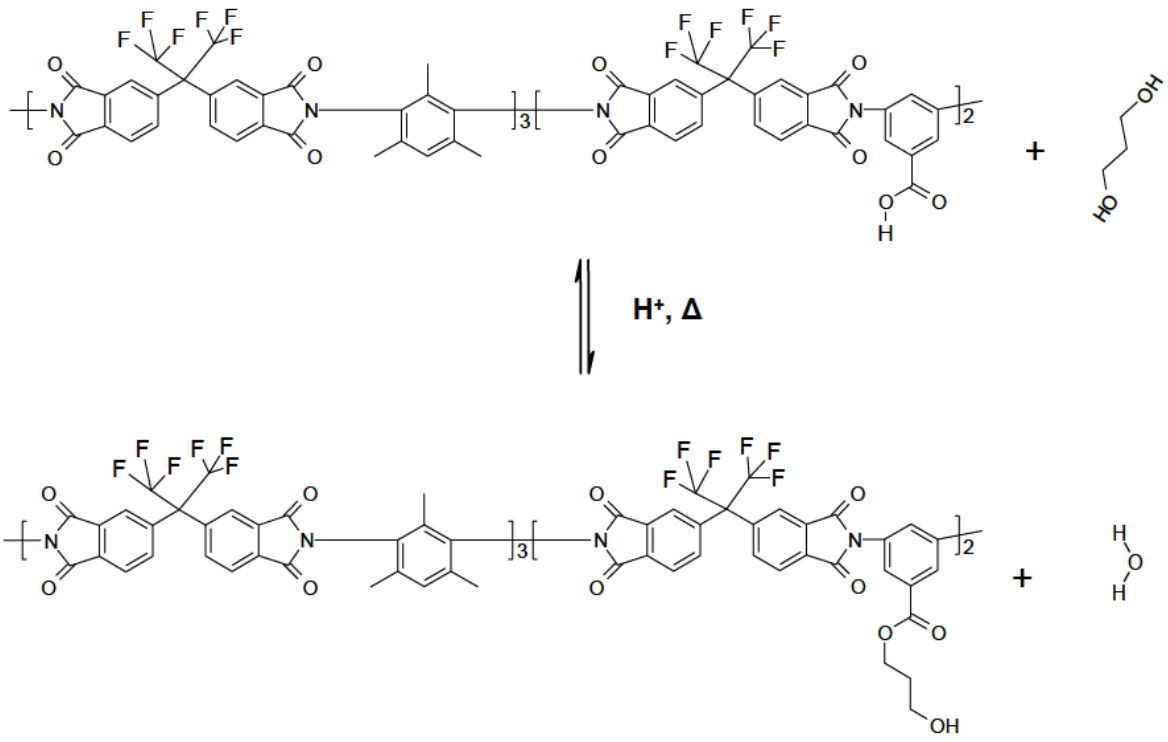

Figure 3.2: Monoesterification reaction mechanism for synthesizing 1, 3-propanediol monoesterified crosslinkable (PDMC) polyimide (3:2).

3.2.3 Polymer characterization

3.2.3.1 Gel permeation chromatography

Gel permeation chromatography (GPC) is a most widely used technique to determine the molecular weight and polydispersity index (PDI) of polymer samples. This technique uses monodisperse polymer standards (e.g. solutions of monodispersed polystyrene in THF) to plot the logarithm of the molecular weight versus the retention volumes (or times). Using this calibration curve and the gel permeation chromatogram of an unknown polymer sample, the molecular weights and the PDI can be determined [11].

3.2.3.2 Nuclear magnetic resonance spectroscopy (NMR)

Solution ^{1}H NMR is commonly used to quantify the yield of monoesterification reaction. The methylene protons closest to the carboxylic acid bond show a peak at 4.2 ppm in the NMR

spectra, shown in the circle in Figure 3.3 [9]. The yield of monoesterification can be calculated by this methlyene proton peak area. Details about this technique are described in reference [9].

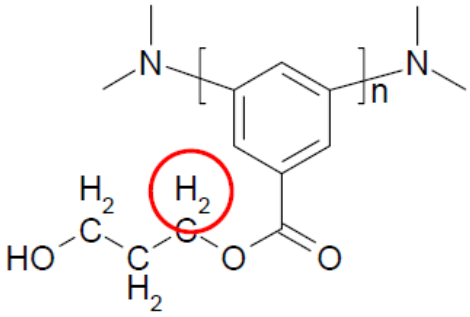

Figure 3.3: The protons in DABA moiety used for the solution ^{1}H NMR determination of yield of moesterification [9].

3.3 Dense film membrane formation

3.3.1 Dense film casting methods

Solution casting and knife casting are commonly used to prepare dense film membranes. In both cases, THF is used as the solvent due to its moderate volatility and PDMC polymer solubility. In solution casting, the polymer concentration is preferred to be 3~10% and the solution is extruded by a filter onto a Teflon® casting dish [12]. The dish is often covered by a funnel to control the evaporation rate of THF to form a uniform dense film membrane. Details about solution casting method is described in reference [3]. On the other hand, knife casting spreads the polymer solution onto a flat glass plate. The casting knife controls the gap between the blade and the plate. Therefore, the thickness of dense film is tunable [11].

After casting, the polymer solution is placed in a bag with THF environment and the evaporation of THF in the polymer solution leads to a uniform thin dense film. The film is then heated overnight under vacuum to remove residual THF in the film. A drying temperature below 70^{o}C is often preferred, since high temperatures can initiate the crosslinking reaction of PDMC.

If no further treatment (such as crosslinking) is needed, the film can be then masked in a permeation cell. Details about masking dense films can be found in reference [10].

3.3.2 Dense film crosslinking

After film casting and drying in the vacuum oven, crosslinking the dense film can be conducted by placing the film under a pre-heated vacuum oven. Vacuum oven serves as the driving force of the crosslinking reaction, as shown in Figure 3.4.

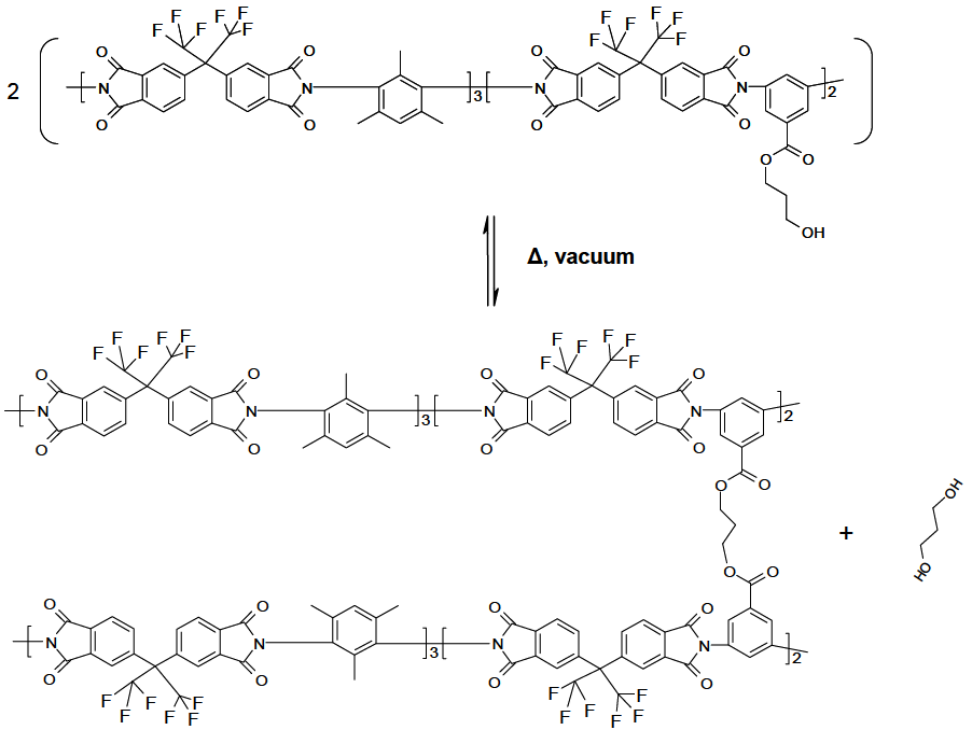

Figure 3.4: Schematic showing the ester-crosslinking of PDMC (3:2).

In this study, the crosslinking conditions for dense films are at 200^{o}C for 2 hrs, which are primarily based on the crosslinking optimization performed on the PDMC hollow fiber membranes [13]. Three different temperatures: 175 ^{o}C, 200 ^{o}C, and 250 ^{o}C have been studied and the optimum crosslinking temperature for hollow fibers is 200^{o}C [3]. Although a higher

crosslinking temperature tends to increase the permeability of dense films [10], it can reduce the permeance of hollow fibers significantly due to the densification of transition layer. Since hollow fibers are the focus of this work, the same 200 ^{o}C hollow fiber crosslinking conditions are used in the dense films. This will also provide consistence in evaluating the morphological features of hollow fibers, as will be described in Section 3.5.2.

3.4 Hollow fiber formation

3.4.1 Dope development

As shown in Section 2.5, the first step for hollow fiber spinning is to develop a spinnable dope. Typically, the spinning dope consists of polymer, solvents and non-solvents [14, 15]. Polymer serves as the framework of hollow fibers and provides mechanical strength. Increasing the polymer concentration will increase the viscosity of the dope and may reduce the "spinnability" of the dope. A typical polymer concentration falls between 25~35% [3]. The solvent dissolves the polymer to form a homogeneous solution. NMP is used in this work due to its low volatility, relatively low toxicity and high boiling point (202~204°C). THF is often added in the dope to promote the skin layer formation during spinning process [16, 17]. Non-solvents are introduced to the dope and keep the dope composition near to the binodal to allow rapid phase separation during wet-quench process. Water and ethanol are often preferred as the non-solvents. Water is a good candidate of the non-solvent since most polymers are hydrophobic. However, ethanol provides more flexibility for the dope composition than water since it allows a relatively larger window of stable one-phase dope. The volatility of ethanol also promotes the skin layer formation [18]. Other "pore-former" additives, such as Polyvinylpyrrolidone (PVP) or

lithium nitrate, can be used in the dope to accelerate phase separation and form an open porous substructure.

After determination of the components in the dope, a ternary phase diagram should be constructed to prepare a spinnable dope. The ternary phase diagram shows the single-phase, two-phase region and the binodal curve, as discussed in Section 2.5.2. The most common and effective method to determine the binodal is through the so-called cloud point technique [19]. The dope composition is chosen near the binodal. The initial dope composition is often determined by prior experience and depends on the properties of the components in the dope. Macroscopically, the dope should be a single phase and have a viscosity similar to or lower than thick honey (about 10,000 cP) when heated up to ~50^{o}C [19]. The dope must also have sufficient volatile solvents, especially THF, for skin layer formation [16]. The complex nature of polymer solutions and multiple requirements that must be met suggests that the dope formulation includes considerable trial and error experiment to develop an optimum dope composition [11].

3.4.2 Hollow fiber spinning

To spin hollow fiber membranes with desirably high separation performance, the following main spinning process variables are typically studied: spinneret temperature, draw ratio, air gap and quench bath.

The spinneret temperature is critical for hollow fiber skin layer formation as it affects the rate of THF evaporation in the air gap to form the nascent skin. An excessively low spinneret temperature can increase the viscosity of the dope and cause the fiber break during drawing. On the other hand, a high spinneret temperature can reduce the viscosity of dope and improve the

"spinnability" of dopes with high polymer concentration; however, limits exist with regard to temperature due to flashing and boiling of the solvent.

The draw ratio is determined by the ratio of hollow fiber take-up rate to the dope extrusion rate. A take-up rate higher than 50 m/min can produce large-scale fibers and is often preferred for industrial application. Moreover, a high draw ratio may introduce elongational forces in the outer layer of nascent fibers, which tends to orientate the segmental chains in polymer and cause selectivities higher than the intrinsic unoriented dense film values [20, 21].

The air gap has been identified as another key spinning parameter in determining the skin layer formation of hollow fibers [16]. A higher air gap height leads to a longer residence time of nascent fibers in the air and can promote the formation of a thicker skin layer. However, a high air gap also causes fiber breaks if the gravity and elongational stress overcome the strength of the nascent fibers. On the other hand, an excessively low air gap can cause skin layer defects or eliminate the skin due to inadequate THF evaporation. Therefore, the air gap must be controlled and optimized carefully.

The quench bath temperature is particularly critical for dual-layer hollow fiber spinning. Since the PDMC polymer is more hydrophilic than other polymers and requires a longer phase separation time, an elevated quench temperature is generally preferred as it accelerates the transport of components in the nascent fibers. However, a higher quench temperature tends to cause delamination of sheath/core layer during dual-layer hollow fiber spinning [22].

3.4 Hollow fiber crosslinking methods

The most commonly studied crosslinking method is by annealing the hollow fibers in a pre-heated vacuum oven for a set period of time. The key crosslinking parameters are mainly the crosslinking temperature and crosslinking time. The reaction mechanism of covalent ester-crosslinking was shown in Figure 3.4.

On the other hand, crosslinking at higher temperature tends to form a thicker skin layer and reduce the CO_2 permeance [3]. Attempts were made to use catalysts to reduce the crosslinking temperature and increase the permeance [11, 19]. The catalysts, such as P-toluenesulfonic acid (PTSA), are believed to reduce the activation energy of the crosslinking reaction and reach a high degree of crosslinking under relatively lower crosslinking temperature [23]. However, preliminary study on catalyst-assisted crosslinking at 150^{o}C showed that the additional catalyst treatment can significantly reduce the permeance; therefore, the approach was not further explored in this work. Details about catalyst-assisted crosslinking and method are described in references [11, 19].

3.5 Membrane characterization methods

3.5.1 Scanning Electronic Microscopy (SEM)

Scanning Electronic Microscopy (SEM) is a particularly important method to characterize the morphology of hollow fibers. SEM image can provide a magnification over 40,000x. To prepare a sample for SEM measurements, the fiber is first soaked in hexane and then cryogenically fractured in liquid nitrogen for perserving its inner morphology, especially the skin layer and open prous substructure. Since the polymeric hollow fiber is non-conductive, the cross-section of the fiber must be coated with a thin gold layer before the SEM test. SEM images

can be also used to estimate the skin layer thickness; however, the effective skin layer thickness should be determined by the gas permeation, as will be discussed in sections below.

3.5.2 Pure gas permeation

3.5.2.1 Dense film permeation

After film masking, the dense film can be tested in a gas permeation system. A schematic depicting the dense film permeation system is shown in Figure 3.5 [24].

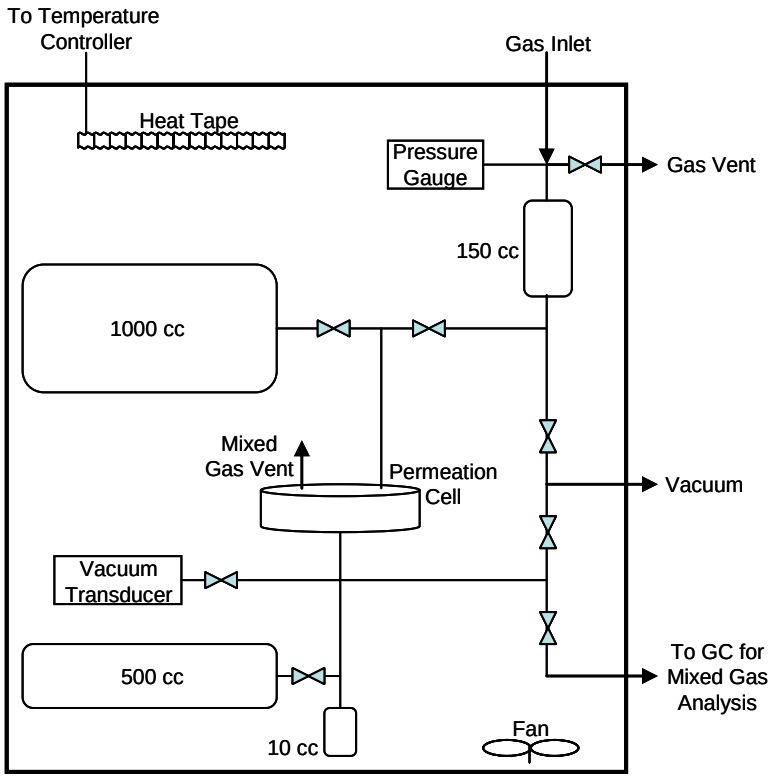

Figure 3.5: Gas permeation system for dense film permeation [24].

For pure gas permeation, gas venting in the upstream and GC analysis are not required. The permeability of a dense film membrane is determined by the Equation 3.1 [3].

$$P = \frac{1.1583\times10^{3}\cdot(\frac{dp}{dt})\cdot l\cdot V_R}{A\cdot T\cdot\Delta p} \quad (3.1)$$

In Equation 3.1, *dp/dt* is the slope of the downstream pressure vs. time (torr/min); *l* is the membrane thickness (μm); V_R is the downstream reservoir volume (cm^3); *A* is the dense film area (cm^2); *T* is the operation temperature (K); Δp represents the partial pressure/fugacity difference. The unit of permeability is the Barrer.

3.5.2.2 Hollow fiber permeation

Pure gas permeation for hollow fibers is performed in a dead-end counter-current flow module with a bore side feed. The permeate flow rate is measured by a bubble meter or digital flow meter in the shell side. Multiple modules can be tested simultaneously if the feed conditions are the same, as shown in Figure 3.6 [3].

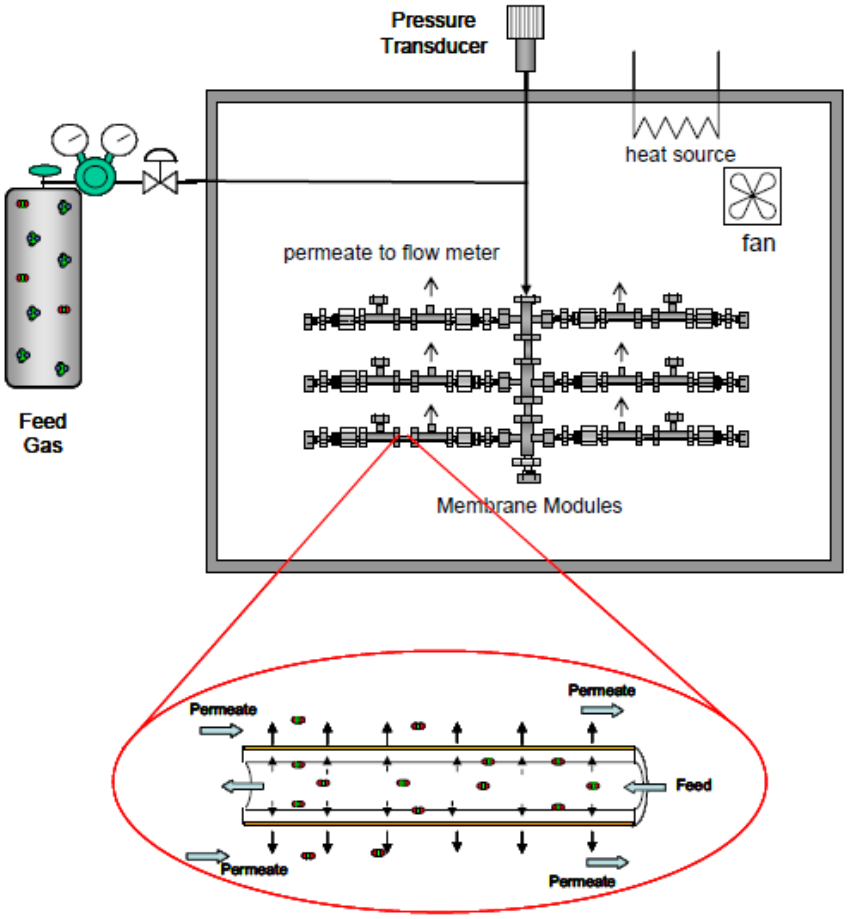

Figure 3.6: Schematic showing the pure gas permeation system for multiple module permeation test [3].

The permeance, *P/l*, of each module is calculated by Equation 3.2 [3, 19].

$$\frac{P}{l} = 10^{-6} \cdot \frac{Vp \cdot 273.15}{5.17 \cdot A \cdot T \cdot \Delta p} \tag{3.2}$$

In this equation, *Vp* is individual permeation flow rate in ml/s; *T* is the test temperature in *Kelvin*; *A* is membrane area in cm^2; Δp is the pressure or fugacity difference in psia. The unit of permeance is the GPU.

Three morphological features of hollow fiber membranes are commonly studied through gas permeation: the skin integrity, skin thickness, and substructure resistance. The skin integrity is measured by comparing the selectivity of hollow fibers with that of dense films for a particular gas pair. A skin is defect-free if the selectivity of hollow fibers is ≥90% of the intrinsic dense film value [18, 25, 26]. Furthermore, the defect-free skin thickness, l_{skin}, is estimated by the ratio of dense film intrinsic permeability to the hollow fiber permeance for a particular gas. Lastly, the substructure resistance of hollow fibers is characterized somewhat by comparing the permselectivity of a high permeability/low permeability gas pair (such as He/N_2) to that of a lower permeability gas pair (such as O_2/N_2). Substructure resistance exists when the He/N_2 selectivity of hollow fibers is a smaller percentage of the intrinsic dense film selectivity than the O_2/N_2 selectivity [27].

Pure gas and mixed gas permeation can be performed for hollow fibers. Non-condensable gases, such as O_2, N_2, He, are often used to study the ideal gas separation performance of hollow fibers. On the other hand, mixed gas permeation is conducted to study the gas separation performance under more realistic feed conditions, where feed conditions can significantly affect the diffusion of each penetrant. Mixed gas permeation will be described in Section 3.5.3 below.

3.5.3 Mixed gas permeation

3.5.3.1 Dense film permeation

Mixed gas permeation was also performed on the dense film membranes in this study. Mixed gas permeation requires a mixed gas venting in the upstream and GC measurements for the gas compositions. The permeation system is shown as Figure 3.5 in Section 3.5.2.1. For mixed gas permeation, the stage cut, determined by the ratio of permeate flow to feed flow, was

kept below 1% by venting the upstream to avoid concentration polarization at the upstream of the dense film. The gas flow compositions were measured by using an Agilent Technologies 6890N Network GC system and ChemStations software. Ultra high purity helium was used as the carrier gas. At least three replicates of GC measurements were taken to minimize the uncertainty of the analysis at each state. Details of the mixed gas permeation system can be found in reference [28].

3.5.3.2 Hollow fiber permeation

The mixed gas permeation of hollow fibers is typically fed through the shell side to allow extremely high feed pressures. The permeate flow rate is measured by a bubble flow meter in this study. The retentate flow rate is controlled by a valve so that the ratio of permeate to feed flow rate (so-called "stage cut") is below 1%. Concentration polarization in the feed was totally avoided by maintaining this low mixed gas stage cut [3].

The gas compositions of permeate and retentate flows are analyzed by the HP5890A Gas Chromatography (GC). The permeance, *P/l*, of each permeant through hollow fibers is calculated by Equation 3.3, as shown in Equation 3.3.

$$\frac{P}{l} = 10^{-6} \cdot \frac{Vp \cdot y_i \cdot 273.15}{5.17 \cdot A \cdot T \cdot (p_x \cdot \phi_{xi} \cdot x_i - p_y \cdot \phi_{yi} \cdot y_i)} \tag{3.3}$$

In the above equation, *Vp* is volumetric flow rate of permeate in ml/s; x_i and y_i are mole fraction of component *i* in permeate and the upstream, respectively; *T* is the operating temperature in Kelvin; *A* is membrane area in cm^2; p_x and p_y are feed pressure and permeate pressures in psia, respectively; ϕ_{xi} and ϕ_{yi} are fugacity coefficients of component *i* in the upstream and permeate streams, respectively.

3.5.4 Crosslinking characterization

3.5.4.1 Dissolution experiment

A dissolution experiment is commonly used to qualitatively determine the crosslinkability of membranes [19, 29]. The *crosslinked* membranes have "infinite" high molecular weight, making them insoluble in THF [3]. In the study, *crosslinked* membranes are placed in vials with THF and sit at room temperature for at least 24 hrs. Completely crosslinked samples are insoluble in the THF. Partially crosslinked samples are highly swollen but not completely soluble in THF. Uncrosslinked samples dissolve in THF rapidly.

3.5.4.2 Gel fraction experiment

The dissolution experiment can only qualitatively measure the crosslinkability since the samples in THF are only observed visually. Gel fraction experiment can somehow characterize the degree crosslinking quantitatively. In this experiment, the crosslinked samples are weighed and then placed in THF for at least 24 hrs on a roller at room temperature. After removing all residual THF in the samples, the weight of samples is re-tested. The gel fraction is determined by the polymer weight after THF dissolution to the initial sample weight.

3.5.4.3 TGA-IR Analysis

TGA-IR (thermogravimetric analysis-infra-red) can also be used to study the crosslinking of polymer samples. TGA measures the weight loss while IR identifies the species during the crosslinking heat treatment. The ratio of actual weight loss of propane diol to theoretical weight loss from stoichiometry can determine the degree of crosslinking. However, the residual NMP in polymer samples makes this approach inaccurate. On the other hand, the ratio of the peak integrals in IR spectra helps quantitatively determine the crosslinking degree. Details about TGA-IR analysis are described in references [19, 29].

3.6 References

[1] A.M.W. Hillock, W.J. Koros, Cross-linkable polyimide membrane for natural gas purification and carbon dioxide plasticization reduction, Macromolecules, 40 (2007) 583-587.

[2] D.W. Wallace, C. Staudt-Bickel, W.J. Koros, Efficient development of effective hollow fiber membranes for gas separations from novel polymers, J Membrane Sci, 278 (2006) 92-104.

[3] I.C. Omole, Crosslinked Polyimide Hollow Fiber Membranes for Aggressive Natural Gas Feed Streams, Ph.D. Dissertation, in: Chemical and Biomolecular Engineering, Georgia Institute of Technology, Atlanta, GA, 2008.

[4] M. Das, MEMBRANES FOR OLEFIN/PARAFFIN SEPARATIONS, PhD Dissertation, in: School of Chemical & Biomolecular Engineering, Georgia Institute of Technology, Atlanta, GA, 2009.

[5] M.H. Kailani, C.S. Sung, S.J. Huang, Syntheses and Characterization of Model Imide Compounds and Chemical Imidization Study, Macromolecules, 25 (1992) 3751-3757.

[6] M.H. Kailani, C.S.P. Sung, Chemical imidization study by spectroscopic techniques. 2. Polyamic acids, Macromolecules, 31 (1998) 5779-5784.

[7] M.H. Kailani, C.S.P. Sung, Chemical imidization study by spectroscopic techniques. 1. Model amic acids, Macromolecules, 31 (1998) 5771-5778.

[8] I.C. Omole, S.J. Miller, W.J. Koros, Increased molecular weight of a cross-linkable polyimide for spinning plasticization resistant hollow fiber membranes, Macromolecules, 41 (2008) 6367-6375.

[9] J.D. Wind, Improving Polyimide Membrane Resistance to Carbon Dioxide Plasticization in Natural Gas Separations, PhD dissertation, in: Chemical Engineering, The University of Texas at Austin, Austin, TX, 2002.

[10] A.M.W. Hillock, CROSSLINKABLE POLYIMIDE MIXED MATRIX MEMBRANES FOR NATURAL GAS PURIFICATION, PhD Dissertation, in: Chemical Engineering, Georgia Institute of Technology, Atlanta, GA, 2005.

[11] C. Ma, OPTIMIZATION OF ASYMMETRIC HOLLOW FIBER MEMBRANES FOR NATURAL GAS SEPARATION, MS THESIS, in: School of Chemical and Biomolecular Engineering, Georgia Institute of Technology, Atlanta, GA, 2011.

[12] J.D. Wind, D.R. Paul, W.J. Koros, Natural gas permeation in polyimide membranes, J Membrane Sci, 228 (2004) 227-236.

[13] I.C. Omole, R.T. Adams, S.J. Miller, W.J. Koros, Effects of CO2 on a High Performance Hollow-Fiber Membrane for Natural Gas Purification, Ind Eng Chem Res, 49 (2010) 4887-4896.

[14] S.A. McKelvey, D.T. Clausi, W.J. Koros, A guide to establishing hollow fiber macroscopic properties for membrane applications, J Membrane Sci, 124 (1997) 223-232.

[15] O.M. Ekiner, G. Vassilatos, Polyaramide hollow fibers for H-2/CH4 separation - II. Spinning and properties, J Membrane Sci, 186 (2001) 71-84.

[16] D.T. Clausi, W.J. Koros, Formation of defect-free polyimide hollow fiber membranes for gas separations, J Membrane Sci, 167 (2000) 79-89.

[17] A.F. Ismail, L.P. Yean, Review on the development of defect-free and ultrathin-skinned asymmetric membranes for gas separation through manipulation of phase inversion and rheological factors, J Appl Polym Sci, 88 (2003) 442-451.

[18] S.B. Carruthers, G.L. Ramos, W.J. Koros, Morphology of integral-skin layers in hollow-fiber gas-separation membranes, J Appl Polym Sci, 90 (2003) 399-411.

[19] D.W. Wallace, Crosslinked Hollow Fiber Membranes for Natural Gas Purification and Their Manufacture from Novel Polymers, Ph.D. Dissertation, in: Chemical Engineering, The University of Texas at Austin, Austin, TX, 2004.

[20] A.F. Ismail, S.J. Shilton, I.R. Dunkin, S.L. Gallivan, Direct measurement of rheologically induced molecular orientation in gas separation hollow fibre membranes and effects on selectivity, J Membrane Sci, 126 (1997) 133-137.

[21] I.D. Sharpe, A.F. Ismail, S.J. Shilton, A study of extrusion shear and forced convection residence time in the spinning of polysulfone hollow fiber membranes for gas separation, Sep Purif Technol, 17 (1999) 101-109.

[22] J. Liu, DEVELOPMENT OF NEXT GENERATION MIXED MATRIX HOLLOW FIBER MEMBRANES FOR BUTANE ISOMER SEPARATION, PhD Dissertation, in: School of Chemical & Biomolecular Engineering, Georgia Institute of Technology, Atlanta, GA, 2010.

[23] C.T. Kuo, S. Chen, Kinetics of polyesterification: Adipic acid with ethylene glycol, 1,4-butanediol, and 1,6-hexanediol, Journal of Polymer Science, Part A: Polymer Chemistry, 27 (1989) 2793-2803.

[24] A.M. Kratochvil, THICKNESS DEPENDENT PHYSICAL AGING AND SUPERCRITICAL CARBON DIOXIDE CONDITIONING EFFECTS ON CROSSLINKABLE POLYIMIDE MEMBRANES FOR NATURAL GAS PURIFICATION, PhD Dissertation, in: School of Chemical & Biomolecular Engineering, Georgia Institute of Technology, Atlanta, GA, 2008.

[25] S.B. Carruthers, Integral-skin formation in hollow fiber membranes for gas separations, Ph.D. Dissertation, in: Chemical Engineering, The University of Texas at Austin, Austin, TX, 2001.

[26] S.C. Pesek, W.J. Koros, Aqueous Quenched Asymmetric Polysulfone Membranes Prepared by Dry Wet Phase-Separation, J Membrane Sci, 81 (1993) 71-83.

[27] D.T. Clausi, S.A. McKelvey, W.J. Koros, Characterization of substructure resistance in asymmetric gas separation membranes, J Membrane Sci, 160 (1999) 51-64.

[28] K.C. Obrien, W.J. Koros, T.A. Barbari, E.S. Sanders, A New Technique for the Measurement of Multicomponent Gas-Transport through Polymeric Films, J Membrane Sci, 29 (1986) 229-238.

[29] D.W. Wallace, J. Williams, C. Staudt-Bickel, W.J. Koros, Characterization of crosslinked hollow fiber membranes, Polymer, 47 (2006) 1207-1216.

CHAPTER 4

SPINNING THIN SKINNED HIGH PERFORMANCE DEFECT-FREE HOLLOW FIBER MEMBRANES

4.1 Introduction

Asymmetric hollow fibers are typically produced in a so-called dry jet/wet quench spinning process. Details of dope development, spinning process and hollow fiber characterization were described in Chapter 3. This chapter will discuss the results of the development of defect-free crosslinkable hollow fibers with relatively thinner skins and significantly improved separation productivity compared to prior work [1] based on the PDMC polymer.

4.2 Hollow fiber formation optimization

In order to reduce the effective skin layer thickness and improve natural gas separation productivity of hollow fibers, three main parameters were examined in this work: spinning conditions, dope composition and molecular weight of polymers. A skin layer thickness on the order of 0.1μm is commercially preferable to provide high separation productivity without loss of separation selectivity. Therefore, this chapter will focus on the optimization of hollow fiber membrane formation process to study the viability of reducing the defect-free skin layer thickness to the order of 0.1 μm.

Previous researchers were able to achieve skin layer thickness of uncrosslinked hollow fibers on the order of 0.2~0.4 μm [1, 2]. To reduce the skin layer thickness and further improve separation productivity, this study aimed to optimize the dope composition and spinning conditions, since these variables can greatly affect the skin layer formation. Clausi and Koros [3]

studied the formation of defect-free Matrimid® polyimide hollow fibers by varying the dope composition and spinning conditions. They showed that a lower air gap and lower THF% resulted in a thinner skin layer, as shown in Figure 4.1. The structure of Matrimid® polyimide is shown in Figure 4.2.

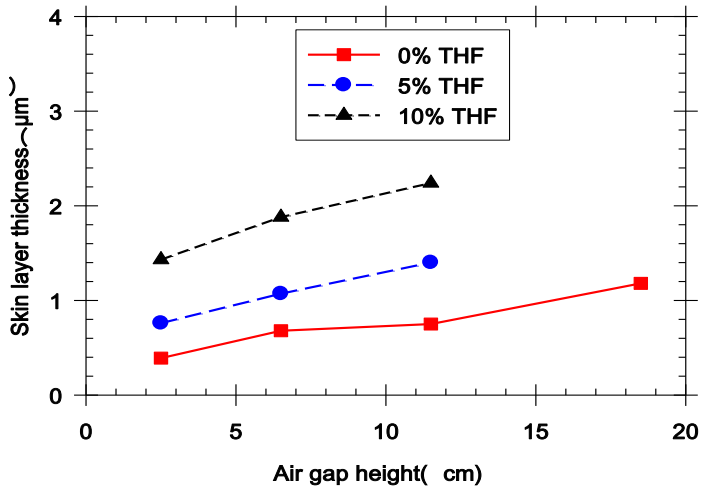

Figure 4.1: Effect of dope compositions and spinning conditions on Matrimid® hollow fiber skin layer thickness[3].

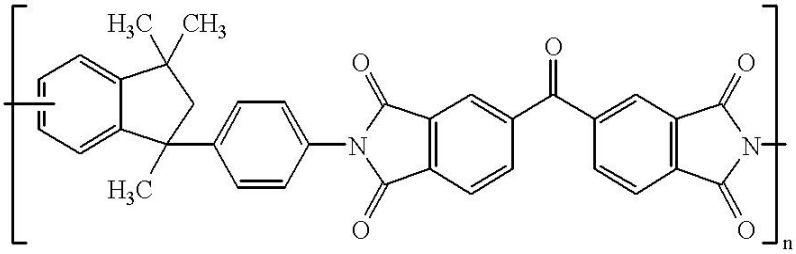

Figure 4.2: Structure of Matrimid® polyimide.

Omole et al [1] demonstrated that a higher molecular weight (Mw~80,000) is favorable for hollow fiber formation since the molecular weight affects viscoelasticity required for fiber drawing. Therefore, two batch polymers with different molecular weight were used in the

spinning to study the effect of molecular weight on the separation performance in this research. Ideal gas permeation was first performed to study the intrinsic separation performance and determine the skin layer thickness of hollow fibers. Moreover, natural gas separation properties of hollow fibers were evaluated by using a CO_2/CH_4 mixed gas.

4.3 Spinning process optimization

4.3.1 Hollow fiber spinning

As discussed in Chapter 3, dry jet/wet-quench hollow fiber spinning process includes a variety of spinning variables, such as spinning temperature, air gap, take-up rate, quench medium and temperature, dope flow rate, and humidity. Three main parameters, air gap, take-up rate and spinning temperature, were studied to optimize spinning process, since those variables are known to significantly affect the skin layer formation and gas separation performance [3-5].

For the first stage of spinning work, the dope composition was chosen based on the previous work done by Omole[1]. He showed that this dope composition provided a relative high CO_2 permeance of 50 GPU with a CO_2/CH_4 selectivity of 42 in testing with 200 psi of 50/50 CO_2/CH_4, 35^oC [1, 6]. The dope composition is shown in Table 4.1.

Table 4.1: Hollow fiber spinning dope compositions from literatures [1, 7].

Component	Wt%
PDMC	35.0
NMP	35.0
Ethanol	8.5
THF	15.0
$LiNO_3$	6.5

The polymer used for spinning process optimization was provided by Chevron Energy Technology Company. The molecular weight of the polymer sample is 74,800 (Mw) with a polydispersity index of 1.8. NMP was used as the primary solvent due to its lower volatility and relatively low toxicity [8, 9]. Including a high volatility component, such as THF, can promote skin layer formation for hollow fibers during the dry jet step [2, 3]. Ethanol is also used as a non-solvent since it provides more flexibility in the dope preparation process by balancing volatility and promotion of phase separation to offset the volatile solvent, THF [3]. Lithium nitrate ($LiNO_3$) is also added as both a non-solvent and "pore-former" to accelerate phase separation and form an open porous substructure during the wet quench process [10].

During the first spinning, the main spinning parameters studied include dope flow rate, air gap, take-up rate and spinning temperature, as shown in Table 4.2. These conditions were chosen based on previous research and personal experience in working with the PDMC polymer [1, 2, 6-8, 11].

Table 4.2: Hollow fibers spinning conditions.

Spinning conditions	
Dope extrusion rate	180~300 ml/hr
Bore fluid composition	NMP/H_2O 80/20wt%
Bore fluid rate	60~100 ml/hr
Spinning temperature	50~75^oC
Air gap	1~30 cm
Quench bath	Tap water, ~55^oC
Take-up rate	25~50 m/min
Nominal draw ratio	2.1~4.2

Table 4.2 shows that two spinning temperatures, 50°C and 75°C, were studied in the first campaign. A higher spinning temperature can accelerate the evaporation of volatile components in the dope, such as THF and ethanol, thereby promoting the skin layer formation and reducing skin layer defects. On the other hand, a lower spinning temperature may reduce the spinnability of hollow fibers due to the high viscoelasticity of the dope under lower temperatures. The air gap, which primarily determines the skin layer thickness of hollow fibers, was varied from 1 to 30 cm. A 1 cm air gap represents an extremely short fiber residence time in the air to produce the thinnest skin layer without defects. The take-up rate was also studied in the spinning. Generally,

a higher take-up rate is preferred for industrial application to improve the productivity of membrane fabrication. Moreover, a higher take-up rate can produce fibers with smaller dimensions, which can withstand high transmembrane pressures [1]. The effective draw ratio is calculated by the ratio of take-up rate to dope extrusion rate.

After the spinning process, the hollow fibers were soaked in water bath for ~3 days to remove residual solvents and non-solvents. The water bath was changed twice a day. After water soaking, solvent exchange on fibers must be conducted to avoid subsequent fiber morphology collapse [12], which is particularly important for preserving the transition porous layer just beneath the skin layer. The fibers from the water bath contain water and must not be dried directly since the capillary force in fibers induced by dehydration may collapse the pores and damage the fibers. Therefore, solvent exchange must be performed as the final spinning step. Typically, alcohol (e.g. ethanol or methanol) is used first to replace water in the fibers for three times (~20 mins each time). Then the alcohol is washed out by using a volatile solvent (e.g. hexane) for three times (~20 mins each time). Through solvent exchange, the fiber surface tension is greatly reduced and the fibers can be dried under vacuum and heating without collapsing the inner structure of fibers. In this study, the fibers were dried in the hood for 1 hr after solvent exchange. Then the fibers were placed in vacuum drying overnight at 70°C to further remove the residual solvents and non-solvents without crosslinking fibers.

4.3.2 Hollow fiber characterization

The *uncrosslinked* hollow fibers were first characterized by using Scanning Electron Microscope (SEM) to observe the cross-sectional structure of hollow fibers. A typical SEM image of hollow fibers spun from this work is shown in Figure 4.3. Fibers with improved concentricity will be discussed later in Section 4.4 on dope reformulation.

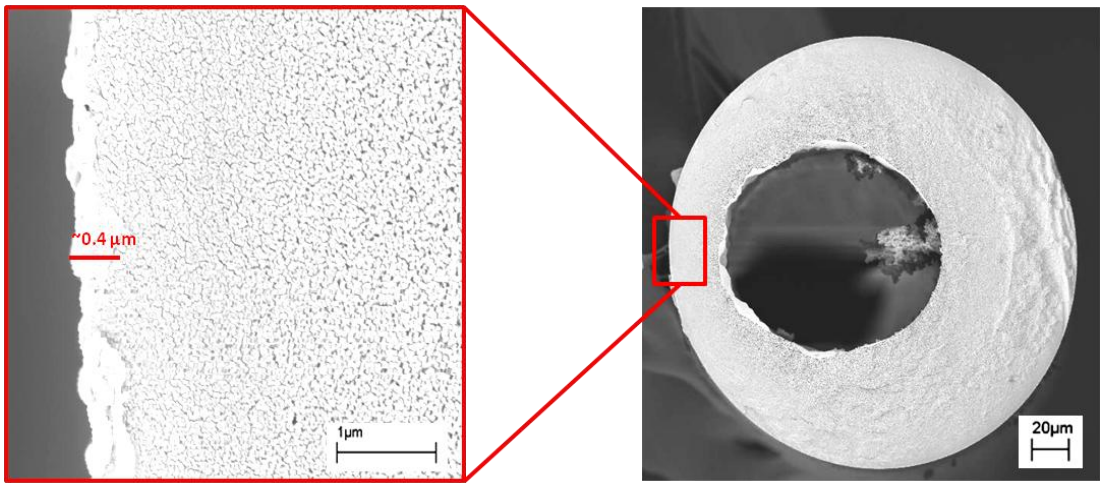

Figure 4.3: SEM images of cross-section of an *uncrosslinked* hollow fiber, showing the apparent skin layer and open porous substructure.

SEM images in Figure 4.3 showed that the hollow fibers are circular, suggesting phase separation occurred rapidly and the fibers were solidified before reaching the guide roller in the quench batch. This morphology allows fibers to withstand high trans-membrane feed pressures. The skin layer is apparent and the SEM estimated skin layer thickness is on the order of ~0.4 µm. The effective skin layer thickness should be determined by the gas permeation experiment.

Gas permeation measurements can characterize three morphological features of hollow fiber membranes: the skin integrity, skin thickness, and substructure resistance. The skin integrity is measured by comparing the permselectivity for a gas pair of hollow fibers with that of dense films. A skin is taken to be defect-free if the selectivity for a gas pair of hollow fibers is ≥90% of the polymer's intrinsic dense film value [5, 13, 14]. The defect-free skin thickness, l_{skin}, is estimated from the dense film intrinsic permeability and the asymmetric membrane's permeance for a particular gas, namely,

$$\ell_{skin} = \frac{\text{Dense Film Permeability}}{\text{Hollow Fiber Permeance}} = \frac{P}{P/\ell}$$

To avoid the complexity of CO_2 induced plasticization in determining the effective skin thickness, the O_2 permeability and permeance are used instead of CO_2 to estimate the skin layer thickness of *uncrosslinked* hollow fibers in this research.

The substructure resistance of hollow fibers can be characterized somewhat by comparing the gas permselectivity of a high permeability/low permeability gas pair such as He/N_2 to that of a lower permeability gas pair such as O_2/N_2. Substructure resistance exists when the He/N_2 selectivity is a smaller percentage of the intrinsic value than the O_2/N_2 selectivity [15].

To characterize the aforementioned three morphological features of hollow fibers, pure gas permeation using N_2, O_2, He and et al. was first performed on uncrosslinked hollow fibers from the first generation. The pure gas permeation for some of the best spinning states from this preliminary campaign are summarized in Table 4.3.

Table 4.3**:** Gas separation properties of *uncrosslinked* hollow fibers [11].

State	Permeance (GPU)		Selectivity	
	O_2	H_e	$\alpha_{O2/N2}$	$\alpha_{He/N2}$
2	25.5±1.5	174±5	4.7±0.5	31.7±4.0
6	16.6±0.9	113.3±2.6	4.5±0.3	30.3±1.4
7	36.4±2.5	-	3.3±0.2	-

Test conditions: feed pressure: ~100 psig, temperature: 35^{o}C.

Uncrosslinked dense film data: O_2 permeability: 7.1 Barrers, $\alpha_{O2/N2}$=4.8, $\alpha_{He/N2}$=40 [1].

Figure 4.3 shows that the State 2 and 6 fibers are defect-free since the O_2/N_2 selectivity is over 90% of intrinsic selectivity (dense film value $\alpha_{O2/N2}$=4.8). Minor substructure resistance may exist in the fibers as the He/N_2 selectivity is ~80% of the intrinsic (dense film value $\alpha_{He/N2}$=40), smaller than the O_2/N_2 selectivity (≥94% of intrinsic O_2/N_2 selectivity). Based on the O_2 permeability of dense films and O_2 permeance of hollow fibers, the calculated effective skin layer thickness of fibers from State 2 and 6 is on the order of 0.3~0.4 μm. State 7 fibers have the thinnest skin layer thickness low to 0.2 μm; however, the O_2/N_2 selectivity is lower than intrinsic value, suggesting that the State 7 fibers are somehow defective; therefore, the skin layer thickness of State 7 fibers is underestimated.

In summary, a first generation defect-free PDMC hollow fiber was developed by using the nominally same dope composition in reference [1]. Despite the optimization of spinning conditions, the defect-free skin layer thickness is on the order of 0.3~.4 μm, close to what

reported in reference [1, 2]. Since the optimized spinning conditions do not result in defect-free fibers with the desired thin skin (ideally 0.1 μm), the dope composition should be modified, which will be discussed in Section 4.4 below.

4.4 Dope reformulation to improve productivity

4.4.1 Phase separation study

As discussed in the last section, spinning conditions have enabled creation of effectively defect-free hollow fibers. However, the hollow fibers showed some evidence for substructure resistance and did not exhibit the desired 0.1 μm skin layer thickness using the nominally same dope composition shown in literature [1], which clearly suggests that this dope composition may be not optimal to make the thinnest skin layer and most productive hollow fibers. Therefore, phase separation of dopes must be studied to reformulate the dope composition so that the defect-free skin layer thickness can be reduced to the desired level.

To optimize the dope composition, the binodal of dope consisting of PDMC/solvents/non-solvents must be determined to ensure that the dope composition is located in the one-phase region for the spinning. The commonly used technique to locate the binodal is through so-called cloud point experiment, as described in references [2, 16]. The results of cloud point experiments are plotted in a ternary phase diagram, as shown in Figure 4.4.

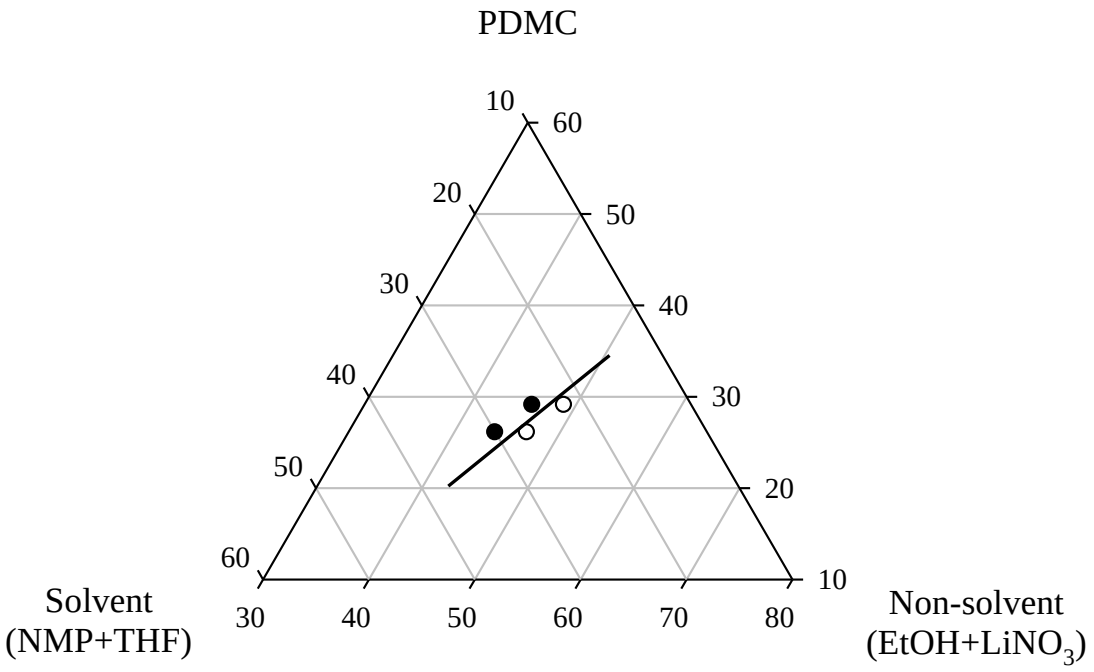

Figure 4.4: Ternary phase diagram depicting the binodal (solid line) of PDMC polymer/solvent/non-solvent system.

In Figure 4.4, the solid dots represent the single-phase samples and open circles represent the two-phase samples. The binodal (shown as the black solid line) lies between the single-phase region and two-phase region. Once the ternary phase diagram is plotted, the dope composition is chosen near the binodal to allow rapid phase separation and thinner skin layer formation. Macroscopically, the dope must be one-phase with a viscosity closer to thick honey [2] and also have sufficient volatile solvents and non-solvents to form the skin layer of hollow fibers. To modify the dope composition, the ratio of two components in the dope can be tuned while the composition of the third component is fixed. The complex nature of polymer solutions and multiple requirements that must be met require that the hollow fiber spinning includes considerable trial and error in dope development to provide the most productive hollow fibers. Based on the ternary phase diagram, the dope composition used in Chapter 4.2, consisting of

35% PDMC polymer, 35% NMP, 15% THF, 8.5% EtOH and 6.5% $LiNO_3$, is located deeply in the 1-phase region. The relative location of this dope composition (indicated as red solid square point) is shown in Figure 4.5.

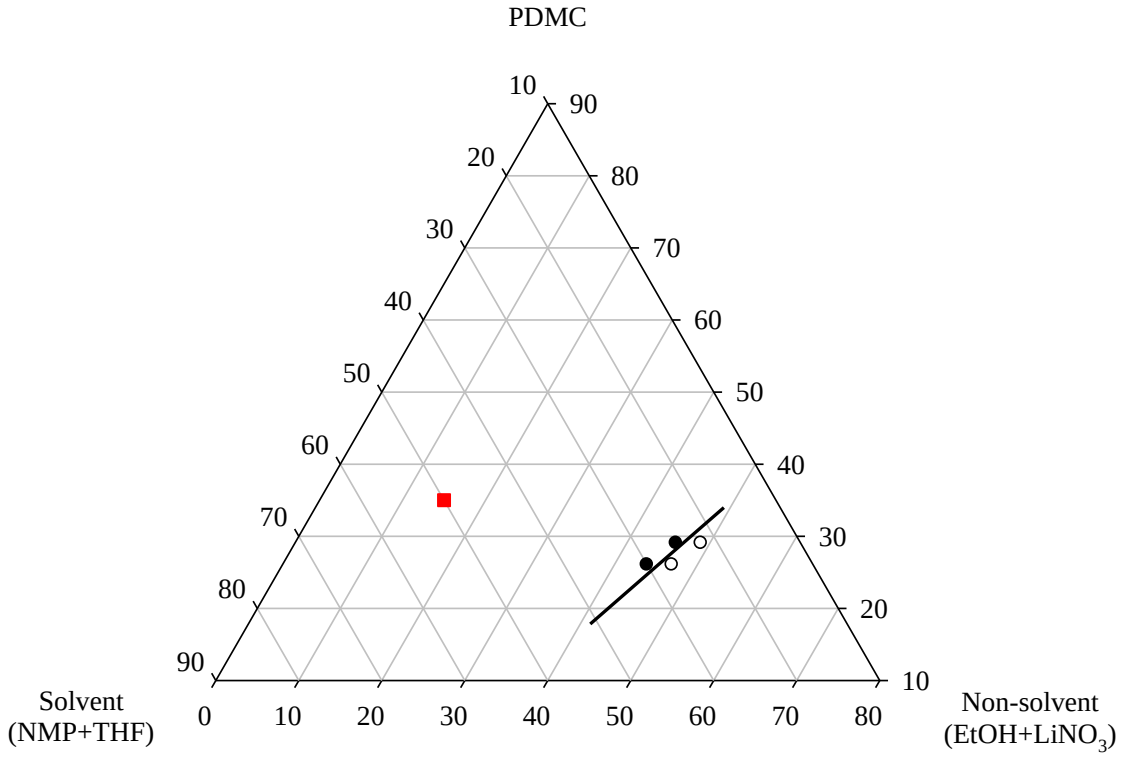

Figure 4.5: Ternary phase diagram depicting the binodal (solid line) of PDMC polymer and dope composition in Chapter 4.2 (red square point).

Since the previous dope composition is far from the binodal, this probably resulted in a relatively thick skin layer (~0.4 μm) and substructure resistance during the transformation into a phase separation structure. Literature [1] shows that hollow fibers spun with this dope composition (red solid point) have a high CO_2/CH_4 selectivity and CO_2 plasticization resistance. However, the CO_2 permeance of crosslinked hollow fibers was only ~50 GPU, making them less desirable for commercial application. Therefore, the dope composition must be reformulated to

achieve high CO_2 permeate flux and high CO_2/CH_4 selectivity, which will be discussed in Section 4.3.2.

4.4.2 Dope reformulation and hollow fiber spinning

Attempts are made in this section to reduce the skin layer thickness through dope reformulation. Starting from the middle range between the first spinning and the binodal, the dope was reformulated and the resultant dope composition is shown as the solid blue diamond point in Figure 4.6. This moves the dope composition closer to the binodal line without crossing it, since moving too close to or crossing the binodal line can cause skin defects or even eliminate the skin layer.

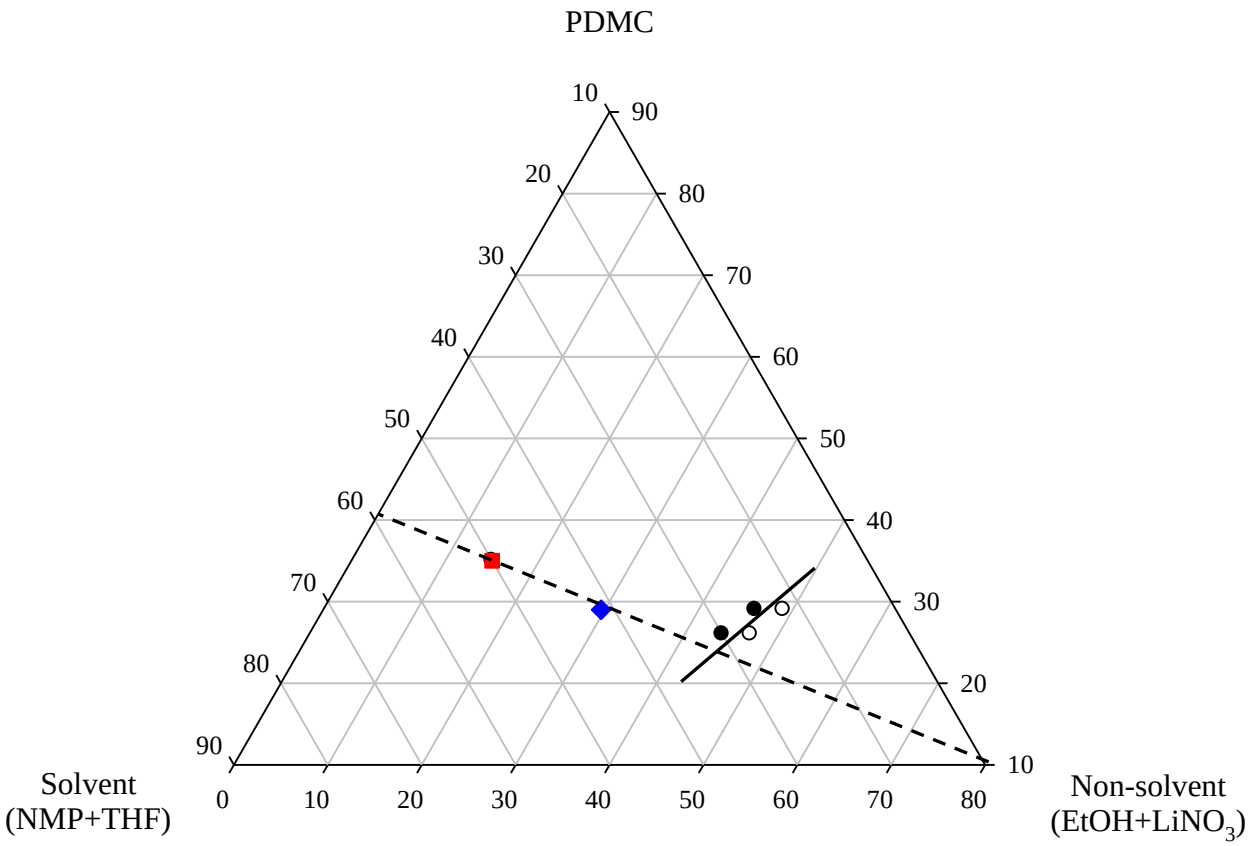

Figure 4.6**:** Ternary phase diagram depicting the binodal (solid line) of PDMC polymer, first dope composition (solid square point) and second dope composition (solid diamond point).

In the second dope, as shown by the trajectory on the dashed line, the ratio of PDMC to solvent was kept the same as first dope composition (35: 50) to allow enough solvent in the dope. The PDMC polymer and THF concentration was reduced from 35% to 29% and 15% to 12.4% respectively, which was expected to reduce the skin layer thickness and improve the separation productivity [3]. The composition of reformulated dope is shown in Table 4.4.

Table 4.4: Reformulated dope composition for hollow fibers spinning.

Component	Wt%
PDMC	29.0
NMP	29.0
Ethanol	23.1
THF	12.4
$LINO_3$	6.5

In the second spinning, two spinning variables, dope flow rate and air gap, were studied to reduce the skin layer thickness and improve separation productivity. The dope flow rate was 120~180 ml/hr, which was the same as the reference [1]. The air gap was varied from 2 to 33 cm to reduce skin layer thickness without introducing defects. The spinning conditions are summarized in Table 4.5.

Table 4.5: Hollow fiber spinning conditions.

Spinning conditions	
Dope extrusion rate	120~180 ml/hr
Bore fluid composition	NMP/H_2O 80/20wt%
Bore fluid rate	40~60 ml/hr
Spinneret temperature	70^oC
Air gap	1~33 cm
Quench bath	Tap water, ~50^oC
Take-up rate	50 m/min
Nominal draw ratio	4.2~6.3

4.4.3 Hollow fiber characterization

The SEM images of uncrosslinked fibers spun in the second spinning were shown in Figure 4.7.

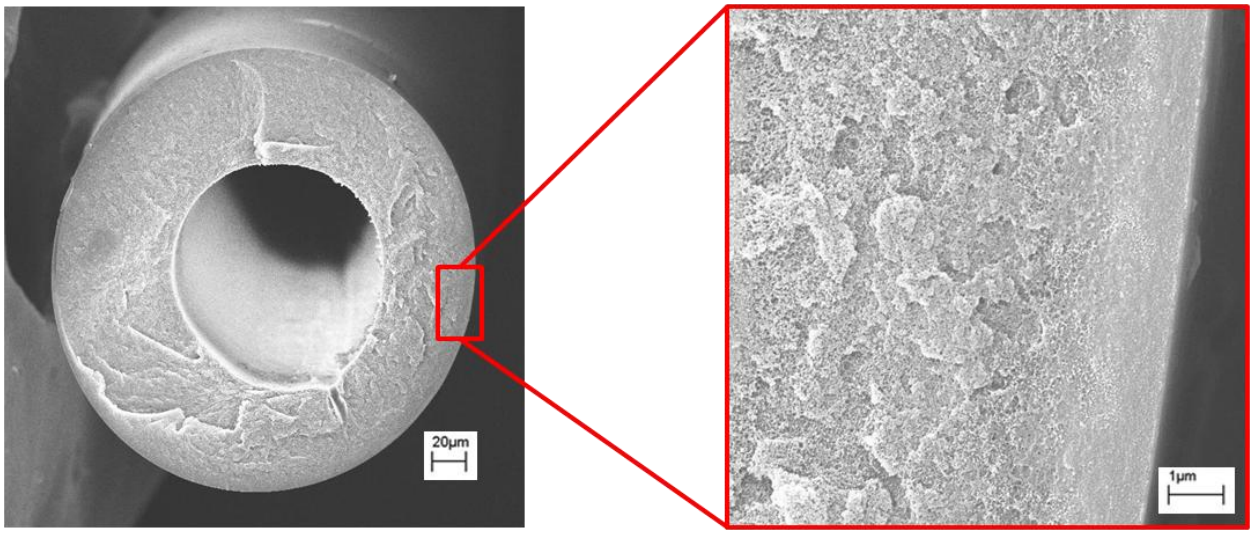

Figure 4.7: SEM images showing the cross-sectional structure of an *uncrosslinked* hollow fiber.

From above SEM images in Figure 4.7, the *uncrosslinked* hollow fibers show more concentric morphology. The concentricity indicates that the alignment of spinneret needle was completed successfully and the needle in the spinneret withstood the high dope flow rate during spinning. The skin layer and open porous substructure of hollow fibers are apparent in the SEM images. The hollow fibers were further tested with pure gases to study ideal gas separation properties and the gas permeation results are shown in Table 4.6.

Table 4.6**:** Pure gas separation properties of *uncrosslinked* hollow fibers.

State	Permeance (GPU)		Selectivity	
	O_2	H_e	$\alpha_{O2/N2}$	$\alpha_{He/N2}$
1	37.2	347	4.8	45
2	33.6	250	5.0	37
3	22.8	160	6.1	43
4	16.4	109	4.8	32

Test conditions: feed pressure: ~100 psig, temperature: 35^{o}C.

Table 4.6 shows that the hollow fibers are defect-free since the O_2/N_2 selectivity is equal or above the intrinsic selectivity (dense film $\alpha_{O2/N2}$=4.8). Possible minor substructure resistance may exist in State 4 since the He/N_2 selectivity is somehow below the intrinsic value (dense film $\alpha_{He/N2}$=40). Based on O_2 permeability and permeance, the thinnest skin layer thickness obtained in the spinning is lower than 0.21 μm. This skin layer thickness is reduced ~50% vs. the previous spinning, suggesting that the dope composition reformulation can effectively reduce the skin layer thickness without introducing defects. However, the skin layer thickness is still higher than the desirable level (<0.1 μm). To further reduce the skin layer thickness, the dope composition was moved even closer to the binodal without crossing the binodal. The relative location of the 3rd dope composition in the ternary phase diagram is shown in Figure 4.8.

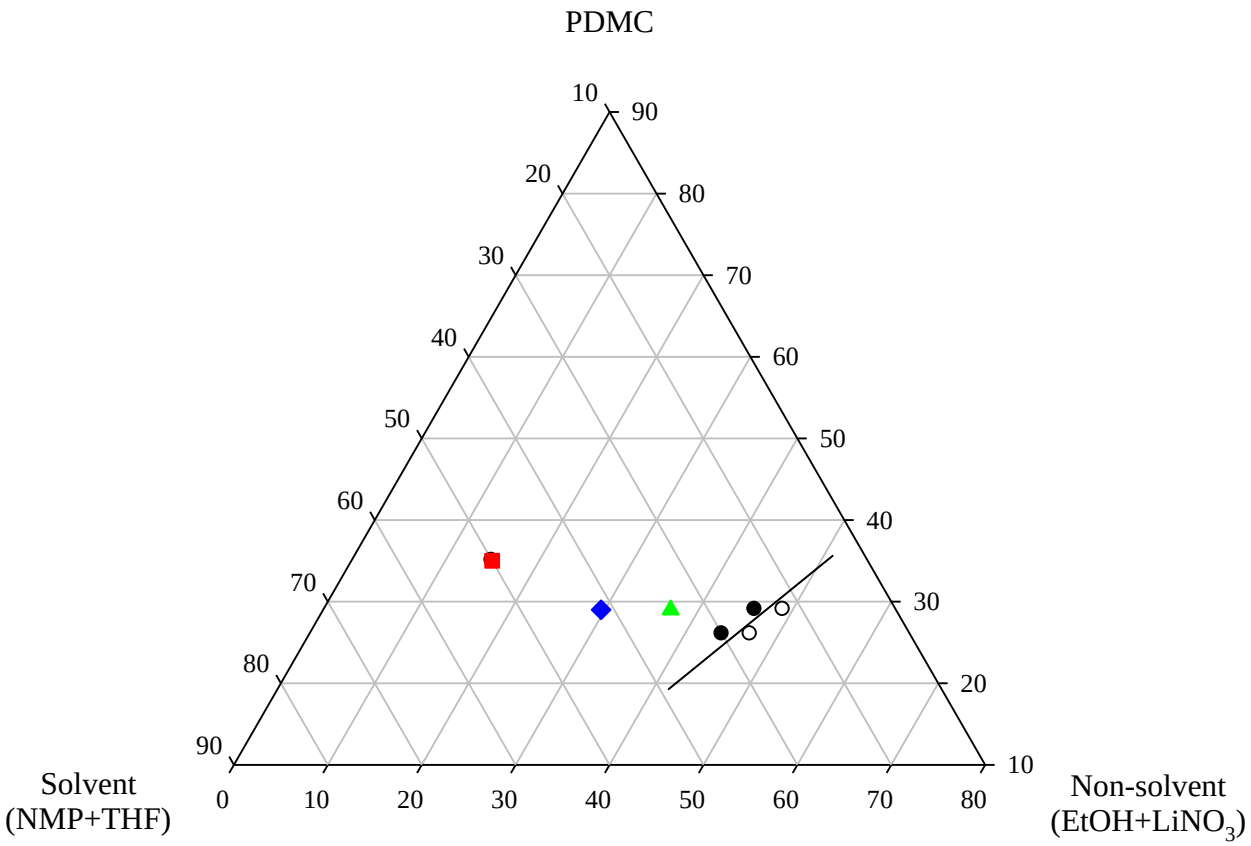

Figure 4.8**:** Ternary phase diagram depicting the 3rd dope composition (solid triangle point), 2nd dope composition (solid diamond point), 1st dope composition (solid square point) and binodal (solid line) of PDMC polymer.

The THF% was reduced from 12.4% to 10.2% in the 3rd dope composition, as shown in Table 4.7.

Table 4.7: Hollow fiber spinning dope composition.

Component	Wt%
PDMC	29.0
NMP	23.8
Ethanol	30.5
THF	10.2
$LiNO_3$	6.5

The key factor in determining the skin layer thickness, air gap, was studied in the 3rd spinning. The spinning conditions are summarized in Table 4.8.

Table 4.8: Hollow fiber spinning conditions.

Spinning conditions	
Dope extrusion rate	180 ml/hr
Bore fluid composition	NMP/H_2O 80/20wt%
Bore fluid rate	60 ml/hr
Spinneret temperature	70^oC
Air gap	1~5 cm
Quench bath	Tap water, ~50^oC
Take-up rate	50 m/min

The SEM images of an *uncrosslinked* hollow fiber spun in the 3rd spinning were shown in Figure 4.9, indicating that the hollow fibers have circular and desirable open porous morphology.

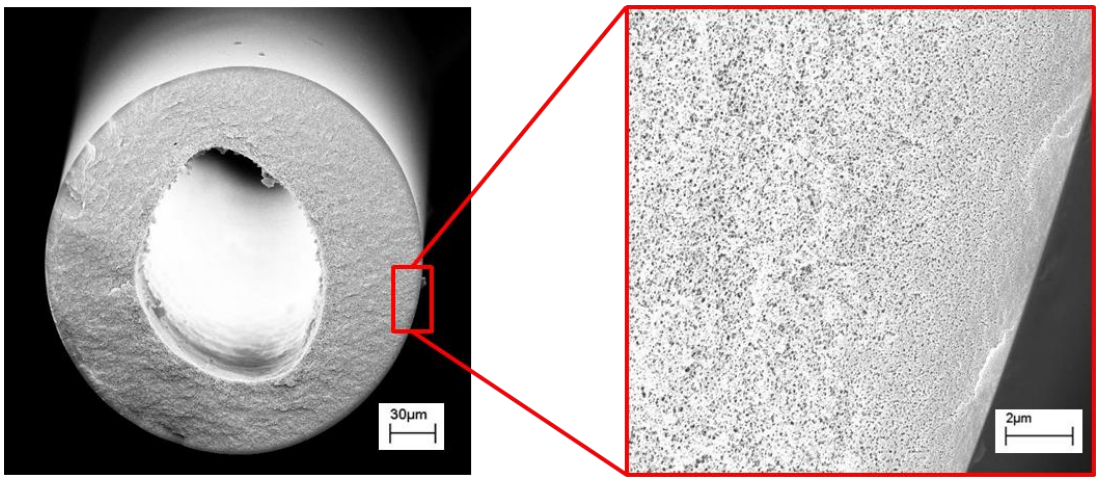

Figure 4.9: SEM images showing the cross-sectional structure of an *uncrosslinked* hollow fiber.

The uncrosslinked hollow fibers were further probed with pure gases and the permeance data are shown in Table 4.9.

Table 4.9: Pure gas separation properties of *uncrosslinked* hollow fibers.

State	Permeance (GPU)		Selectivity	
	O_2	H_e	$\alpha_{O2/N2}$	$\alpha_{He/N2}$
1	45.8	321	2.0	14
2	49.6	478	2.7	26
3	80.3	594	2.3	17

Test conditions: feed pressure: ~100 psig, temperature: 35^{o}C.

Table 4.9 shows that the *uncrosslinked* hollow fibers are defective since the O_2/N_2 selectivity is considerably lower than the intrinsic (dense film $\alpha_{O2/N2}$=4.8). The defects are possibly due to the relatively lower THF concentration in the dope, which is reduced 22% vs. the 2nd dope. Since THF has been identified as a key factor in determining the skin layer formation [3], the relatively lower THF concentration is detrimental for the formation of skin layer and cause the skin defects of hollow fibers.

As discussed in Section 4.3 and 4.4, the optimization of spinning variables and dope composition does not reduce the skin layer thickness to the desirable level (<0.1 μm) without introducing defects. A higher molecular weight polymer can maintain significant polymer chain entanglement and also promote the formation of defect-free skin layer [7]. Therefore, another batch polymer with relatively higher molecular weight was utilized to study the feasibility of reducing the effective skin layer thickness to 0.1 μm without introducing skin defects, which will be discussed in Section 4.5.

4.5 Polymer molecular weight effect on separation performance

4.5.1 Phase separation study

A new batch polymer with a higher molecular weight Mw=120k and PDI=2.0 was used to study the effect of molecular weight on separation performance in this chapter. By using this high molecular weight version polymer and the same solvents and non-solvents described in Section 4.4, a new ternary phase diagram was constructed to determine the dope composition. The ternary phase diagram with the binodal is shown in Figure 4.10.

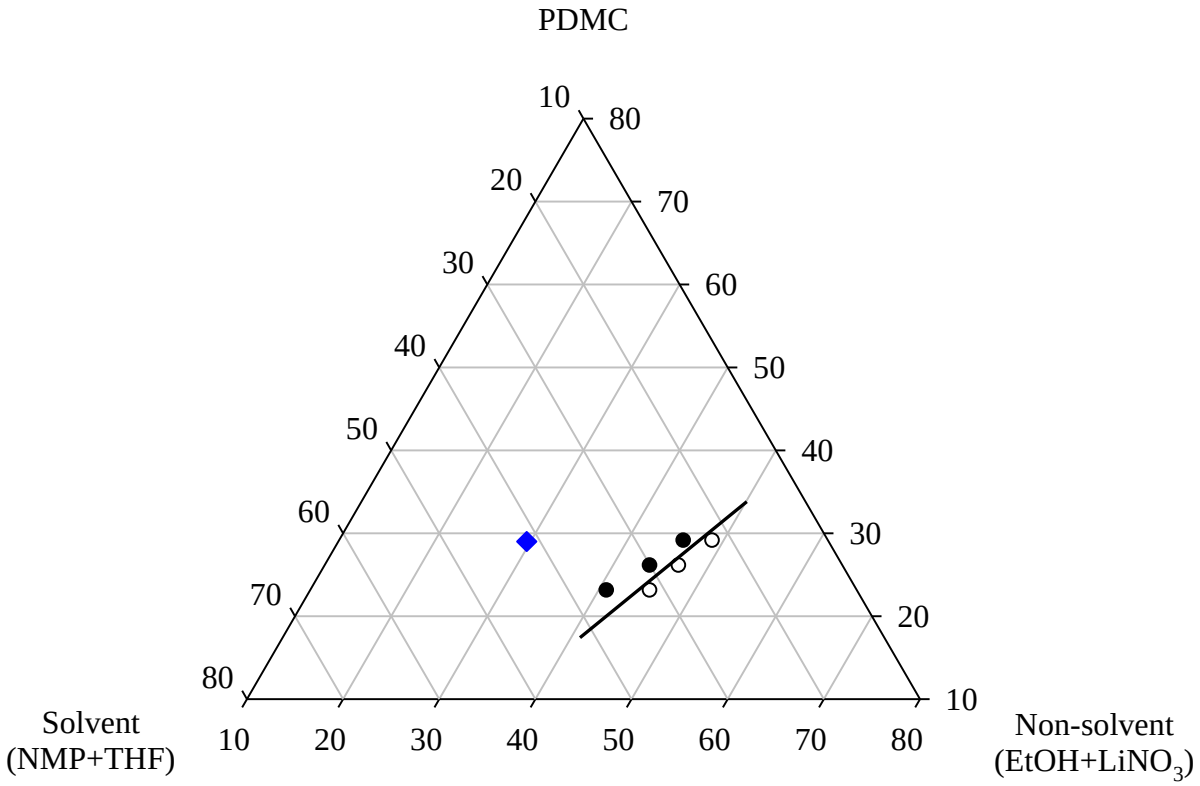

Figure 4.10: Ternary phase diagram showing the binodal (black solid line) of PDMC polymer/solvent/non-solvent system and dope composition (blue diamond point). Black solid dots and open circles represent one-phase dope and two-phase dope, respectively.

In Figure 4.10, the solid dots represent the single-phase samples and open circles represent the two-phase samples. The binodal (shown as the black solid line) lies between the one-phase region and two-phase region. The binodal line for this higher molecular weight sample is very similar to that found for the lower molecular weight sample. Further experiments will be needed to determine the accurate locations of binodal for different batch polymers. The dope composition used for the 4th spinning consists of 35% PDMC polymer, 35% NMP, 15% THF, 8.5% EtOH and 6.5% $LiNO_3$, and is safely located in one-phase region.

4.5.2 Hollow fiber spinning

For the 4th spinning, the main studied spinning parameter was the air gap. The air gap up to 33 cm represented a good spinnability while 1 cm air gap was used to minimize the residence time of nascent fibers in the air to achieve the thinnest skin. The greater "skinnability" of the higher molecular weight sample does appear to be helpful. Table 4.10 shows the spinning conditions.

Table 4.10: Hollow fiber spinning conditions.

Spinning conditions	
Dope extrusion rate	180 ml/hr
Bore fluid composition	NMP/H_2O 80/20wt%
Bore fluid rate	60 ml/hr
Spinneret temperature	70^oC
Air gap	1~33 cm
Quench bath	50^oC
Take-up rate	50 m/min

4.5.3 Hollow fiber characterization

The cross-sectional structure of an uncrosslinked hollow fiber from the 4th spinning is shown in Figure 4.11.

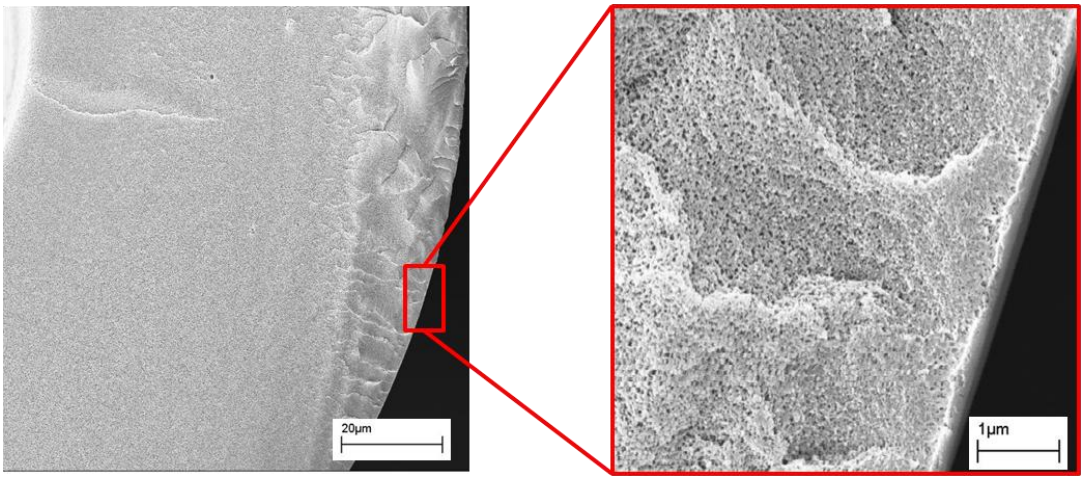

Figure 4.11: SEM images showing cross-sectional structure of an *uncrosslinked* fiber with apparent skin layer and open porous transition layer.

Figure 4.11 show that the skin layer and open porous substructure are apparent in the *uncrosslinked* hollow fibers. The pure gas permeation was then performed on *uncrosslinked* hollow fibers, and the permeation results are shown in Table 4.11. At least two modules were prepared to check the experimental reproducibility for each state.

Table 4.11: Pure gas separation properties of *uncrosslinked* hollow fibers.

State	Permeance (GPU)		Selectivity	
	O_2	N_2	$\alpha_{O2/N2}$	$\alpha_{He/N2}$
3	63±7	13.7±1.3	4.6±0.1	39±1

Test conditions: feed pressure: ~100 psia, temperature: 35°C.

From Table 4.11, the uncrosslinked hollow fibers are defect-free since the O_2/N_2 selectivity is over 90% of the intrinsic selectivity (dense film $\alpha_{O2/N2}$=4.8). There is no substructure resistance since the $\alpha_{He/N2}$ is intrinsic (dense film $\alpha_{He/N2}$=40). An O_2 permeance up to 63 GPU was achieved. Based on the O_2 permeance and permeability, the defect-free skin layer thickness is ~0.1 μm. The desired skin layer thickness (0.1 μm) without defects is achieved in the 4th spinning on a higher molecular weight PDMC polymer, suggesting that a higher molecular weight is preferable to achieve the desirable thin skins without introducing defects.

To further probe the separation performance of defect-free hollow fibers with the desirably thin skins, the *uncrosslinked* hollow fibers were tested with a mixed CO_2/CH_4 gas to study the natural gas separation performance. The mixed gas permeation results are shown in Table 4.12.

Table 4.12: Mixed gas separation properties of *uncrosslinked* hollow fibers.

	CO_2 Perm. (GPU)	$\alpha_{CO2/CH4}$
This study	237±23	27.7±2.7
Reference[6]	203±3	30±0.5

Test conditions: 20/80 CO_2/CH_4, 200 psia, 35°C.

From Table 4.12, the CO_2 permeance of *uncrosslinked* hollow fibers is improved ~20% vs. the reference [6]. The high molecular weight polymer in this spinning produced a CO_2 permeance up to 237 GPU with a CO_2/CH_4 selectivity close to the reference [6]. Despite the high separation performance, the uncrosslinked PDMC hollow fibers tend to plasticize by high partial CO_2 feeding pressures. Therefore, the hollow fibers are subsequently crosslinked in order to suppress the CO_2 plasticization for natural gas purification under realistic operation environments. Chapter 5 will discuss the results on the development of crosslinked hollow fibers with significantly improved natural gas separation performance.

4.6 Summary and conclusions

Defect-free selective *uncrosslinked* hollow fibers with ideally thin skins were successfully developed through the dry jet/wet quench spinning process by simultaneously optimization of dope composition and spinning process variables.

Phase separation of the polymer solution was explored to reformulate the dope composition to reduce skin layer thickness and improve the gas separation productivity. Defect-

free hollow fibers with a skin layer thickness lower than 0.2 μm were developed by using reformulated dope composition and optimum spinning conditions on a lower molecular weight batch polymer. The resultant hollow fibers exhibit ideally circular and concentric morphology.

Another relatively higher molecular weight version was implemented to develop defect-free hollow fibers with a desired skin layer thickness of 0.1 μm and significantly improved gas separation productivity. The *uncrosslinked* hollow fibers with significantly reduced skin layer thickness were further crosslinked to stabilize hollow fibers against CO_2 induced plasticization, which will be discussed in Chapter 5.

4.7 References

[1] I.C. Omole, Crosslinked Polyimide Hollow Fiber Membranes for Aggressive Natural Gas Feed Streams, Ph.D. Dissertation, in: Chemical and Biomolecular Engineering, Georgia Institute of Technology, Atlanta, GA, 2008.

[2] D.W. Wallace, Crosslinked Hollow Fiber Membranes for Natural Gas Purification and Their Manufacture from Novel Polymers, Ph.D. Dissertation, in: Chemical Engineering, The University of Texas at Austin, Austin, TX, 2004.

[3] D.T. Clausi, W.J. Koros, Formation of defect-free polyimide hollow fiber membranes for gas separations, J Membrane Sci, 167 (2000) 79-89.

[4] D.T. Clausi, Formation and characterization of asymmetric polyimide hollow fiber membranes for gas separations, Ph.D. Dissertation, in, The University of Texas at Austin,, Austin, TX, 1998.

[5] S.B. Carruthers, Integral-skin formation in hollow fiber membranes for gas separations, Ph.D. Dissertation, in: Chemical Engineering, The University of Texas at Austin, Austin, TX, 2001.

[6] I.C. Omole, R.T. Adams, S.J. Miller, W.J. Koros, Effects of CO2 on a High Performance Hollow-Fiber Membrane for Natural Gas Purification, Ind Eng Chem Res, 49 (2010) 4887-4896.

[7] I.C. Omole, S.J. Miller, W.J. Koros, Increased molecular weight of a cross-linkable polyimide for spinning plasticization resistant hollow fiber membranes, Macromolecules, 41 (2008) 6367-6375.

[8] D.W. Wallace, C. Staudt-Bickel, W.J. Koros, Efficient development of effective hollow fiber membranes for gas separations from novel polymers, J Membrane Sci, 278 (2006) 92-104.

[9] D.W. Wallace, J. Williams, C. Staudt-Bickel, W.J. Koros, Characterization of crosslinked hollow fiber membranes, Polymer, 47 (2006) 1207-1216.

[10] J. Liu, DEVELOPMENT OF NEXT GENERATION MIXED MATRIX HOLLOW FIBER MEMBRANES FOR BUTANE ISOMER SEPARATION, PhD Dissertation, in: School of Chemical & Biomolecular Engineering, Georgia Institute of Technology, Atlanta, GA, 2010.

[11] C. Ma, OPTIMIZATION OF ASYMMETRIC HOLLOW FIBER MEMBRANES FOR NATURAL GAS SEPARATION, MS THESIS, in: School of Chemical and Biomolecular Engineering, Georgia Institute of Technology, Atlanta, GA, 2011.

[12] H.C. Park, Y.S. Moon, H.W. Rhee, J. Won, Y.S. Kang, U.Y. Kim, Effect of solvent exchange on the morphology of asymmetric membranes, Acs Sym Ser, 744 (2000) 110-124.

[13] S.C. Pesek, W.J. Koros, Aqueous Quenched Asymmetric Polysulfone Membranes Prepared by Dry Wet Phase-Separation, J Membrane Sci, 81 (1993) 71-83.

[14] S.B. Carruthers, G.L. Ramos, W.J. Koros, Morphology of integral-skin layers in hollow-fiber gas-separation membranes, J Appl Polym Sci, 90 (2003) 399-411.

[15] D.T. Clausi, S.A. McKelvey, W.J. Koros, Characterization of substructure resistance in asymmetric gas separation membranes, J Membrane Sci, 160 (1999) 51-64.

[16] R.M. Boom, T. Vandenboomgaard, J.W.A. Vandenberg, C.A. Smolders, Linearized Cloudpoint Curve Correlation for Ternary-Systems Consisting of One Polymer, One Solvent and One Nonsolvent, Polymer, 34 (1993) 2348-2356.

CHAPTER 5

DEVELOPMENT AND CHARACTERIZATION OF THIN-SKINNED HIGH-PERFORMANCE CROSSLINKED HOLLOW FIBER MEMBRANES

5.1 Introduction

In Chapter 4, defect-free *uncrosslinked* PDMC hollow fibers with ideally thin skins were developed through simultaneous optimization of the spinning dope and spinning process variables. PDMC hollow fibers can be further crosslinked to suppress plasticization induced by high CO_2 partial pressure and achieve high separation efficacy under aggressive feed conditions. This chapter will focus on the development of ester-crosslinked hollow fibers with significantly reduced skin layer thickness and improved separation productivity. The ester-crosslinked hollow fibers will be characterized under aggressive feed conditions, including high CO_2 partial pressures, high operating temperatures and extended natural gas exposure. Physical aging and active CO_2 feed will be also discussed.

5.2 Defect-free hollow fiber spinning

Previous researches showed that the PDMC polymer can be spun into defect-free hollow fibers with a solution containing 35% polymer, 8.5% ethanol, 35% NMP, 6.5% $LiNO_3$, and 15% THF, which is *far away* from the binodal determined in Section 4.1 [1]. The resultant crosslinked hollow fibers show a CO_2 permeance only ~50 GPU in testing with 200 psi of 50/50 CO_2/CH_4 mixed gas feed at 35^oC [2]. Increasing the separation productivity under realistic operation conditions to reach a CO_2 permeance above 100 GPU is desirable if selectivity can be maintained. Therefore, a reformulation of dope composition was performed to further improve the productivity. Chapter 4 show that a reformulated dope with 29% polymer, 29% NMP, 23.1%

Ethanol, 12.4% THF and 6.5% $LiNO_3$ used in the 4th spin produces high productivity *uncrosslinked* hollow fibers with a defect-free skin layer thickness of ~0.1 μm; however, by using the crosslinking method described in reference [1, 3], the *ester-crosslinked* hollow fibers show a CO_2 permeance of ~65 GPU with a CO_2/CH_4 selectivity of 32.4 in testing at 200 psi with 50/50 CO_2/CH_4 feed, 35°C [3]. The CO_2/CH_4 selectivity is lower than the literature data [1, 2, 4], suggesting that further dope optimization should be performed to produce *ester-crosslinked* hollow fibers with significantly improved permeance without loss of selectivity.

In this chapter, a 5th spin was done by increasing the polymer concentration from 29% to 32% and moving the dope composition slightly further from the binodal vs. the 4th spin. The THF% was increased from 12.4% to 13.7% to promote the formation of defect-free skins and thereby improve the CO_2/CH_4 selectivity. The reformulated dope consisted of 32% polymer, 32% NMP, 15.8% Ethanol, 13.7% THF and 6.5% $LiNO_3$. The spinning conditions for the 5th spin are summarized in Table 5.1.

Table 5.1: Hollow fiber spinning conditions.

Spinning conditions	
Dope extrusion rate	180 ml/hr
Bore fluid composition	NMP/H_2O 80/20wt%
Bore fluid rate	60 ml/hr
Spinning temperature	70^oC
Air gap	1~33 cm
Quench bath	Tap water, ~50^oC
Take-up rate	50 m/min

The spinning conditions shown in Table 5.1 are primarily based on what reported in Chapter 4, and this chapter reports *crosslinked* properties for those optimized fibers. The main spinning parameter studied during the spinning was the air gap, which was identified as *a key factor in determining the skin layer formation and intrinsic separation properties of hollow fibers* [5, 6]. The hollow fibers created from the prior spinning were crosslinked by annealing the "as-spun" fibers at 200^oC for 2 hrs under vacuum [3]. The cross-section structures of *uncrosslinked* and *crosslinked* hollow fibers are shown in Figure 5.1~5.2.

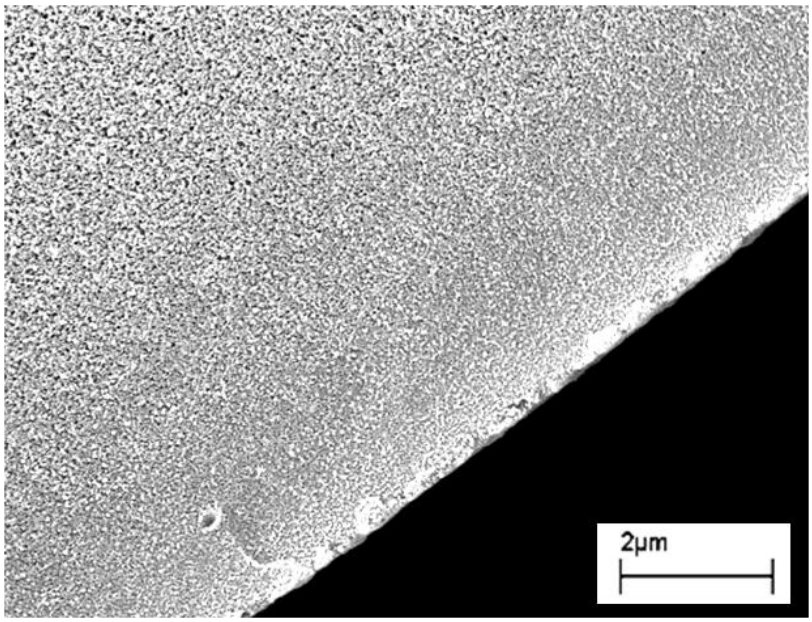

Figure 5.1**:** Scanning electron micrograph (SEM) of the cross-section of an *uncrosslinked* hollow fiber, showing the dense skin layer and the porous substructure of the hollow fiber.

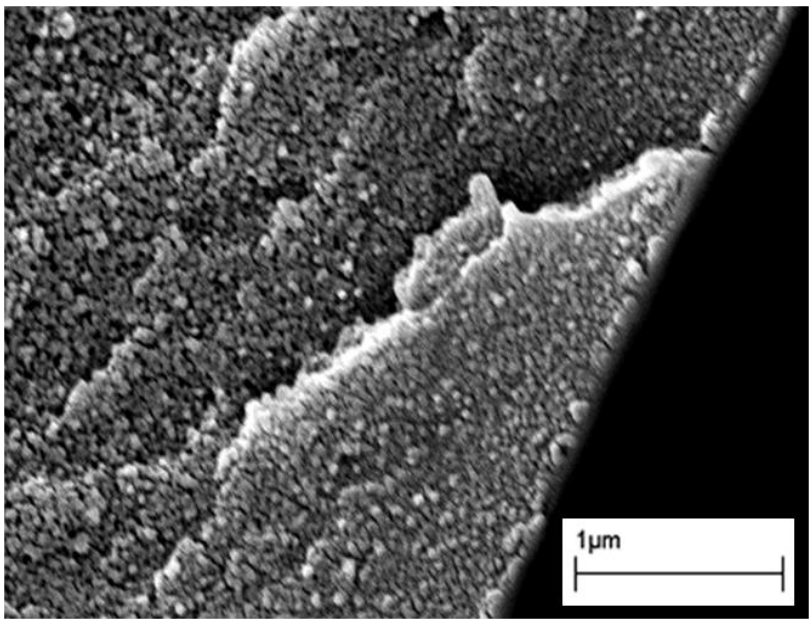

Figure 5.2**:** Scanning electron micrograph (SEM) of the cross-section of a *crosslinked* hollow fiber, showing the dense skin layer and the porous substructure of the hollow fiber.

Figure 5.1~5.2 show that the skin layer and porous substructure are quite apparent in the SEM images for both uncrosslinked and crosslinked hollow fibers. The integrated dense skin layer and transition layer of *crosslinked* hollow fibers suggest that the crosslinking does not cause a collapse of the fiber wall. The open porous substructure is also preserved, which will allow a high permeate flux for natural gas separations.

As mentioned above, the key spinning parameter, air gap, was varied in the spinning to produce the most productive hollow fibers. The effect of air gap on the separation performance of ester-crosslinked hollow fibers was studied by spinning hollow fibers at different air gaps, which were translated into different residence time of fibers in the air gap. The permeation results on the resultant ester-crosslinked hollow fibers are shown in Figure 5.3~5.4.

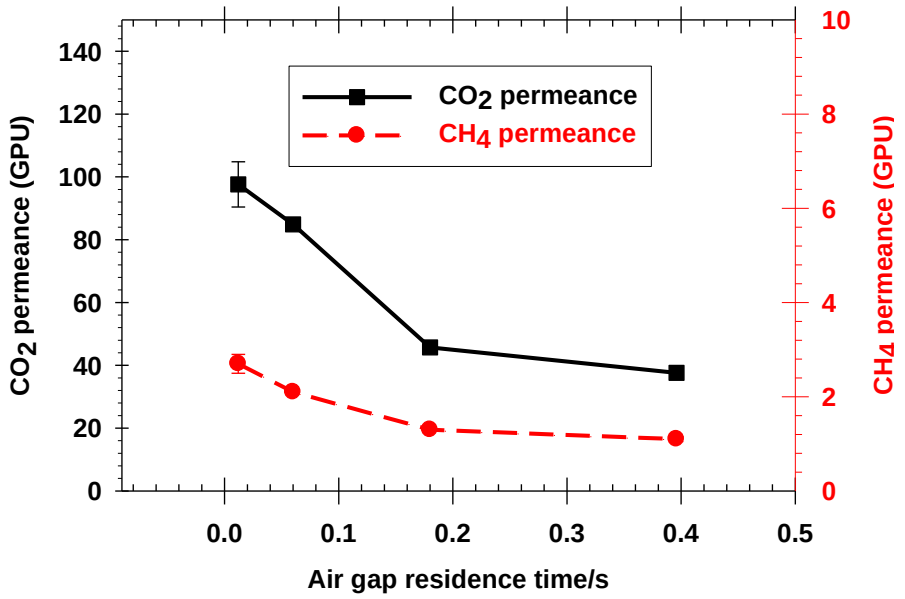

Figure 5.3: CO_2 and CH_4 permeance at different air gap residence time for 200^{o}C, 2 hrs crosslinked hollow fibers. Approximate air gap residence time was determined by the ratio of air gap to take-up rate. Test conditions: 50/50 CO_2/CH_4 at 200 psia, 35^{o}C.

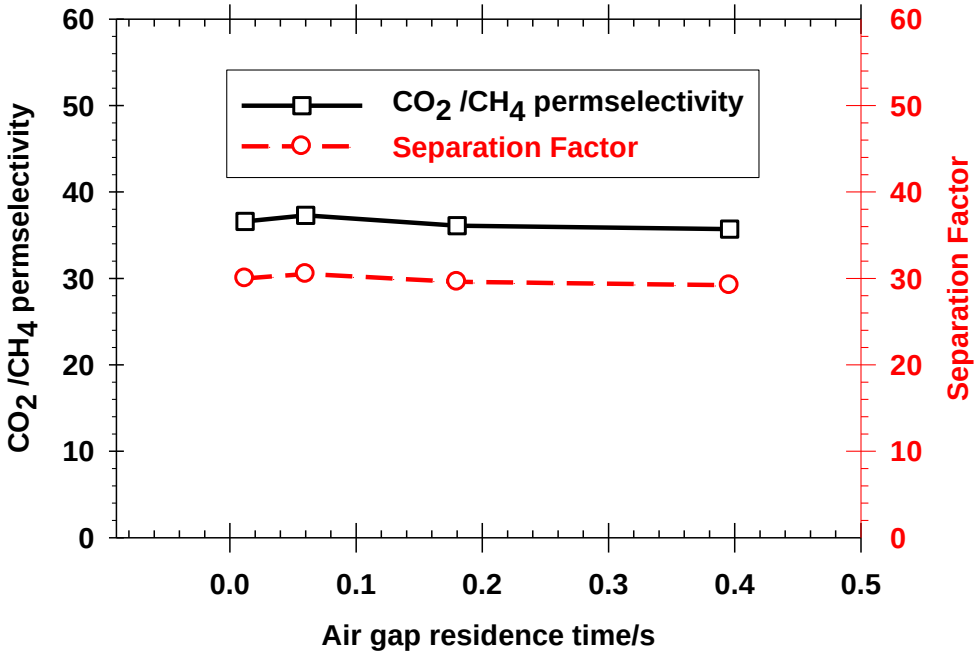

Figure 5.4: CO_2/CH_4 separation efficacy at different air gap residence time for 200°C, 2 hrs crosslinked hollow fibers. Approximate air gap residence time was determined by the ratio of air gap to take-up rate. Test conditions: 50/50 CO_2/CH_4 at 200 psia, 35°C.

Figure 5.3 shows that the air gap residence time affects the crosslinked fiber separation productivity significantly. The CO_2 and CH_4 permeance decreases when increasing the air gap/residence time. A higher CO_2 permeance indicates a thinner skin layer for the hollow fiber, which is formed due to less evaporation of volatile solvent and non-solvent at a lower air gap. A similar phenomenon was also found in Matrimid® hollow fibers described in the reference [5]. Fortunately, on the other hand, the curves in Figure 5.4 show that a lower air gap does not cause an apparent loss of CO_2/CH_4 selectivity or separation factor. The difference between selectivity and separation factor was discussed in Chapter 2. In fact, the crosslinked hollow fibers display attractively high separation efficacy over a long range of air gaps. This suggests that hollow fibers can be developed with a thinner-skinned layer at an air gap lower than 1 cm to achieve desirable high separation productivity *without loss of selectivity*, as shown in Table 4.10.

5.3 Dope optimization to improve separation productivity

In the 5th spinning work described in Section 5.2, ester-crosslinked hollow fibers with a CO_2 permeance up to 100 GPU was achieved by using a polymer solution containing 32% polymer. To further improve the separation productivity of hollow fibers, a solution with a slightly lower polymer and THF concentration was used for the 6th spinning to locate the optimal spinning dope composition. The resultant dope consisted of 30.5% polymer, 30.5% NMP, 19.5% Ethanol, 13.0% THF and 6.5% $LiNO_3$.The spinning conditions for this spin are summarized in Table 5.2.

Table 5.2: Hollow fiber spinning conditions.

Spinning conditions	
Dope extrusion rate	120~180 ml/hr
Bore fluid composition	NMP/H_2O 80/20wt%
Bore fluid rate	40~60 ml/hr
Spinning temperature	50~70^oC
Air gap	1~33 cm
Quench bath	Tap water, ~50^oC
Take-up rate	50~75 m/min

In the 6th spinning, spinning variables, including the dope flow rate, spinneret temperature, air gap and take-up rate, were adjusted to probe the optimum spinning conditions. A

take-up rate higher than 75 m/min represents a superior high hollow fiber fabrication rate, which is even higher than some industrial rate of 50 m/min [1]. The resultant *crosslinked* hollow fibers with the highest separation productivity were characterized by using 50/50 CO_2/CH_4 mixed gas at a feed pressure of 200 psia. Table 5.3 shows the mixed permeation results of 200^oC, 2 hrs crosslinked hollow fibers from the 5th, 6th spin and were compared with literature data [2].

Table 5.3: Mixed gas separation properties of *crosslinked* hollow fibers.

	CO_2 Permeance (GPU)	$\alpha_{CO2/CH4}$
5th spin	98±7	36.6±0.6
6th spin	117±6	36.5±0.8
Reference [2]	~50	~42

Crosslinking conditions: 200^oC, 2 hrs; test conditions: 50/50 CO_2/CH_4, 200 psi, 35^oC

Table 5.3 shows that a high take-up rate of 50~75 m/min in the spinning can produce ester-crosslinked hollow fibers with a CO_2 permeance up to 117 GPU and a CO_2/CH_4 selectivity of 36.5. Compared to the 5th spin, the 6th spin improved CO_2 permeance of hollow fibers by ~20%, due to a thinner skin formed by lowering THF% in the spinning dope. Compared to the literature data [2], the separation productivity (CO_2 permeance) of crosslinked hollow fibers *was enhanced over 130%*, although the CO_2/CH_4 selectivity was a slightly lower than the literature data, which is possibly due to different intrinsic separation properties of polymers used. This difference is presumably due to the different imidization and monoesterification processes, since chemical imidization and two-step monoesterification was used in this work vs. thermal imidization and one-pot monoesterification in literature [1, 2]. The side-reactions in chemical

imidization and depolymerization in thermal imidization may produce significantly different chemical structures of polymer backbones and essentially affect the separation properties of polymers [7-9].

5.4 Effect of high CO_2 partial pressures

The crosslinked hollow fibers with the highest separation productivity were further characterized by using a 50/50 CO_2/CH_4 mixed gas at a feed pressure up to 800 psi to probe the CO_2 plasticization resistance. Figure 5.5~5.6 show the mixed permeation results of 200°C, 2 hrs crosslinked hollow fibers from the 5th spin, 6th spin and literature [2].

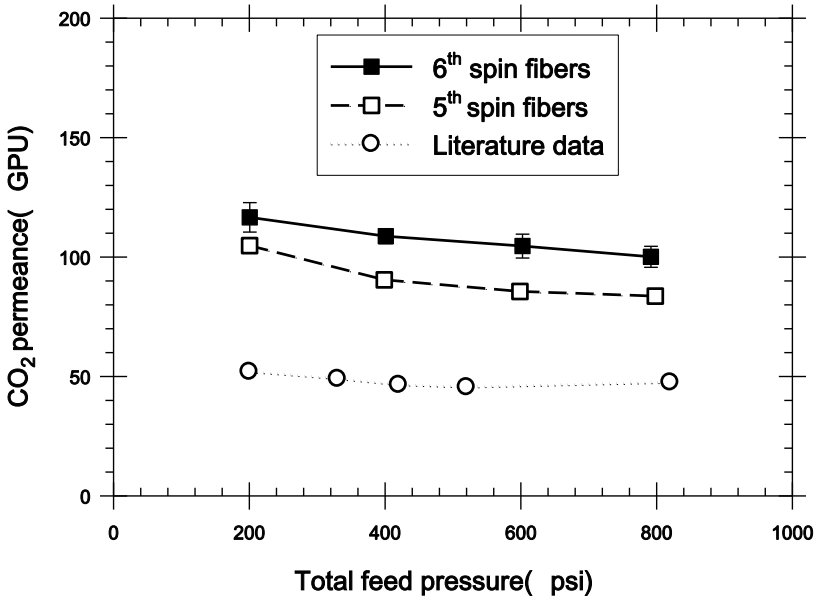

Figure 5.5: CO_2 permeance of *crosslinked* hollow fiber membranes at elevated feed pressures from this work and literature. Permeance calculated by using fugacity. Test conditions: 50/50 CO_2/CH_4, at 35°C. 6th spin fiber permeance uncertainty: ±5%.

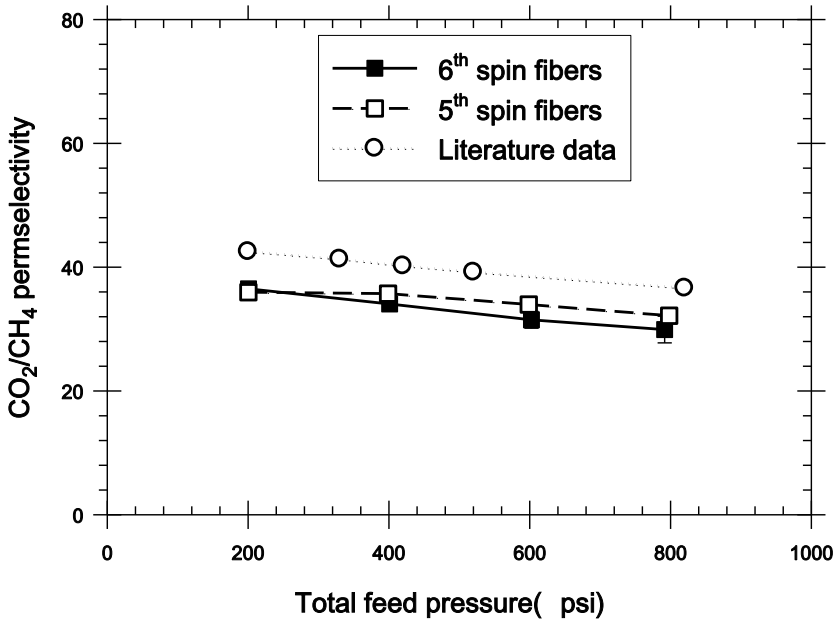

Figure 5.6**:** CO_2/CH_4 selectivity of *crosslinked* hollow fiber membranes at elevated feed pressures from this work and literature. Selectivity calculated by using fugacity. Test conditions: 50/50 CO_2/CH_4, at 35°C. 6^{th} spin fiber selectivity uncertainty: ±7%.

As indicated by Figure 5.5, the crosslinked fibers from the 6^{th} spin demonstrate a CO_2 permeance over 100 GPU at all testing pressures from 200 to 800 psi. The significant improvement of separation productivity is primarily due to *a much thinner skin layer* formed when a reformulated dope composition and optimized spinning conditions were used in this work. It is also found that compared to the slight increase of CO_2 permeance at a pressure above 500 psi in the literature. There is no upswing at the maximum test pressure of 800 psi for the crosslinked hollow fibers in this work, suggesting an improved CO_2 plasticization resistance was also achieved in this study. Moreover, the CO_2/CH_4 selectivity was attractively high over the long range of feed pressures with a CO_2/CH_4 of 36.5 at 200 psi of 50/50 CO_2/CH_4, 35^oC. Those impressive high-pressure permeation data reflect that the dope reformulation and spinning

conditions optimization can effectively improve natural gas separation performance of crosslinked hollow fibers under high feed pressures.

5.5 Effect of operating temperatures

The crosslinked hollow fibers from 6th spin were further characterized by using different operating temperatures from room temperature (22°C) to elevated temperature of 50°C to probe their performance under more aggressive conditions. The CO_2 permeance and CO_2/CH_4 selectivity are summarized in Figure 5.7~5.8.

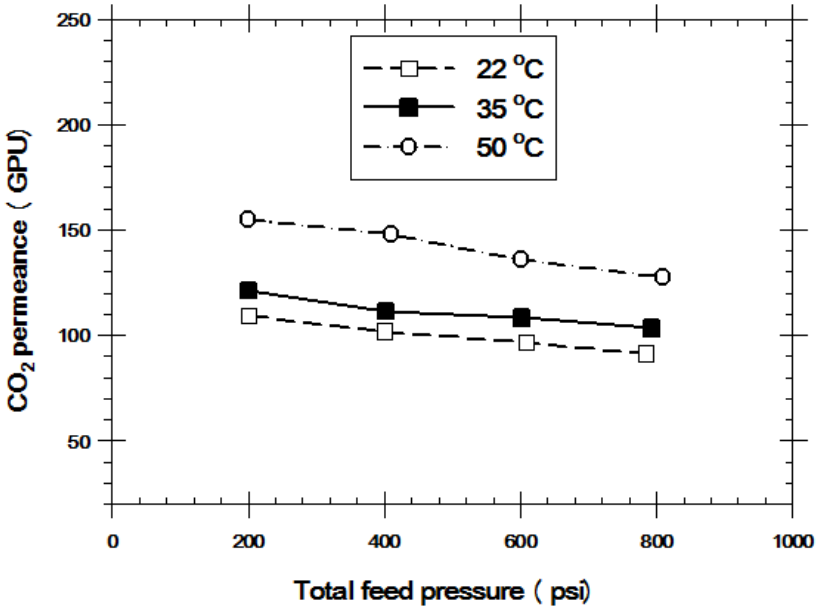

Figure 5.7: CO_2 permeance of crosslinked hollow fibers from the 6th spin at different operating temperatures. Permeances calculated by using fugacity at corresponding temperatures and pressures. Test conditions: 50/50 CO_2/CH_4, 22~50^{o}C.

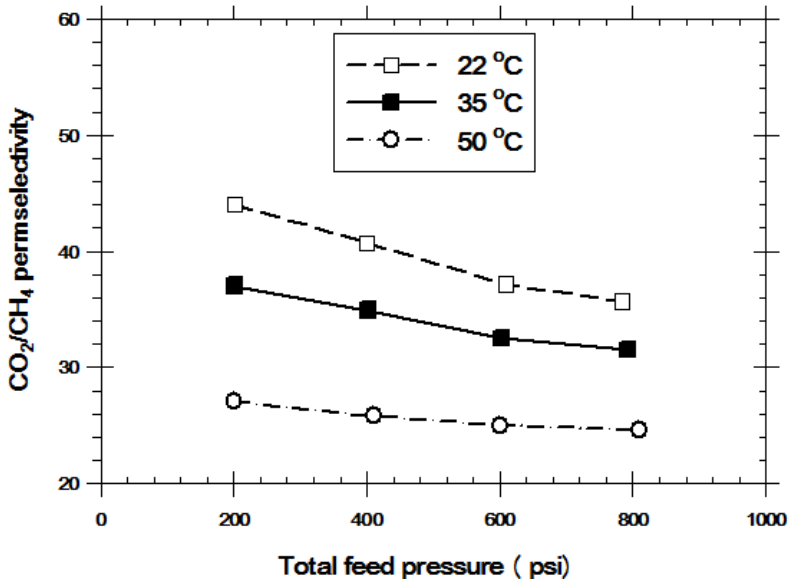

Figure 5.8: CO_2/CH_4 selectivity of crosslinked hollow fibers from the 6th spin at different operating temperatures. Selectivities calculated by using fugacity at corresponding temperatures and pressures. Test conditions: 50/50 CO_2/CH_4, 22~50^{o}C.

Figure 5.7~5.8 show that a higher operating temperature can increase the CO_2 permeance while decrease the CO_2/CH_4 selectivity. A lower operating temperature at 22^{o}C produces a CO_2 permeance of 110 GPU and a CO_2/CH_4 selectivity up to 44 at 200 psi. Moreover, this low testing temperature does not cause any CO_2 plasticization at the maximum feed pressure of 800 psi. At elevated temperatures, the increased polymer chain mobility increases diffusion coefficients for both CO_2 and CH_4. However, the larger CH_4 molecule is affected to a larger extent over CO_2; as a result, the higher temperature decreases the diffusion advantage of CO_2 over CH_4. Furthermore, the sorption advantage of CO_2 over CH_4 is also reduced when increasing the temperature. Those factors can cause a loss of CO_2/CH_4 selectivity at higher temperatures. Therefore, a lower temperature is preferable for the CO_2/CH_4 separation.

The temperature dependence of permeance can be explained by Equation (5.1) below [10]:

$$\frac{P}{l} = \frac{P_0}{l} \exp\left[\frac{-E_p}{RT}\right] \qquad (5.1)$$

In this equation, P/l represents the CO_2 permeance; E_p is the activation energy; P_0/l is pre-exponential factor. By plotting log (P) vs. 1/T as show in Figure 5.9, the activation energy and P_0 can be calculated.

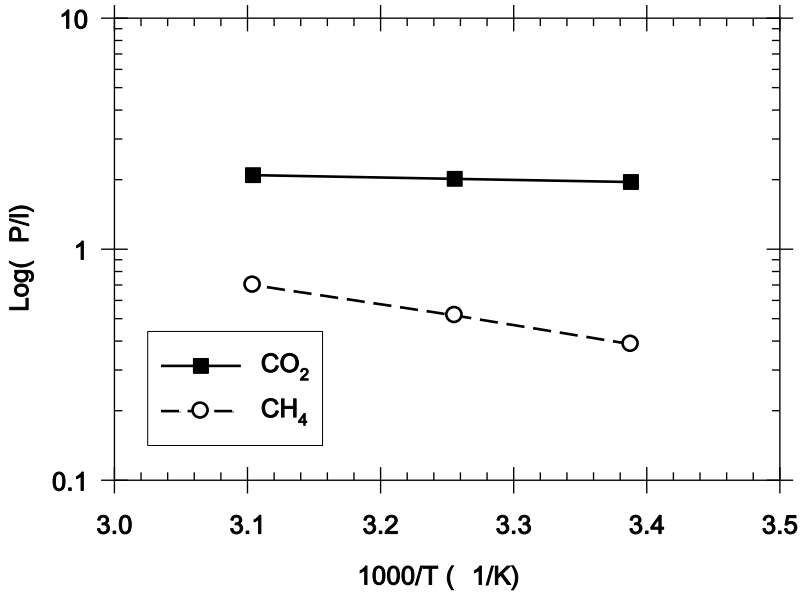

Figure 5.9: Temperature dependence of CO_2 and CH_4 permeance. Permeances calculated by using fugacity. Test conditions: 50/50 CO_2/CH_4 at 800 psi, 22~50°C.

Figure 5.9 shows that there exists a good linearity between log (P/l) and 1/T as the R^2 approaches to 1 for both CO_2 and CH_4 permeance ($R^2 = 0.9998$ for CO_2; $R^2 = 0.9963$ for CH_4), indicating that the experimental permeation data agrees well the model described by Equation 9.

5.6 Stability of fibers under high feed pressures

As discussed above, the ester-crosslinked hollow fibers showed significantly improved separation productivity with good selectivity under a total feed pressure up to 800 psi of 50/50 CO_2/CH_4. Despite this high performance, it is desirable to expose those crosslinked hollow fibers under a high feed pressure for a long period to simulate more realistic operation conditions. This is because the stability over time is critical for the application of hollow fibers in the field. Therefore, the crosslinked fibers were examined by using a 50/50 CO_2/CH_4 feed with a pressure of 600 psi at 35^{o}C and the separation performance was continuously tested during the ~120 hrs' exposure. The permeation results are shown in Figure 5.10~5.11.

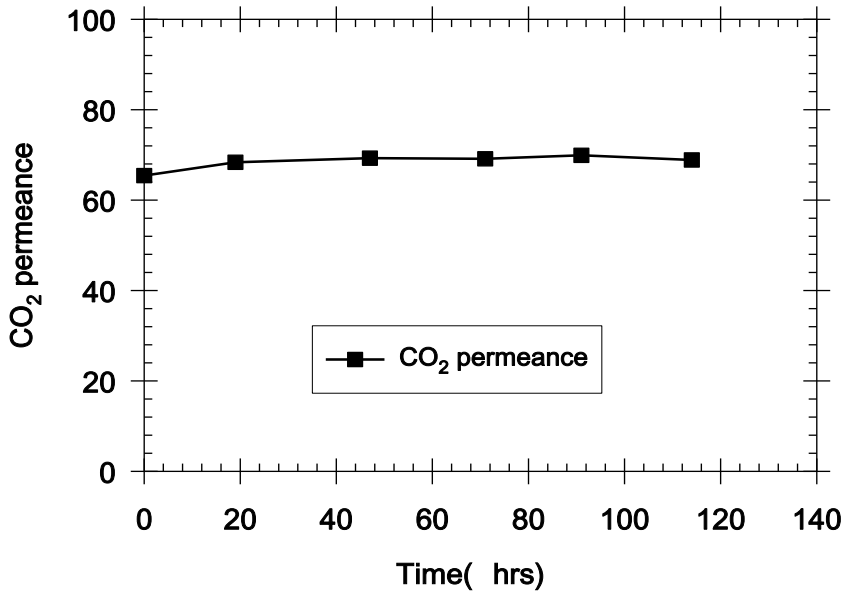

Figure 5.10: CO_2 permeance of *crosslinked* hollow fiber membranes over extended time exposure in a feed pressure of 600 psi. Permeance calculated by using fugacity. Test conditions: 50/50 CO_2/CH_4, at 35°C.

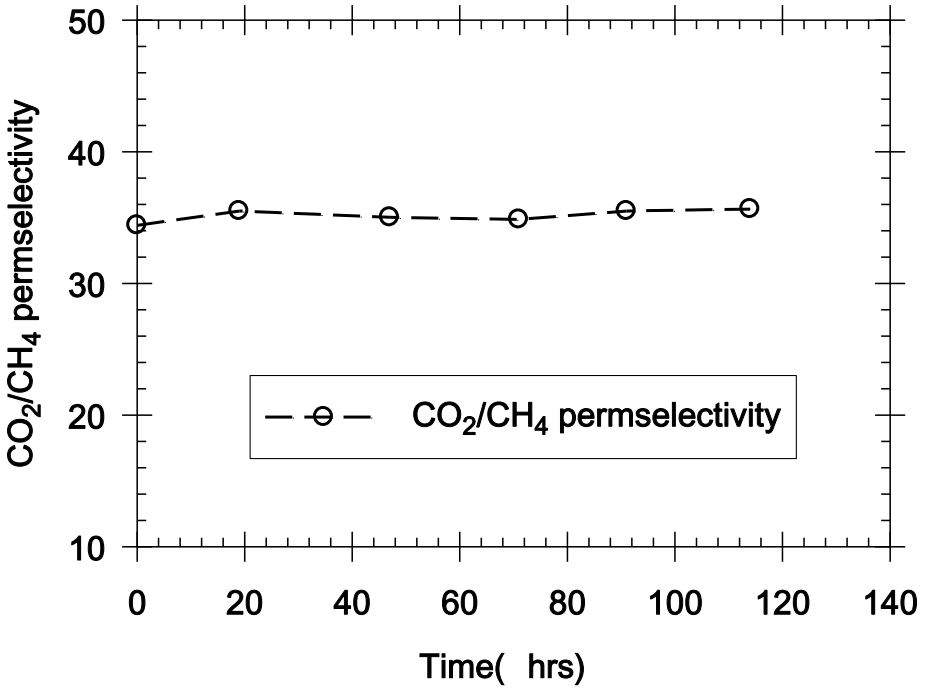

Figure 5.11: CO_2/CH_4 selectivity of *crosslinked* hollow fiber membranes over extended time exposure in a feed pressure of 600 psi. Permeance calculated by using fugacity. Test conditions: 50/50 CO_2/CH_4, at 35°C.

In Figure 5.10, the ester-crosslinked hollow fibers showed a slight increase of CO_2 permeance up to 7% over the 120 hrs exposure under 600 psi of 50/50 CO_2/CH_4 feed. On the other hand, only a small variance of CO_2/CH_4 selectivity up to 4% was found during this extended time exposure. The stable permeance and selectivity over time clearly suggests that the ester-crosslinked hollow fibers are viable for extended time natural gas separation in the realistic operation environment.

5.7 Skin layer thickness dependent physical aging

Notwithstanding the high separation performance under aggressive feed conditions, physical aging can cause a drastic loss of permeability or permeance of membranes [1, 11]. Although crosslinking accelerates the physical aging process, the crosslinked hollow fibers may still undergo aging. To study the aging effect on hollow fibers, crosslinked fibers with different skin layer thickness (or different initial CO_2 permeance) from the 5^{th} spin were considered. The samples were systematically tested for a long period of ~230 days to monitor the changes of CO_2 permeance and selectivity during physical aging. Those hollow fiber module samples were stored in dry air. The CO_2 permeance and CO_2/CH_4 selectivity of crosslinked fibers at different aging time are shown in Figure 5.12~5.13.

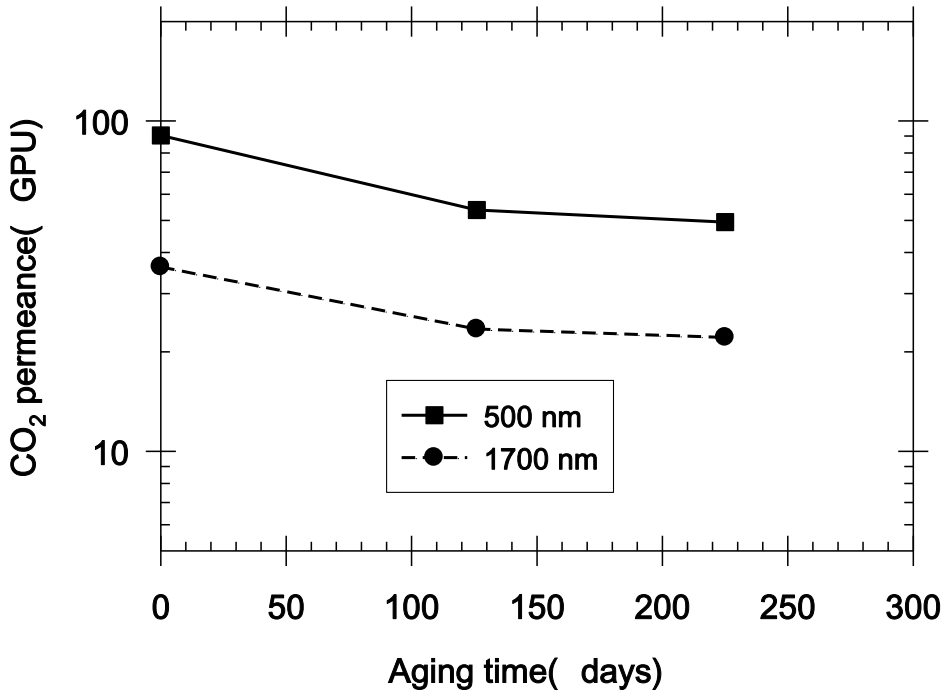

Figure 5.12: CO_2 permeance of crosslinked hollow fibers with different skin layer thickness at different aging time. Test conditions: 50/50 CO_2/CH_4, 35°C.

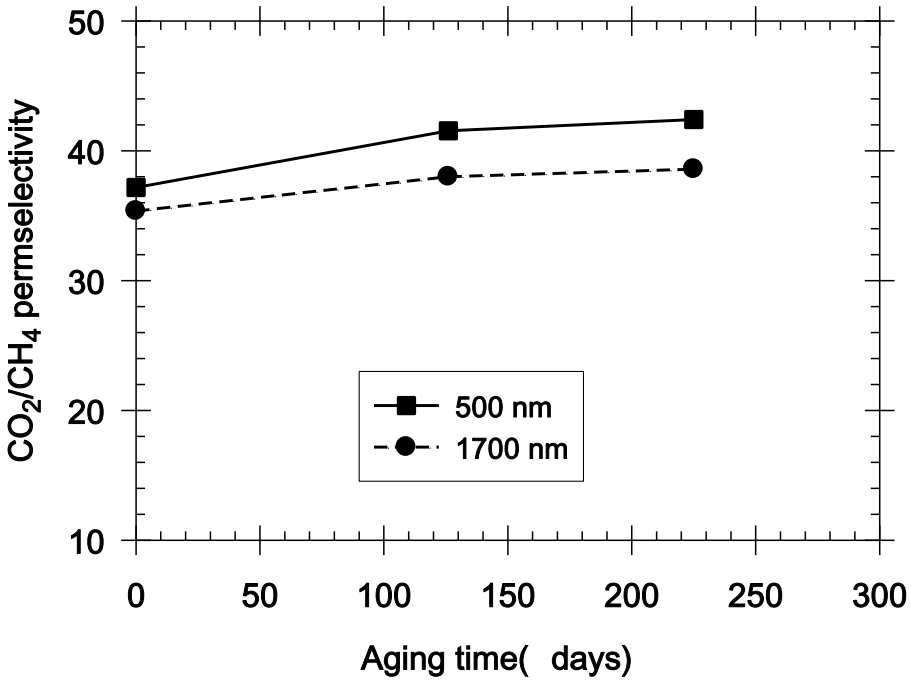

Figure 5.13: CO_2/CH_4 selectivity of crosslinked hollow fibers with different skin layer thickness at different aging time. Test conditions: 50/50 CO_2/CH_4, 35°C.

Figure 5.12 shows that the CO_2 permeance of crosslinked hollow fibers with a thinner skin dropped ~45% while the ones with a thicker skin dropped ~39% during the 230 days' aging. On the other hand, the CO_2/CH_4 selectivity of thinner skin fibers was increased by ~14% vs. 9% for the thicker ones. The trends shown in the Figure 5.12~13 clearly suggest that the aging rate of hollow fiber membranes is dependent of the skin layer thickness of hollow fibers.

Physical aging can cause the decrease of permeance but increase of selectivity, which is presumably due to the polymer contraction and the removal of unrelaxed freed volume, as shown in Figure 5.14 [11].

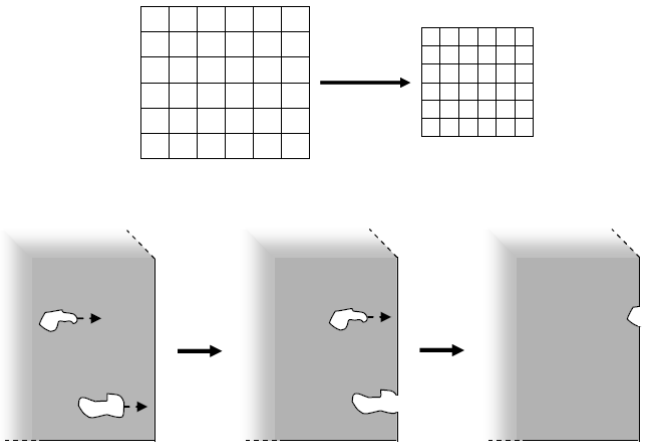

Figure 5.14: Physical aging mechanism in polymeric membranes: lattice contraction and diffusion of free volume.

Physical aging is hypothesized to be a complex combination of the two physical aging processes, lattice contraction and diffusion of free volume [11]. The lattice contraction process is identical throughout the whole sample and does not depend on the size of samples [12]. On the other hand, assuming the diffusion process of free volume follows Fick's second law of diffusion, the free volume flux will be inversely proportional to the square of the skin layer thickness [13]. This can explain why the thinner skin hollow fiber samples tend to age faster than the thicker samples.

A similar phenomenon was also found for dense films with different membrane thickness (720 nm or 49 μm) from Kratochvil's work, as shown in Figure 5.15 [11].

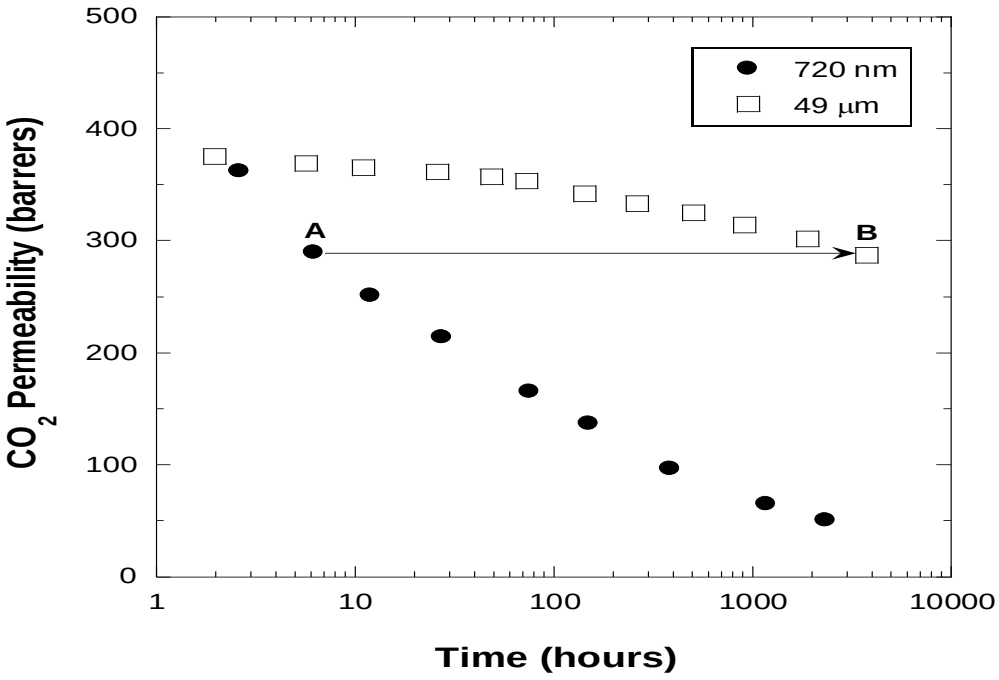

Figure 5.15: CO_2 permeability of 6FDA-DAM:DABA (2:1) dense films at different aging time from Kratochvil's work [11].

Figure 5.15 shows that the CO_2 permeability of 0.72 μm films drops much faster than 49 μm films during the period of ~120 days' aging, suggesting that the aging rate of thin films is much higher than that of thicker films. This agrees with what was found in crosslinked hollow fibers with different skin layer thickness, where the fibers with a thinner skin ages faster than that with a thicker skin.

5.8 Effect of active CO_2 feed

As discussed in Section 5.7, there exists physical aging on crosslinked hollow fibers and the rate of physical aging depends on skin layer thickness of fibers. Since physical aging reduces the separation productivity, it is desirable to study the feasibility of alleviating the physical aging to achieve high separation performance for a long period. In this work, the effect of active CO_2

feed on crosslinked hollow fibers was studied. Two hollow fiber modules from the same spinning state were selected to eliminate the inference of skin layer thickness, which affects physical aging rate as shown in Section 5.7. One ester-crosslinked hollow fiber module was fed with a positive ~30 psia of pure CO_2 through the shell side while the other one was stored in a bag with air and desiccants. The CO_2 permeance and CO_2/CH_4 selectivity were monitored by using mixed gas permeation. The permeation results are summarized and shown in Figure 5.16~5.17.

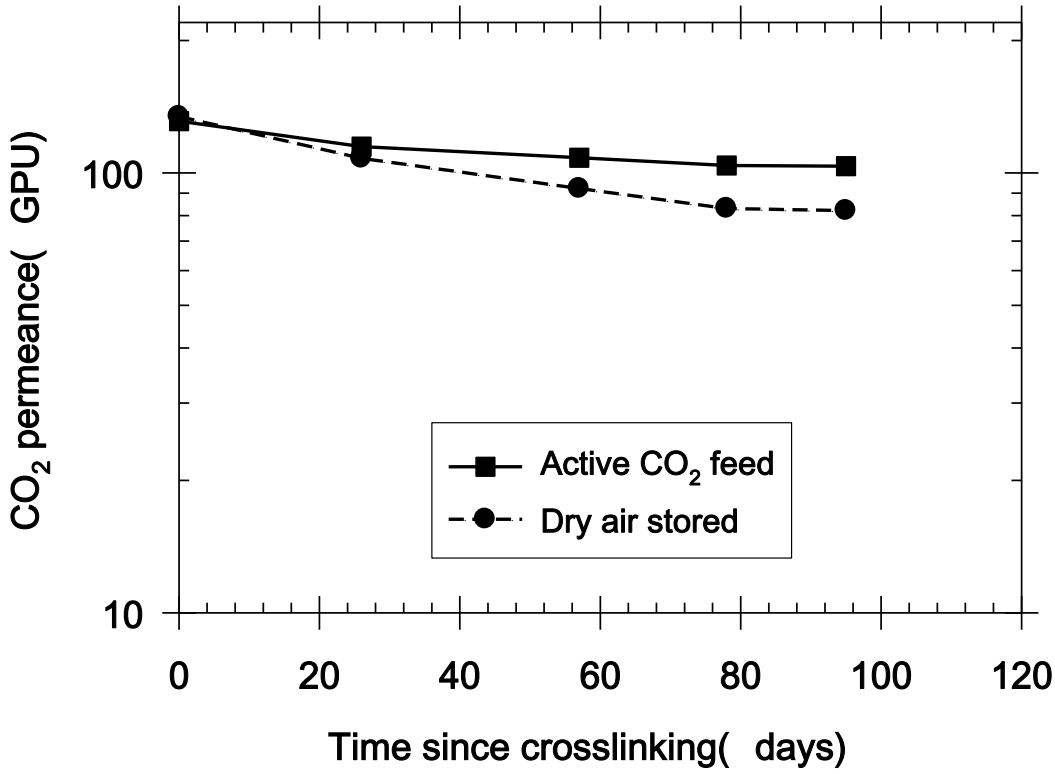

Figure 5.16: CO_2 permeance of crosslinked hollow fibers stored at different environments. Test conditions: 200 psi, 50/50 CO_2/CH_4, 35^oC.

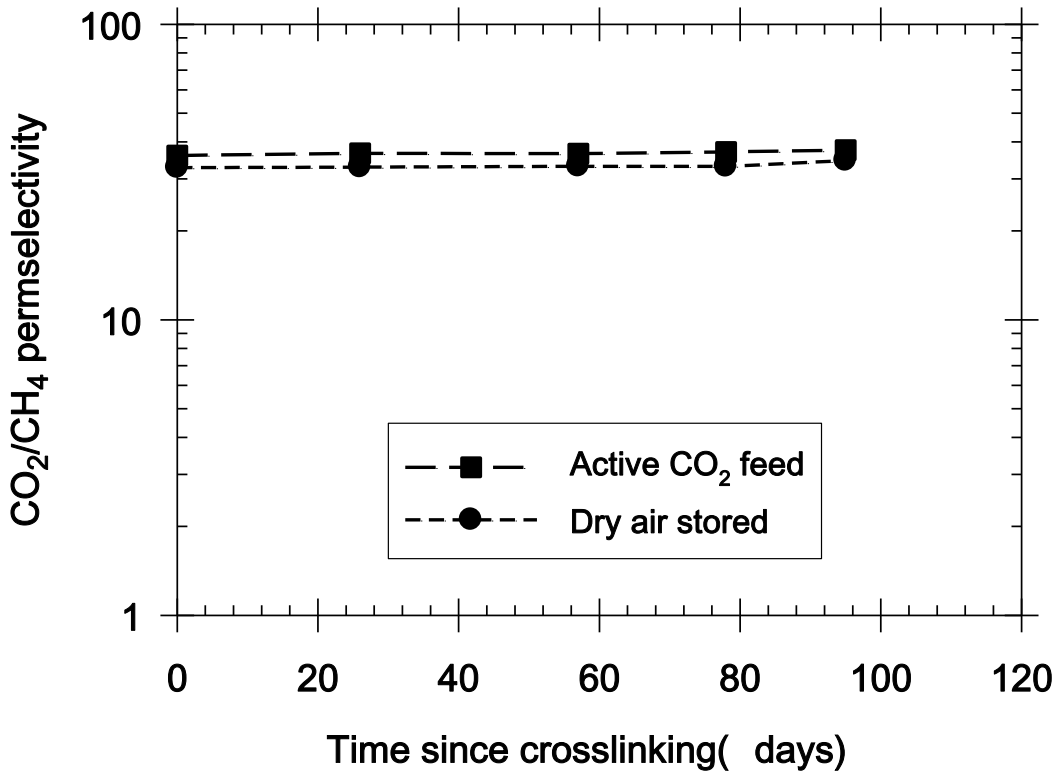

Figure 5.17: CO_2/CH_4 selectivity of crosslinked hollow fibers stored at different environments. Test conditions: 200 psi, 50/50 CO_2/CH_4, 35^{O}C.

Figure 5.16 shows that the active CO_2 feed can slow down the depression of CO_2 permeance of crosslinked hollow fibers experienced physical aging. The positive CO_2 feed fibers show a CO_2 permeance loss of only 21% vs. 39% loss in dry air stored ones during the ~100 days' aging. On the other hand, the CO_2/CH_4 selectivity increases 4% and 6% for active CO_2 feed fibers and dry air stored fibers, respectively. The slow physical aging in active CO_2 feed hollow fibers is possibly due to the unrelaxed volume in the polymer matrix *occupied by CO_2 molecules*, which may restrain the polymer chain relaxation. Therefore, the fibers tend to maintain the original packing status and the relaxation of polymer matrix to a more equilibrium state is retarded. Presumably, the physical aging might be totally quenched if the fibers were

under an active feed under high feed pressure (say 800 psi of 50/50 CO_2/CH_4). Nevertheless, the active CO_2 feed does provide a simple and effective method for preserving the superior high separation productivity for extended time natural gas separations.

5.9 Summary and conclusions

A significantly improved defect-free *ester-crosslinked* hollow fiber membrane was developed through simultaneous optimization of the spinning solution and dry-jet/wet-quench spinning process variables. The ester-crosslinked hollow fibers show extremely high separation productivity and efficacy with improved CO_2 plasticization resistance under aggressive feed conditions.

The *ester-crosslinked* hollow fibers were characterized under aggressive feed conditions, including high CO_2 partial pressures, high operation temperatures and extended time exposure under high pressures. The crosslinked hollow fibers maintain a high CO_2 permeance and CO_2/CH_4 selectivity under a feed pressure up to 800 psi of 50/50 CO_2/CH_4, suggesting that the crosslinked hollow fibers withstand a CO_2 partial pressure up to 400 psi without plasticization. Moreover, the study on operation temperatures shows that a lower operating temperature can improve the CO_2/CH_4 selectivity significantly without apparent loss of CO_2 permeance. An operating temperature at 22^oC produces a CO_2 permeance of 110 GPU and a CO_2/CH_4 selectivity up to 44 at 200 psi of 50/50 CO_2/CH_4. Furthermore, the extended time exposure with high feed pressures show that the crosslinked hollow fibers demonstrate strong stability over time in more realistic operation conditions.

The crosslinked hollow fibers show physical aging after crosslinking and the fibers with a thinner skin ages faster than that with a thicker skin. However, the active CO_2 feed can

effectively slow down physical aging of CO_2 permeance due to the slower polymer chain relaxation. The high permeance and selectivity retained by the active CO_2 feed provides an effective method for preserving high separation performance of crosslinked hollow fibers and make them viable for long-term natural gas separations.

5.10 References

[1] I.C. Omole, Crosslinked Polyimide Hollow Fiber Membranes for Aggressive Natural Gas Feed Streams, Ph.D. Dissertation, in: Chemical and Biomolecular Engineering, Georgia Institute of Technology, Atlanta, GA, 2008.

[2] I.C. Omole, R.T. Adams, S.J. Miller, W.J. Koros, Effects of CO2 on a High Performance Hollow-Fiber Membrane for Natural Gas Purification, Ind Eng Chem Res, 49 (2010) 4887-4896.

[3] C. Ma, OPTIMIZATION OF ASYMMETRIC HOLLOW FIBER MEMBRANES FOR NATURAL GAS SEPARATION, MS THESIS, in: School of Chemical and Biomolecular Engineering, Georgia Institute of Technology, Atlanta, GA, 2011.

[4] I.C. Omole, D.A. Bhandari, S.J. Miller, W.J. Koros, Toluene impurity effects on CO2 separation using a hollow fiber membrane for natural gas, J Membrane Sci, 369 (2011) 490-498.

[5] D.T. Clausi, W.J. Koros, Formation of defect-free polyimide hollow fiber membranes for gas separations, J Membrane Sci, 167 (2000) 79-89.

[6] D.T. Clausi, Formation and characterization of asymmetric polyimide hollow fiber membranes for gas separations, Ph.D. Dissertation, in, The University of Texas at Austin,, Austin, TX, 1998.

[7] M.H. Kailani, C.S. Sung, S.J. Huang, Syntheses and Characterization of Model Imide Compounds and Chemical Imidization Study, Macromolecules, 25 (1992) 3751-3757.

[8] P.R. Dickinson, C.S.P. Sung, Kinetics and Mechanisms of Thermal Imidization Studies by Uv-Visible and Fluorescence Spectroscopic Techniques, Macromolecules, 25 (1992) 3758-3768.

[9] M.H. Kailani, C.S.P. Sung, Chemical imidization study by spectroscopic techniques. 2. Polyamic acids, Macromolecules, 31 (1998) 5779-5784.

[10] T.S. Chung, C. Cao, R. Wang, Pressure and temperature dependence of the gas-transport properties of dense poly[2,6-toluene-2,2-bis(3,4dicarboxylphenyl)hexafluoropropane diimide] membranes, J Polym Sci Pol Phys, 42 (2004) 354-364.

[11] A.M. Kratochvil, THICKNESS DEPENDENT PHYSICAL AGING AND SUPERCRITICAL CARBON DIOXIDE CONDITIONING EFFECTS ON CROSSLINKABLE POLYIMIDE MEMBRANES FOR NATURAL GAS PURIFICATION, PhD Dissertation, in: School of Chemical & Biomolecular Engineering, Georgia Institute of Technology, Atlanta, GA, 2008.

[12] L.C.E. Struik, Physical Aging in Plastics and Other Glassy Materials, Polym Eng Sci, 17 (1977) 165-173.

[13] J.G. Curro, R.R. Lagasse, R. Simha, Diffusion-Model for Volume Recovery in Glasses, Macromolecules, 15 (1982) 1621-1626.

CHAPTER 6

EFFECTS OF CONTAMINANTS ON HIGH PERFORMANCE ESTER-CROSSLINKED HOLLOW FIBERS

6.1 Introduction

Notwithstanding the excellent separation productivity and high CO_2 plasticization resistance demonstrated in Chapter 5, the ester-crosslinked hollow fibers were characterized by using a model natural gas feed consisting of only CO_2 and CH_4. However, some feeds might be more challenging to process. Specifically, some raw natural gas contains undesirable hydrocarbon and even after pre-treatment, those compounds may be detrimental to the membrane performance [1-3]. Hydrocarbon-induced antiplasticization can significantly reduce the permeate flux and cause loss of separation efficacy [3, 4]. Therefore, it is desirable to characterize membranes in the presence of high-level impurities to probe their separation performance under realistic operation conditions.

This chapter will discuss the effects of contaminants on the performance of ester-crosslinked hollow fibers, including aliphatic, aromatic, and water impurities. The effect of high contaminant concentrations, stability of hollow fibers under high level contaminant at high feed pressures, and recovery of performance after contaminant exposure will be studied. The effect of skin layer thickness on the toluene sensitivity was also discussed.

6.2 Effect of toluene impurity

6.2.1 Introduction

The effect of toluene on dense film and asymmetric hollow fiber membrane separation performance has been investigated by previous researches [1, 3-6]. Omole showed that the CO_2 permeance of 200^oC 2 hrs crosslinked *hollow fibers* dropped ~70% when exposing the membrane in a 10/90 CO_2/CH_4 mixture with 500 ppm toluene [3, 4]. Ward showed the CO_2 permeability of 220^oC, 24 hrs crosslinked *dense films* dropped ~10% when exposing the membrane to the same feed as in Omole's work [3, 5]. This may suggest that high-level toluene impurity in the feed causes different degrees of depression of permeate flux for dense films and asymmetrics [4, 5]. To explore the effect of toluene on PDMC polymer, both crosslinked *dense film* and *hollow fiber* membranes were studied by using high-level toluene impurity, as discussed in sections below.

6.2.1 Effect of toluene on dense films

Dense film permeation was performed in order to study the effect of toluene on the intrinsic separation properties of crosslinked PDMC membranes. Clean mixed gas permeation without toluene was first conducted as the control experiments. Then mixed gas with 500 ppm toluene in the 10/90 CO_2/CH_4 feed was also used on crosslinked *dense films*. The permeation results are shown in Figure 6.1~6.2. At least two films were prepared to check the reproducibility for each state.

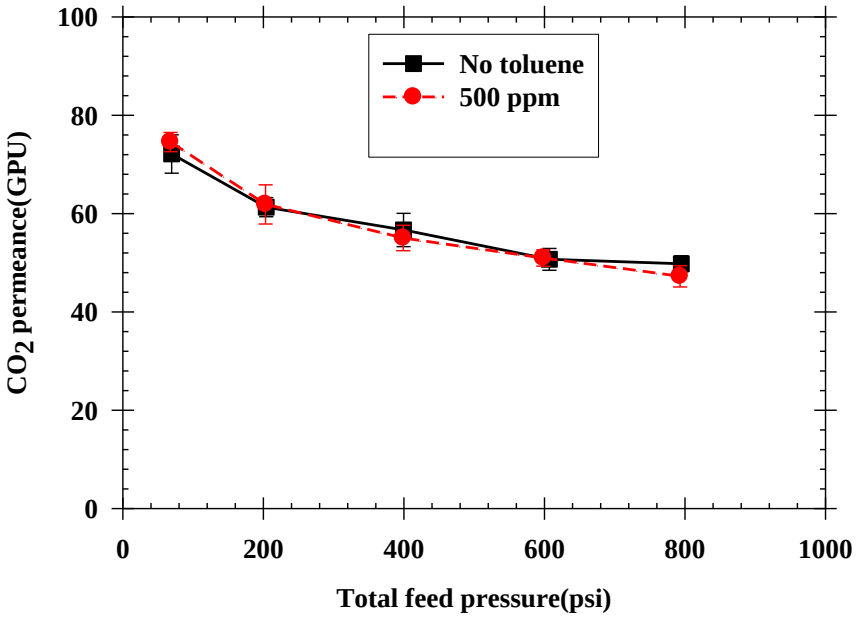

Figure 6.1: CO_2 permeability of *crosslinked* dense films in a clean mixed gas and in the presence of toluene impurity. Test conditions: 10/90 CO_2/CH_4, 35°C.

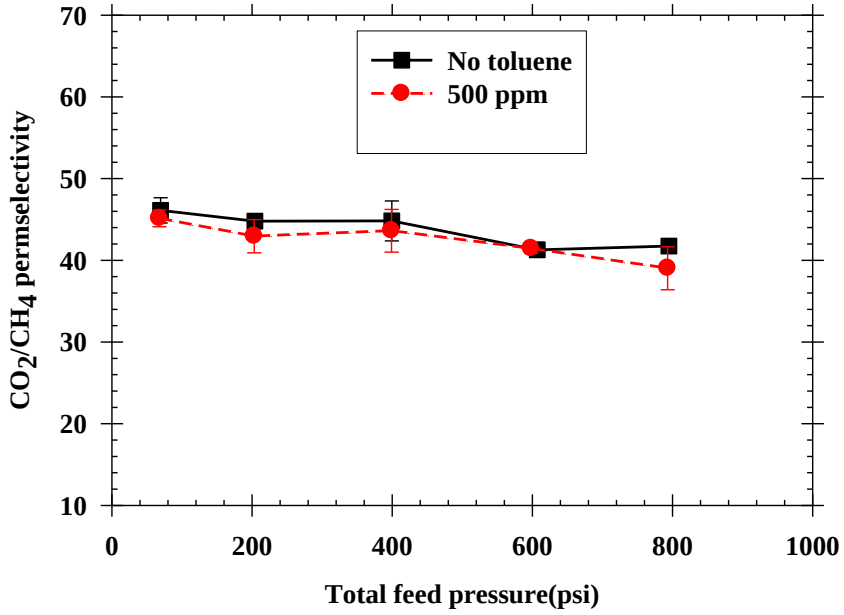

Figure 6.2: CO_2/CH_4 selectivity of *crosslinked* dense films in a clean mixed gas and in the presence of toluene impurity. Test conditions: 10/90 CO_2/CH_4, 35°C.

Figure 6.1 shows that 500 ppm toluene impurity does not significantly affect CO_2 permeability up to a total feed pressure of 800 psi. The presence of toluene only causes a loss of permeability of ~5% vs. clean mixed gas feed. The causes of permeability loss will be discussed in the Section 6.2.3. The low depression of permeability in the presence of toluene suggests the robust *crosslinked* dense films can resist the loss of permeability under high pressures with high-level toluene impurity. On the other hand, the toluene impurity shows a similar effect on $\alpha_{CO2/CH4}$ in this work vs. Ward's work [5]. The 500 ppm toluene tends to cause a decrease of $\alpha_{CO2/CH4}$ within 5%. Overall, the *crosslinked* dense films demonstrate excellent separation performance in the presence of high content toluene impurity.

The toluene effect on membrane separation performance was further studied on *crosslinked* hollow fibers since fibers are the industrially preferred membrane format, as described in the section below.

6.2.3 Effect of toluene on crosslinked hollow fibers

The high performance crosslinked hollow fibers developed in Chapter 5 were characterized using high level hydrocarbon contaminants in the feed. Figure 6.3~6.4 show the CO_2 permeance and selectivity of crosslinked hollow fibers by using 30~1000 ppm toluene in the feed under a maximum test pressure of 800 psi at 35^{o}C.

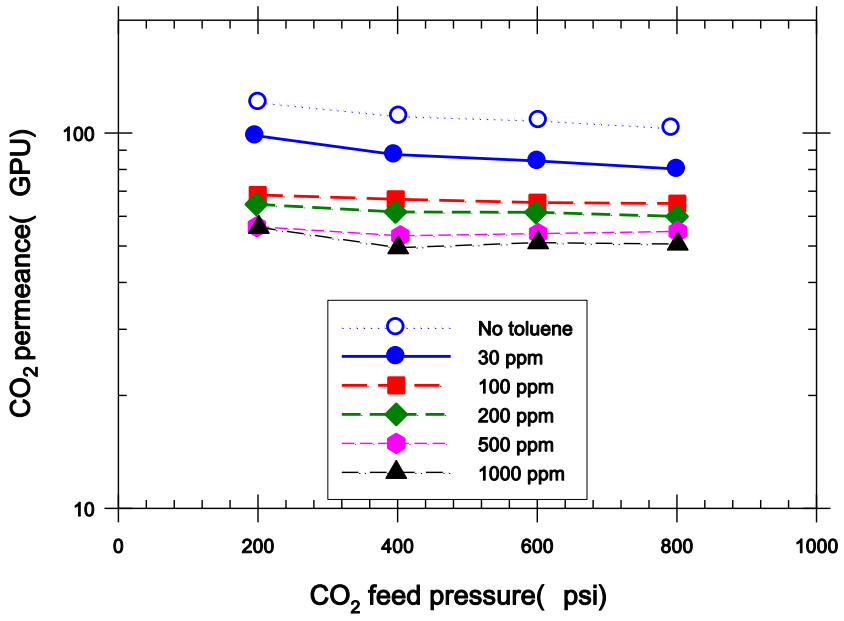

Figure 6.3: CO_2 permeance of *crosslinked* hollow fibers in the presence of different levels of toluene impurity. Test conditions: 50/50 CO_2/CH_4, 35°C.

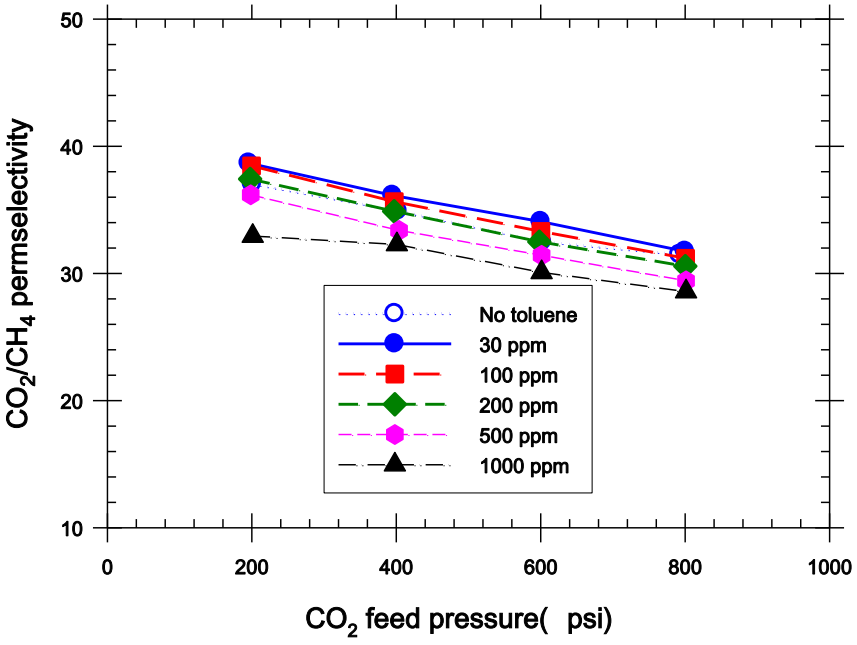

Figure 6.4: CO_2/CH_4 selectivity of *crosslinked* hollow fibers in the presence of different levels of toluene impurity. Test conditions: 50/50 CO_2/CH_4, 35°C.

Figure 6.3 shows that the CO_2 permeance is reduced when increasing the toluene concentration in the feed; however, the CO_2 permeance at the 1000 ppm toluene level is significantly improved to 50 GPU vs. ~10 GPU reported in reference [3, 4]. Note that the mixed gas used in the study contains 50% of CO_2 in the feed, which is more aggressive than the 10% CO_2 used in the reference [3, 4]. On the other hand, the CO_2/CH_4 selectivity is attractively high, which is close or above 30 at all testing toluene levels under a feed pressure up to 800 psi. The high permeance and selectivity under 1000 ppm toluene with a pressure up to 800 psi suggests that the ester-crosslinked hollow fibers are viable under extremely challenging feeding conditions. To demonstrate the effect of toluene concentration, the CO_2 permeance and selectivity at a 400 psi feed pressure with different toluene levels are summarized in Figure 6.5~6.6, compared with literature data [4].

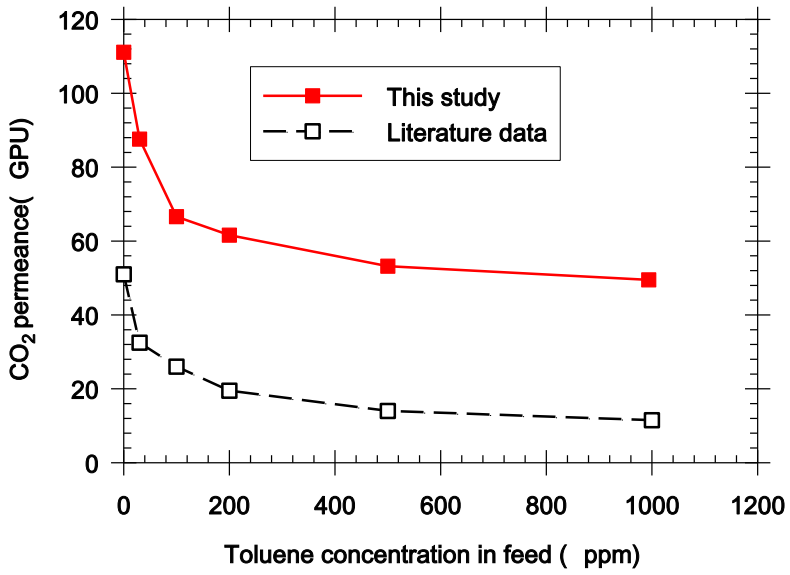

Figure 6.5**:** CO_2 permeance of *crosslinked* hollow fibers under different toluene concentrations from this study and literature. Test conditions: 400 psi, 50/50 CO_2/CH_4, 35^{o}C; literature test conditions: 10/90 CO_2/CH_4 [4].

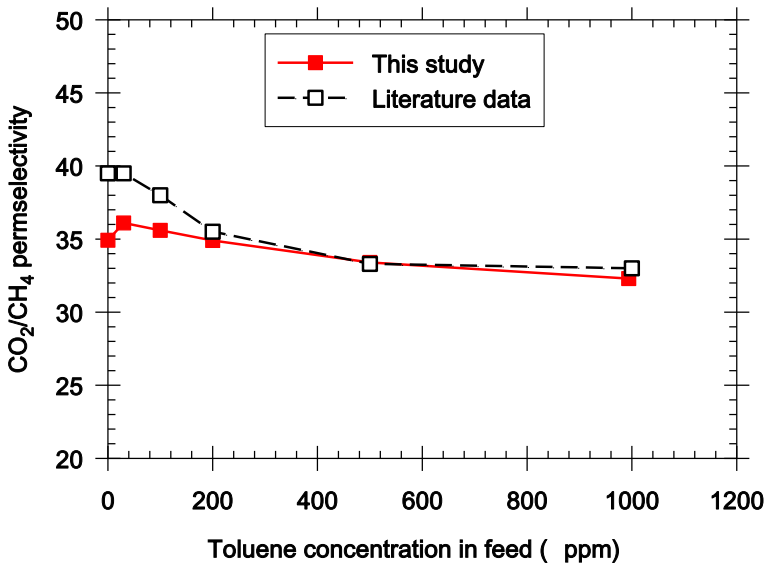

Figure 6.6: CO_2/CH_4 selectivity of *crosslinked* hollow fibers under different toluene concentrations from this study and literature. Test conditions: 400 psi, 50/50 CO_2/CH_4, 35°C; literature test conditions: 10/90 CO_2/CH_4 [4].

Figure 6.5 shows that the CO_2 permeance in literature-reported membranes dropped drastically under a toluene level of 30~200 ppm; however, the decrease of permeance leveled off at a concentration of ~500 ppm, similar to the trend reported in reference [4]. The CO_2 permeance decreased about 52% vs. 76% in reference when introducing the 500 ppm toluene. This suggests the ester-crosslinked hollow fibers developed in this work are less sensitive to toluene vs. the fibers reported in reference [4]. On the other hand, despite a slightly lower selectivity under the low toluene content, the CO_2/CH_4 selectivity is quite close to literature data at 200~1000 ppm toluene levels [4].

The significantly reduced depression of permeance under high toluene concentrations indicates that the *ester-crosslinked* hollow fibers developed in this study are less sensitive to toluene vs. the literature [4]. The lower loss of CO_2 permeance in this study vs. Omole's work [4] is possibly due to different properties of polymer batch used for the hollow fiber spinning. To

check the intrinsic properties of polymer samples, dense film permeation was performed in this work and the results are compared with Omole's work, as shown in Table 6.1 [7].

Table 6.1: Ester-crosslinked dense film separation properties.

Membrane form	CO_2 permeability	$\alpha_{CO2/CH4}$
Crosslinked dense films	57.4±6.9 Barrer	44.8±0.6
Crosslinked dense films [7]	133±0.3 Barrer	45±0.6

Test conditions: 10/90 CO_2/CH_4, 200 psi, 35^oC.

Table 6.1 shows that CO_2 permeability in this work is significantly lower than that reported by Omole et al. in reference [7]. This difference is possibly due to the different imidization and monoesterification processes, since chemical imidization and "two-pot" monoesterification were used in this work vs. thermal imidization and "one-pot" monoesterification in literature [7]. The details about polymer synthesis can be found in Section 3.2.1. However, the permeance, *P/l*, (actual productivity) in this work is significantly *higher* than the literature due to optimized membrane formation protocol.

The decrease of CO_2 permeability or permeance in the presence of toluene is believed to be primarily due to antiplasticization induced by toluene. Antiplasticization occurs when an antiplasticizer reduces the fractional free volume (*FFV*) and increases the stiffness by lowering the glass transition temperature, as shown in Figure 6.7 [8, 9].

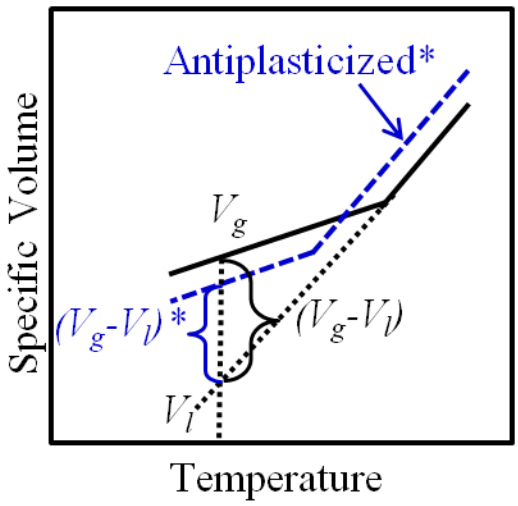

Figure 6.7: Specific volume of pure polymer (solid black line) and antiplasticized polymer (blue dashed line), showing *FFV'*<*FFV* for antiplasticized vs. neat polymer.

In Figure 6.7, *FFV* and *FFV'* represent the Fractional Free Volume of neat polymer and antiplasticized polymer, respectively. As shown in Figure 6.7, toluene induced antiplasticization can reduce Fractional Free Volume (*FFV*) and thereby hinder the diffusion of each penetrant and reduce permeability accordingly. Park et al correlated the gas permeability with the Fractional Free Volume of polymer and the relation is shown below [10]:

$$P_A = A_A \exp\left(\frac{-B_A}{FFV}\right) \qquad (6.1)$$

P_A represents the permeability of a membrane and A_A and B_A are constants for a particular gas. For the same gas, the permeability decreases when *FFV* is reduced. As Table 6.1 shows, the crosslinked dense films in this work have relatively lower permeability, which is believed to reflect smaller *FFV* vs. the ones used in literature [7]. It is hypothesized that the membrane with a small *FFV* is less sensitive to toluene impurity. Therefore, the membrane in this study is hypothesized to have a lower *FFV* and hence shows less tendency to antiplasticize by toluene vs.

higher permeability membrane used in the literature [4]. The data in Figure 6.6 and Table 6.1 at 0 ppm toluene supports this hypothesis that the current material has lower FFV (and hence lower permeability based on Equation 6.1). This fact notwithstanding, further density and FFV measurements will be beneficial for verifying this hypothesis.

6.2.4 Effect of skin layer thickness on toluene sensitivity

As shown in Section 6.2.2 and 6.2. 3, dense films showed much less depression of CO_2 permeate flux in the presence of toluene than hollow fibers using the same PDMC polymer. The significantly different sensitivities to toluene are presumably due to the different thickness (and FFV) of the selective layer for dense films and hollow fibers. To understand the different toluene sensitivities of the various samples from the same polymer batch, three *crosslinked* hollow fiber modules with different skin layer thickness were considered. Those fibers samples were not only from the same batch polymer but also were spun at the same time. Moreover, the samples experienced the same physical aging histories for ~200 days after crosslinking. The aged fiber samples with different skin layer thickness were retested by using the same feed conditions. The effective skin layer thickness of *crosslinked* hollow fibers was estimated by mixed gas permeation on dense films and hollow fibers using a 50/50 CO_2/CH_4 feed. High CO_2 partial feed pressure permeation was first performed on *crosslinked* hollow fibers, as shown in Figure 6.8~6.9.

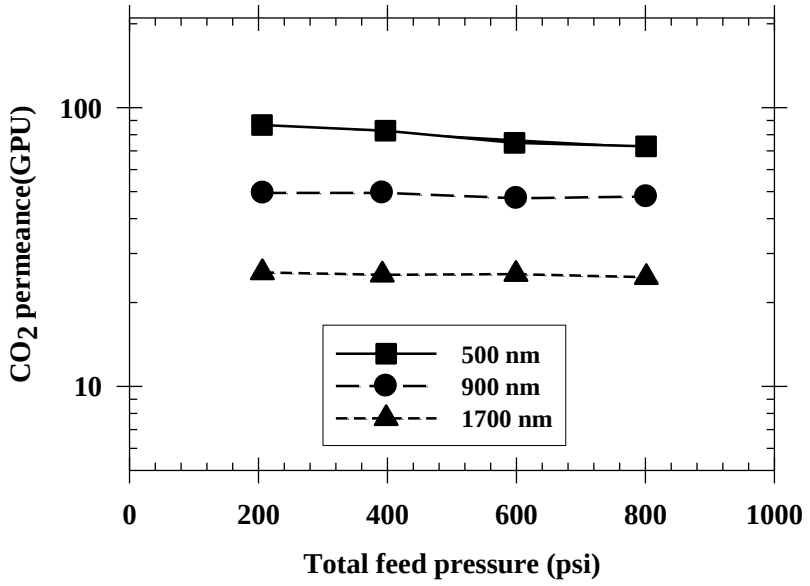

Figure 6.8: CO_2 permeance of *crosslinked* hollow fibers with different skin layer thickness under different feed pressures. Test conditions: 50/50 CO_2/CH_4, 35°C.

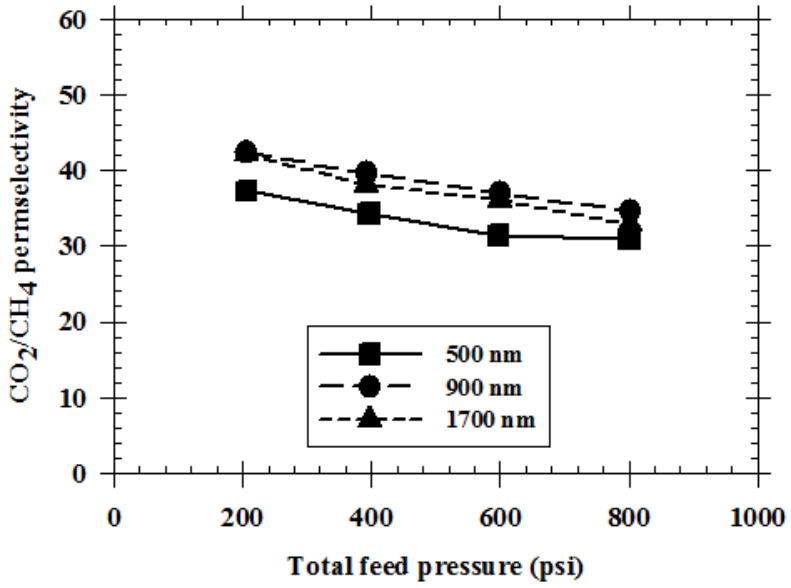

Figure 6.9: CO_2/CH_4 selectivity of *crosslinked* hollow fibers with different skin layer thickness under different feed pressures. Test conditions: 50/50 CO_2/CH_4, 35°C.

Figure 6.8 shows that despite the different skin layer thickness, no CO_2 plasticization was found in any of those *crosslinked* hollow fibers. All hollow fibers demonstrate a CO_2/CH_4

selectivity nearly or over 90% of the intrinsic (dense film $\alpha_{CO2/CH4}$=43.8±1.4 tested with 200 psi 50/50 CO_2/CH_4), suggesting the fibers are defect-free. Based on the CO_2 permeability (43.6±0.1 Barrers) and permeance tested at 200 psi of 50/50 CO_2/CH_4, the skin layer thickness of those crosslinked hollow fibers are estimated to be 500 nm, 900 nm and 1700 nm. The three crosslinked hollow fiber samples were then further subjected to a toluene impurity. The mixed gas permeation under a 400 psi 50/50 CO_2/CH_4 feed with a toluene level from 30~750 ppm is shown in Figure 6.10~6.11. The detailed percentage reductions in permeance and selectivity due to 750 ppm toluene, shown in Table 6.2, are revealing.

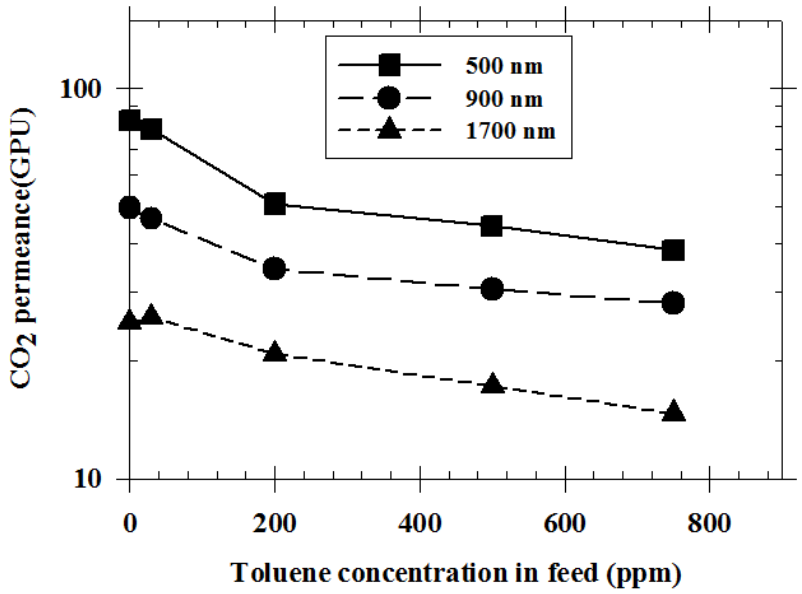

Figure 6.10: CO_2 permeance of *crosslinked* hollow fibers with different skin layer thickness under different toluene contents. Test conditions: 400 psi, 50/50 CO_2/CH_4, 35^oC.

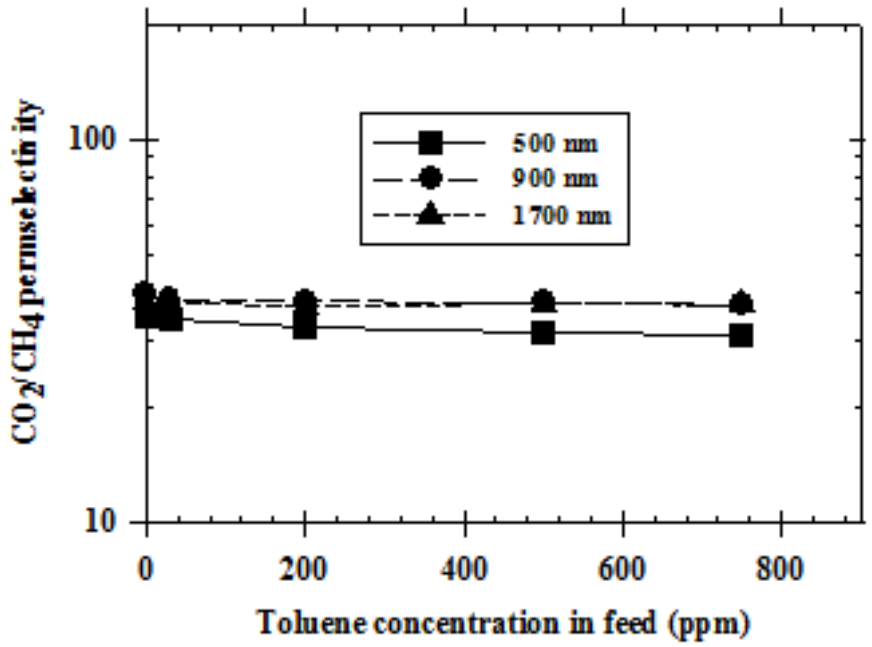

Figure 6.11: CO_2/CH_4 selectivity of *crosslinked* hollow fibers with different skin layer thickness under different toluene contents. Test conditions: 400 psi, 50/50 CO_2/CH_4, 35°C.

Table 6.2: CO_2 permeance reduction during toluene exposure.

Sample ID	Skin layer thickness/nm	CO_2 permeance reduction/%	$\alpha_{CO2/CH4}$ reduction/%
1	500	53.4	10.4
2	900	43.1	6.4
3	1700	41.5	2.5

Specifically, Table 6.2 shows that the *thinner* skin crosslinked hollow fibers show a relatively greater loss of CO_2 permeance and selectivity vs. the *thicker* skinned samples in the presence of 750 ppm toluene. The significantly different behavior against toluene suggests that

the skin layer thickness can affect the membrane sensitivity to toluene. Due to the more rapid quenching process of the thinner skin fibers during the spinning, there may exist additional micro-void packing defects or unrelaxed free volume in the *thinner* skinned hollow fibers. Presumably, the higher FFV tends to be more affected by the toluene contaminant due to the combined effect of competitive sorption and antiplasticization [9]. Therefore, the *thinner* hollow fibers show greater depression of CO_2 permeance and thereby are *more* sensitive to toluene than the *thicker* ones.

To further study skin layer thickness dependent toluene sensitivity of hollow fibers, another hollow fiber module was characterized in the *fresh state* without aging by exposure to toluene for comparison to the aged samples. Because the ~500 nm selective layer sample was the most technologically important, it was selected for this aging study. The CO_2 permeance and selectivity before and during exposure to toluene are shown in Figure 6.12~6.13. In each case, the samples were exposed to the toluene-laden feeds until apparent steady state was achieved (typically ~2 hrs) for both fresh and aged samples. As discussed later, even with extended exposure for 100 hrs, negligible change was observed as compared to the 2 hr exposure steady state case.

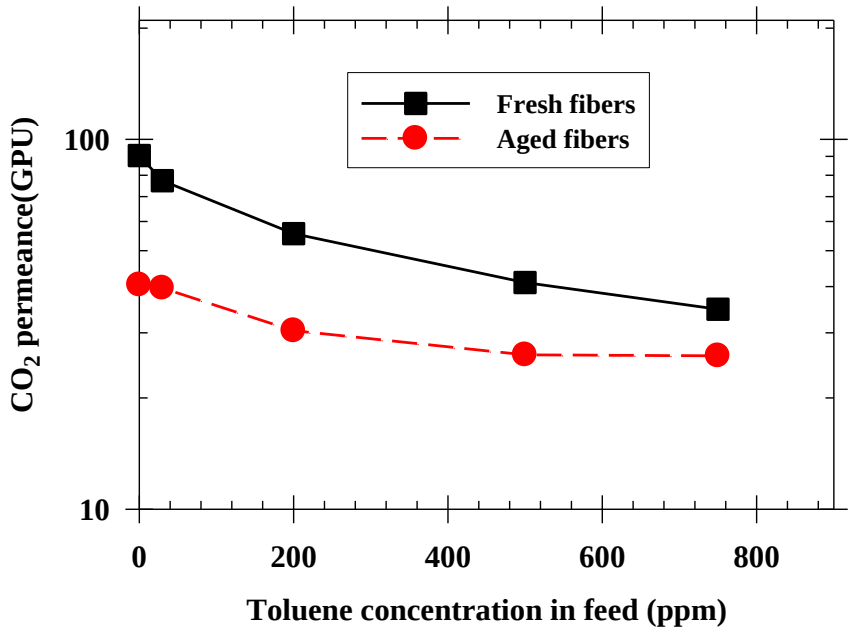

Figure 6.12: CO_2 permeance of *crosslinked* hollow fibers before and after ageing 240 days under different toluene contents. Test conditions: 400 psi, 50/50 CO_2/CH_4, 35°C.

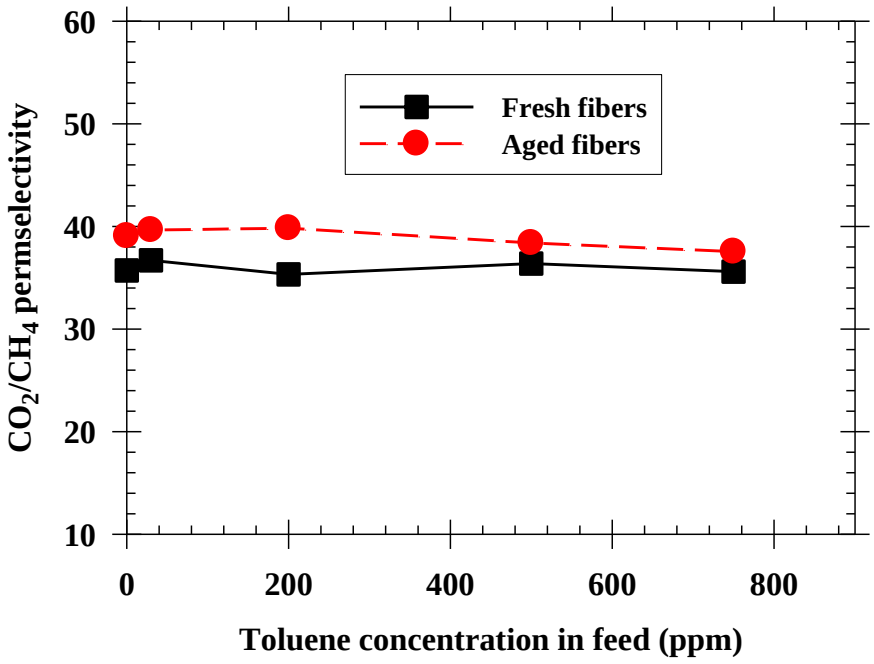

Figure 6.13: CO_2/CH_4 selectivity of *crosslinked* hollow fibers before and after ageing 240 days under different toluene contents. Test conditions: 400 psi, 50/50 CO_2/CH_4, 35°C.

Figure 6.12 shows that the fresh hollow fibers showed ~62% depression of CO_2 permeance vs. ~36% in aged fibers when increasing the toluene concentration from 0 to 750 ppm. This behavior is consistent with a larger FFV in the freshly made samples as opposed to the ~200 day aged samples. Moreover, this supports the observation that the more highly quenched thin skinned samples (which were argued to contain higher FFV vs. the thicker skinned samples) showed more CO_2 permeance sensitivity to toluene. Although not tested due to time constraints, these results suggest that the thicker skinned samples (which are believed to start with lower FFV and higher intrinsic skin thickness) will show less ageing dependence as well as less toluene sensitivity for CO_2 permeance. This fact notwithstanding, the results in Fig. 6.8 and 6.9 suggest that despite greater CO_2 permeance sensitivity to toluene (Fig. 6.10), the ultimate performance is still higher for the aged ~500 nm skinned sample exposed to toluene.

6.3 Effect of heptane impurity

As another common impurity in the natural gas feed, heptane was chosen to study the aliphatic contaminant resistance of crosslinked hollow fibers. In this study, a mixed gas feed with a heptane content of 750 and 33.4 ppm is used to simulate the typical contaminant concentration prior and after the pre-treatment of the feed. The crosslinked hollow fibers were tested with a 50/50 CO_2/CH_4 feed under a total feed pressure up to 800 psi. The mixed gas permeation results are shown in Figure 6.14~6.15.

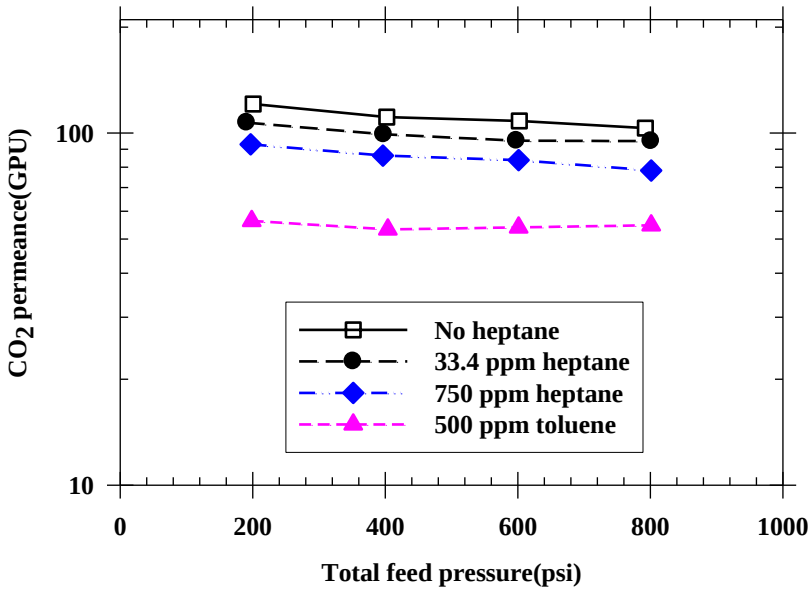

Figure 6.14: CO_2 permeance of *crosslinked* hollow fibers in the presence of different level of heptane and toluene impurities. Test conditions: 50/50 CO_2/CH_4, 35°C.

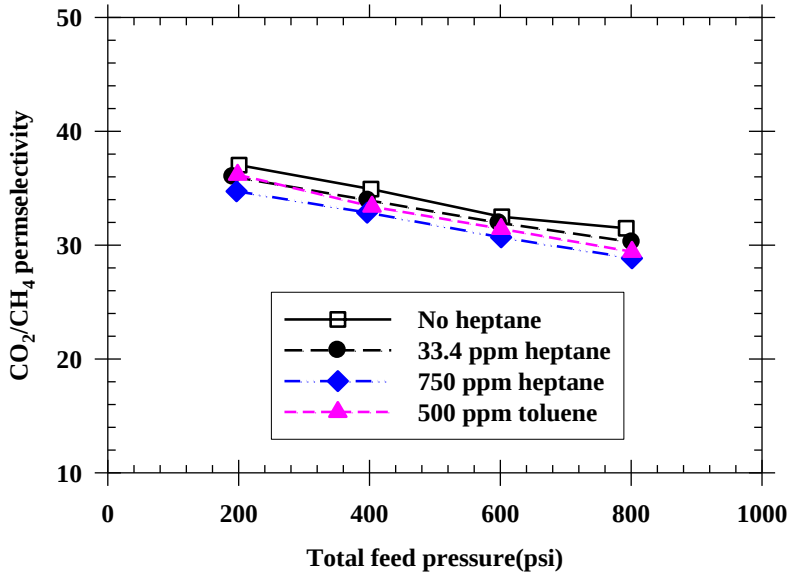

Figure 6.15**:** CO_2/CH_4 selectivity of *crosslinked* hollow fibers in the presence of different level of heptane and toluene impurities. Test conditions: 50/50 CO_2/CH_4, 35°C.

Figure 6.14~6.15 show that the low 33.4 ppm heptane level does not affect either the CO_2 permeance or selectivity significantly. This indicates that a pre-treatment may be unnecessary to achieve the desirable separation performance at a contaminant level below 33.4 ppm. Moreover, the crosslinked hollow fibers showed a CO_2 permeance above 80 GPU at the maximal 750 ppm heptane level. The highest testing heptane level does not cause a very serious effect on the CO_2/CH_4 selectivity. Furthermore, Figure 6.14 shows that the permeance dropped ~24% and ~47% in the 750 ppm *heptane* and 500 ppm *toluene*, respectively. Studies on toluene and heptane in Matrimid® polyimide showed that toluene has a significantly higher sorption capacity than heptane [9]. The sorption advantage of toluene may explain the larger depression of CO_2 permeance vs. heptane since the antiplasticization is affected by the sorption competition between the antiplasticizer and permeants. Further sorption study will provide a better understanding on the different sensitivities of toluene and heptane for the crosslinked hollow fibers. Nevertheless, the permeation results with heptane demonstrate the excellent separation performance of crosslinked hollow fibers under realistic operation conditions with high-level aliphatic contaminants.

6.4 Effect of water impurity

A pre-treatment using absorbents can remove most of the high-level contaminants in the feed, including both hydrocarbon and moisture impurities. However, the water impurity in the raw natural gas feed has potential to hydrolyze the covalent bonds and could be detrimental to the membrane separation performance. To study the separation performance of ester-crosslinked hollow fibers in the presence of water impurity, the fibers were subjected to a N_2 feed containing 101 ppm water at a pressure up to 600 psi. The hollow fiber module was tested with clean 50/50 CO_2/CH_4 to monitor the changes of permeance and CO_2/CH_4 selectivity over time. Specifically,

the crosslinked hollow fibers were first tested with clean mixed gas, and then subjected to 600 psi of N_2 feed with 101 ppm H_2O and conditioned for ~2 hrs. After removal of the feed with water impurity, the crosslinked hollow fibers were re-tested with clean mixed gas. The permeation results are summarized in Figure 6.16~6.17.

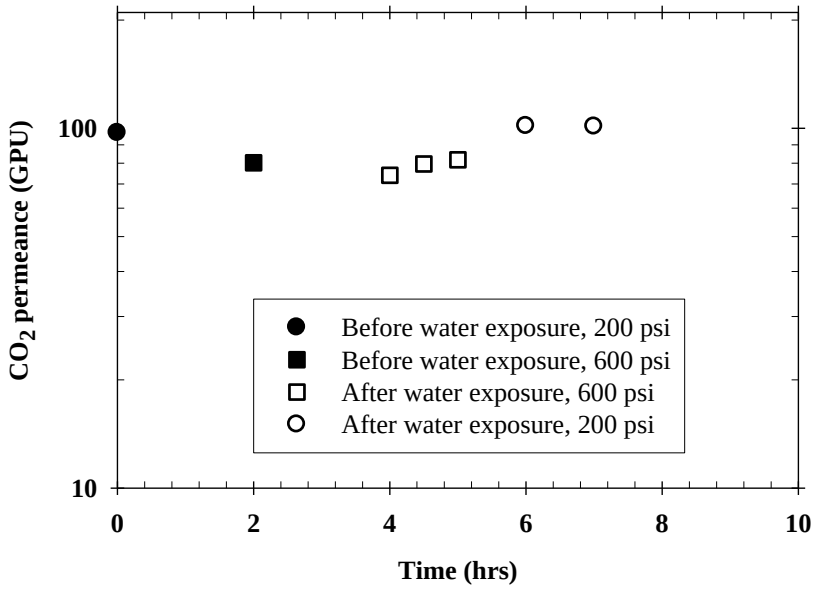

Figure 6.16: CO_2 permeance of *crosslinked* hollow fibers before and after water exposure. Test conditions: 50/50 CO_2/CH_4, 35°C. Water feed conditions: 600 psi, 101 ppm in N_2.

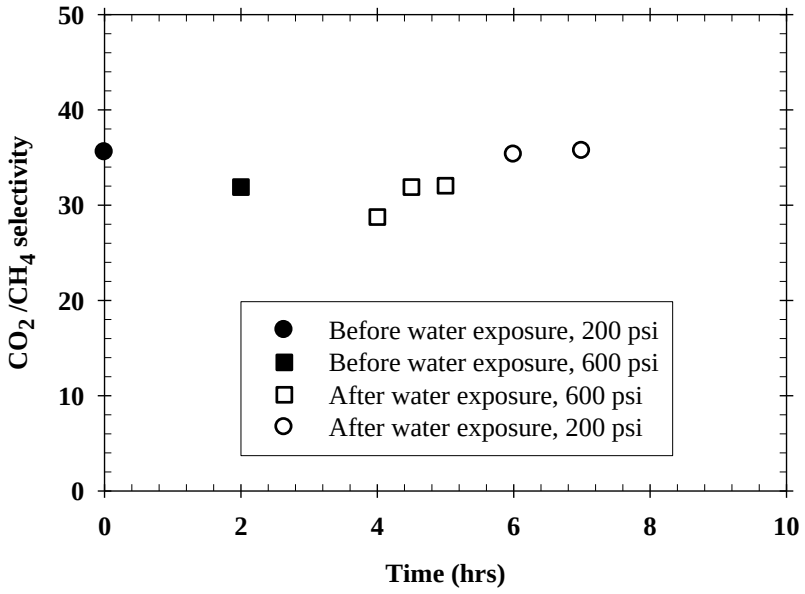

Figure 6.17: co_2/ch_4 selectivity of *crosslinked* hollow fibers before and after water exposure. Test conditions: 50/50 CO_2/CH_4, 35°C. Water feed conditions: 600 psi, 101 ppm in N_2.

Figure 6.16~6.17 shows that the water impurity causes a slight loss of permeance and selectivity after water exposure; however, after purging the hollow fiber module with clean mixed gas for ~ 2 hrs, the high CO_2 permeance and selectivity can be regenerated quickly. The high permeance and selectivity recovered after purging fibers with clean gas suggests the water does not cause an irreversible damage to the fibers. An extended time up 100 hrs exposure in water impurity was also performed to study the stability and reversibility of hollow fibers, as will be discussed in Section 6.6.3.

6.5 Stability under toluene impurity

As discussed above, the *ester-crosslinked* hollow fibers showed high separation performance in the presence of high-level hydrocarbon impurities. Despite this high performance, it is also desirable to expose those *crosslinked* hollow fibers under a high-pressure

feed with contaminant for an extended period to simulate realistic operation conditions. This is particularly important since the stability over time is required for the application of hollow fibers in the real field. Therefore, the crosslinked fibers were examined by using 600 psi 50/50 CO_2/CH_4 feed with a 750 ppm toluene and the separation performance was continuously tested during the ~100 hrs' exposure. The permeation results are shown in Figure 6.18~6.19.

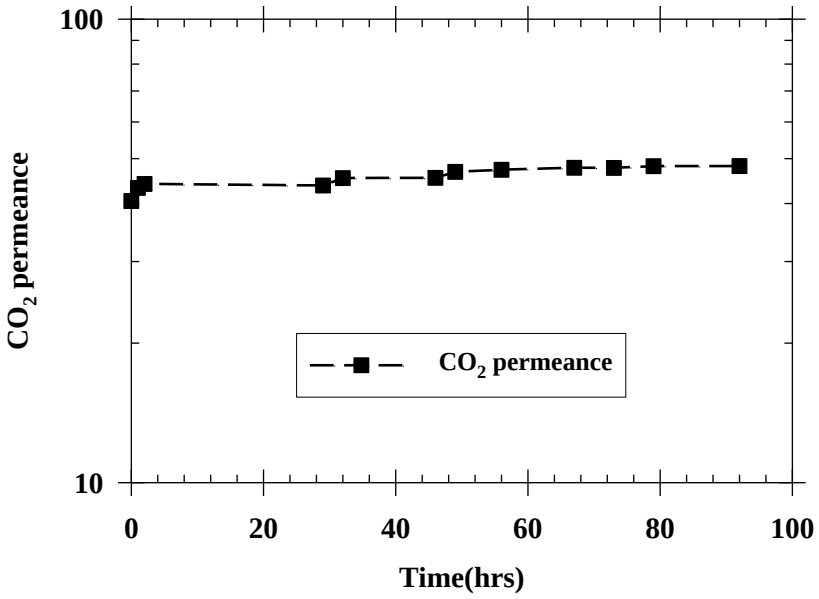

Figure 6.18: CO_2 permeance of *crosslinked* hollow fiber membranes over extended time exposure in a feed pressure of 600 psi. Permeance calculated by using fugacity. Test conditions: 50/50 CO_2/CH_4, 750 ppm toluene, at 35°C.

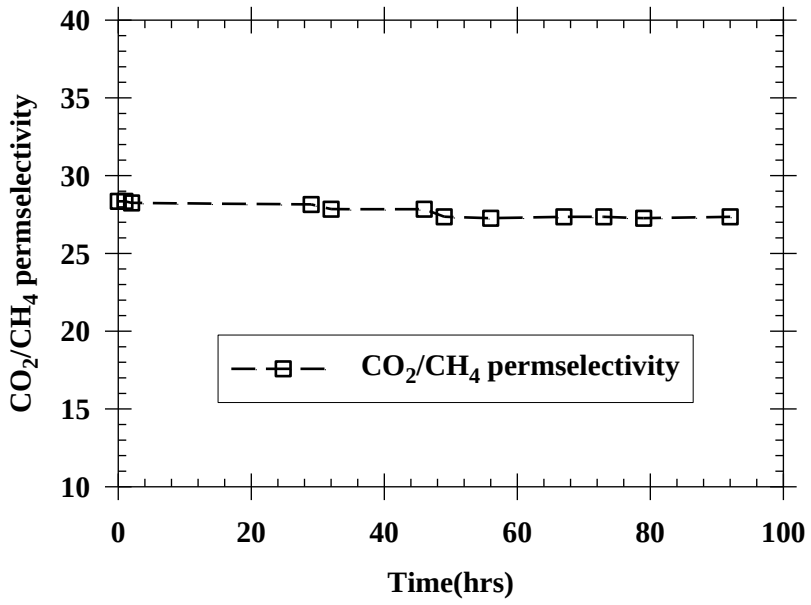

Figure 6.19: CO_2/CH_4 selectivity of *crosslinked* hollow fiber membranes over extended time exposure in a feed pressure of 600 psi. Permeances calculated by using fugacity. Test conditions: 50/50 CO_2/CH_4, 750 ppm toluene, at 35°C.

In Figure 6.18, the ester-crosslinked hollow fibers showed a slight increase of CO_2 permeance in the first 2 hrs exposure. However, the CO_2 permeance quickly reached a steady state after 2 hrs. On the other hand, the CO_2/CH_4 selectivity was found rather stable during this extended time exposure. The stable permeance and selectivity over time suggests that the ester-crosslinked hollow fibers are applicable for extended time natural separation with high-level contaminants under high feed pressures.

6.6 Reversibility of contaminant exposure

To determine whether the hydrocarbon contaminant causes a permanent damage of the integrated skin or inner structure, it is necessary to check the separation performance of hollow fibers after removal of impurities. In this study, the ester-crosslinked hollow fibers were first tested with clean mixed gas permeation and then exposed in a mixed gas with a high-level

contaminant. Three common contaminants, toluene, heptane and water, were selected to study the reversibility of contaminant effect on the crosslinked hollow fibers, as discussed below.

6.6.1 Reversibility of toluene exposure

Prior to the toluene exposure, the crosslinked hollow fibers were re-tested to check the CO_2 permeance and selectivity to eliminate the interference of physical aging. Then the fibers were exposed in a mixed gas with toluene. Since the CO_2 permeance tends to reach a plateau when increasing the toluene content to 500 ppm, a toluene concentration of 500 ppm was chosen and represents a high-level content. After the toluene exposure, the fibers were purged with clean mixed gas and the permeance and selectivity were re-tested by a 50/50 CO_2/CH_4 feed. The permeation results are shown in Figure 6.20.

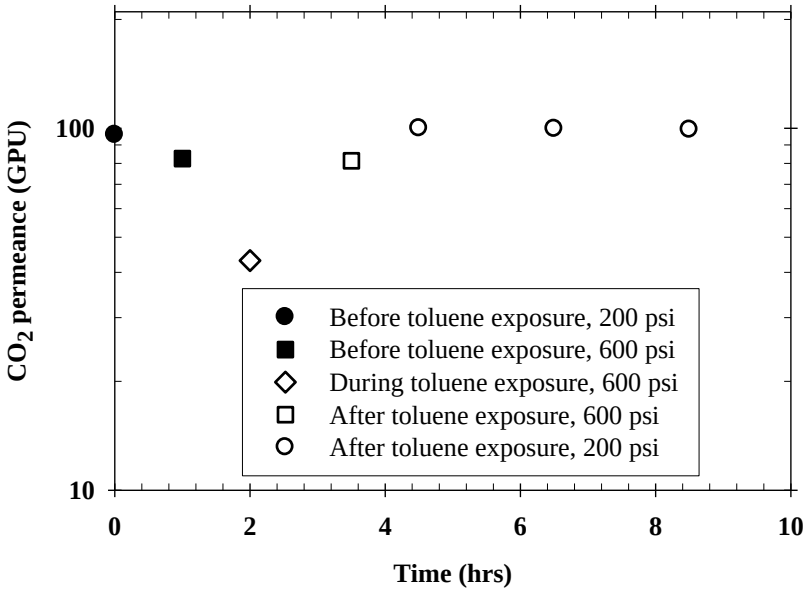

Figure 6.20: CO_2 permeance of crosslinked hollow fibers before, during and after toluene exposure. Test conditions: 50/50 CO_2/CH_4, 35°C. Toluene content: 500 ppm in 50/50 CO_2/CH_4.

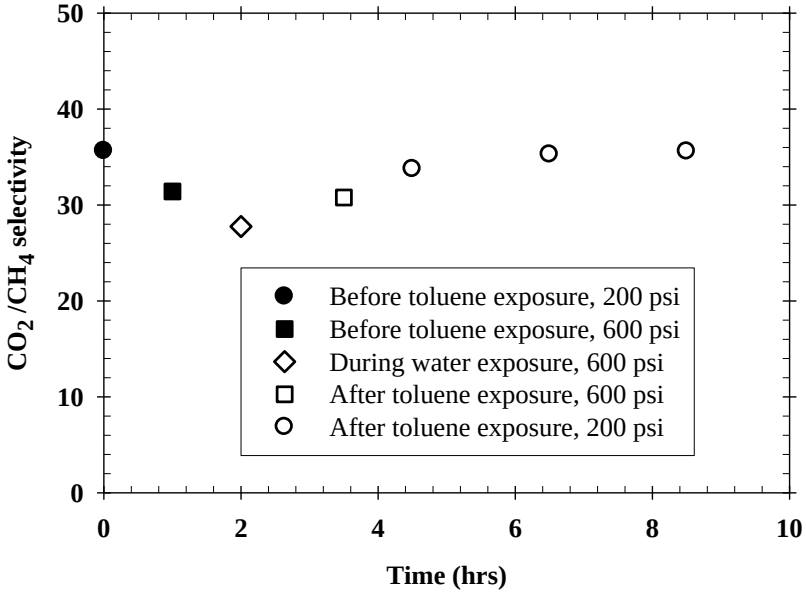

Figure 6.21: CO_2/CH_4 selectivity of crosslinked hollow fibers before, during and after toluene exposure. Test conditions: 50/50 CO_2/CH_4, 35°C. Toluene content: 500 ppm in 50/50 CO_2/CH_4.

Figure 6.20 shows that the loss of CO_2 permeance during toluene exposure was recovered rapidly by purging with clean mixed gas for ~ 2 hrs. The high permeance prior to exposure was completely regained after removal of toluene and purging with clean gas. Moreover, the high CO_2/CH_4 selectivity was also recovered upon removing the toluene impurity. The high permeance and selectivity regenerated after purging fibers with clean gas suggests the presence of toluene does not cause permanent damage to the integrated skins or the inner structure.

6.6.2 Reversibility of heptane exposure

Another common aliphatic contaminant was also studied to probe the reversibility of crosslinked hollow fibers in the presence of another category impurity. In this study, a heptane content of 750 ppm represents a significantly high level of contaminants. The permeation results prior to the heptane exposure, during and after exposure were shown in Figure 6.22~6.23.

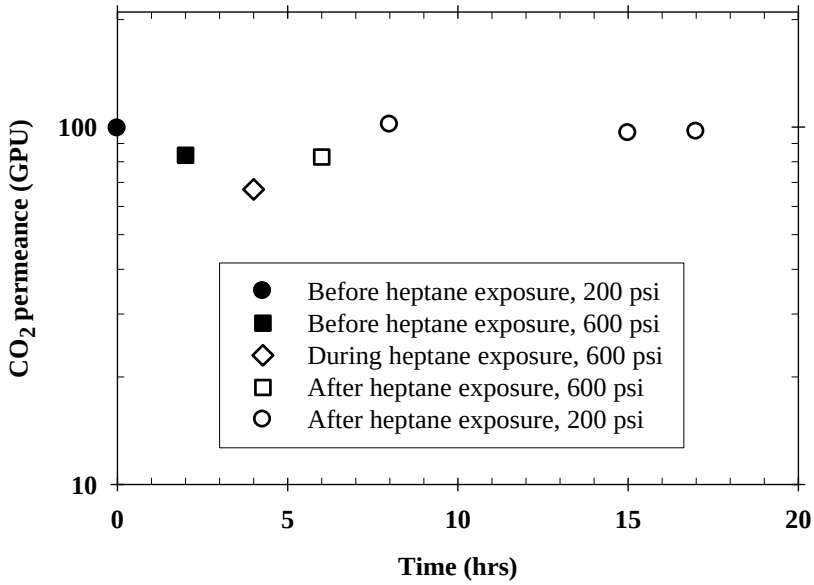

Figure 6.22: CO_2 permeance of crosslinked hollow fibers before, during and after heptane exposure. Test conditions: 50/50 CO_2/CH_4, 35°C. Heptane content: 750 ppm in 50/50 CO_2/CH_4.

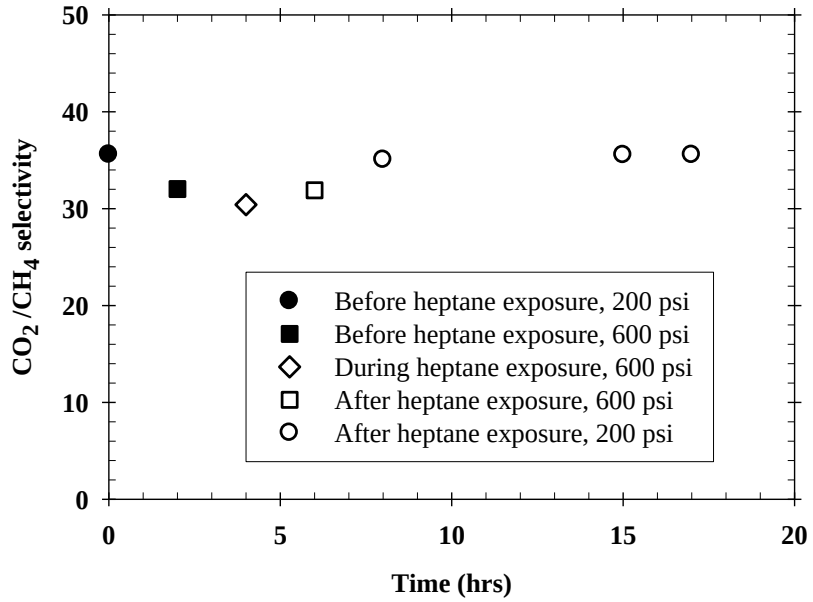

Figure 6.23: CO_2/CH_4 selectivity of crosslinked hollow fibers before, during and after heptane exposure. Test conditions: 50/50 CO_2/CH_4, 35°C. Heptane content: 750 ppm in 50/50 CO_2/CH_4.

Figure 6.22 shows that the loss of CO_2 permeance during heptane exposure was recovered quickly by purging with clean mixed gas for ~ 2 hrs. Moreover, the permeance and CO_2/CH_4 selectivity were regained ~100% after removal of heptane and purging with clean gas. The high permeance and selectivity recovered after removing heptane suggests the presence of heptane could not cause permanent damage to the integrated skins or the inner structure either.

6.6.3 Reversibility of water impurity

To study the recovery of the separation performance of ester-crosslinked hollow fibers after removing water impurity, the fibers were subjected to a N_2 feed containing 101 ppm water at a pressure up to 600 psi for a period of ~100 hrs. The permeance and CO_2/CH_4 selectivity of hollow fibers were tested with a clean 50/50 CO_2/CH_4 during the ~100 hrs exposure to study their stability. After each permeance test, the fibers were removed from the permeation system and immediately exposed to the water contaminant environment. After exposing in water impurity for ~100 hrs, the hollow fibers were then re-tested with clean mixed gas to explore if the high performance can be recovered after removal of water contaminant. The permeation results are shown in Figure 6.24~6.25.

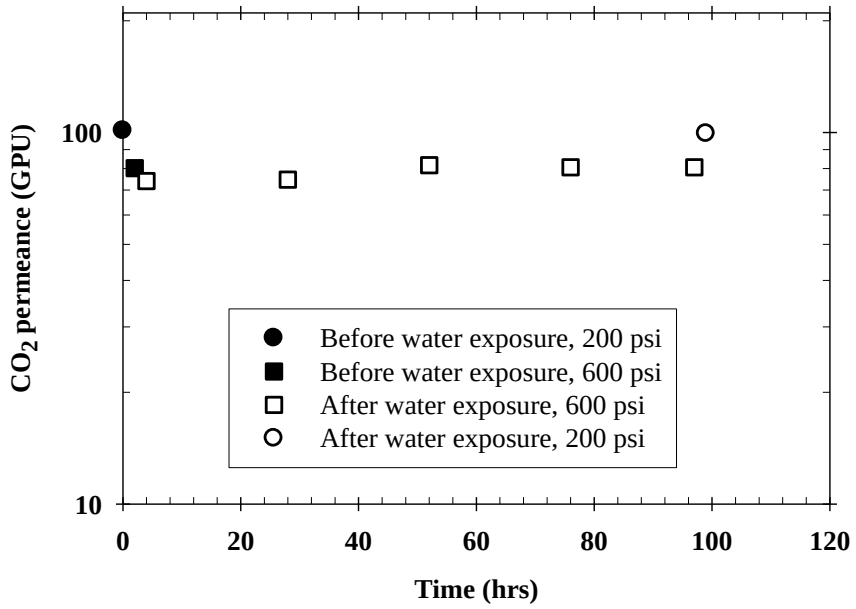

Figure 6.24: CO_2 permeance of *crosslinked* hollow fibers in the presence of water impurity. Test conditions: 50/50 CO_2/CH_4, 35°C.

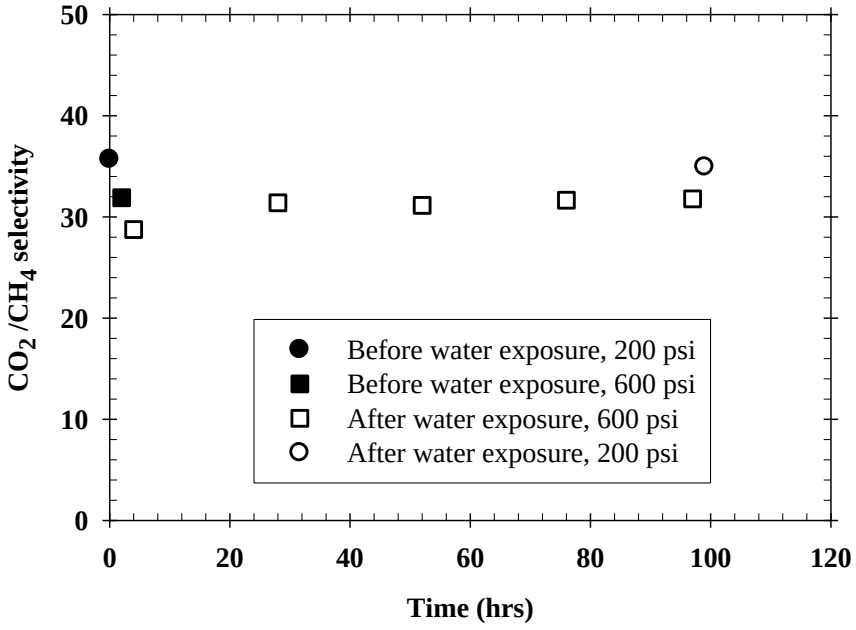

Figure 6.25**:** CO_2/CH_4 selectivity of *crosslinked* hollow fibers in the presence of water impurity. Test conditions: 50/50 CO_2/CH_4, 35°C.

Figure 6.24~6.25 show that the water impurity causes a slight loss of permeance and selectivity during the first 48 hrs' water exposure. However, after exposing the hollow fiber module in the high-pressure water impurity for ~ 48 hrs, the permeance and selectivity tends to level off. Moreover, the high CO_2 permeance and selectivity can be regenerated ~100% after removing the water contaminant. This clearly suggests the 101 ppm water impurity does not cause permanent damage to the integrated skin of the fibers. The ester-crosslinked hollow fibers are also viable for natural gas separation with the moderate level water impurity.

6.7 Summary and conclusions

Mixed gas permeation in the presence of toluene showed that ester-crosslinked *dense films* show much less depression in the presence of toluene than fibers. Moreover, ester-crosslinked hollow fibers spun from a *lower* permeability batch polymer created in a two-pot synthesis vs. one-pot synthesis show *less* tendency to antiplasticize by toluene impurity. It was hypothesized that this tendency reflects a smaller factional free volume (FFV) for the sample produced in the two-pot approach. This hypothesis will need to be verified by subsequent researchers.

Furthermore, for the same two-pot synthesis samples, thinner skinned hollow fibers are more sensitive to toluene than the *thicker* ones. It was again hypothesized that fractional free volume differences are factors in explaining the observed difference between thin and thick skin samples.

Similarly, aged thin-skinned samples from the two-pot synthesis batch were shown to exhibit less toluene sensitivity vs. freshly spun fiber samples. This trend is also consistent with expected fractional free volume changes in aged vs. freshly spun fibers. Both of these FFV based

explanations (unlike the one related to one-pot vs. two-pot batches) cannot be explored by future studies until independent methods are available to probe the thin skin regions of polymer fibers.

The ester-crosslinked hollow fibers demonstrated high strong stability over time in the presence of high-level toluene under high feed pressures. Moreover, they showed significant reversibility in the presence of contaminants and the high separation properties can be regenerated after removal of impurities. The attractive separation performance in the presence high-level contaminants clearly suggests that the ester-crosslinked hollow fibers developed in this work are viable for natural gas separation under extremely challenging feed conditions.

6.8 References

[1] D. Vu, W.J. Koros, S.J. Miller, Effect of condensable impurity in CO2/CH4 gas feeds on performance of mixed matrix membranes using carbon molecular sieves, J Membrane Sci, 221 (2003) 233-239.

[2] M. Al-Juaied, W.J. Koros, Performance of natural gas membranes in the presence of heavy hydrocarbons, J Membrane Sci, 274 (2006) 227-243.

[3] I.C. Omole, Crosslinked Polyimide Hollow Fiber Membranes for Aggressive Natural Gas Feed Streams, Ph.D. Dissertation, in: Chemical and Biomolecular Engineering, Georgia Institute of Technology, Atlanta, GA, 2008.

[4] I.C. Omole, D.A. Bhandari, S.J. Miller, W.J. Koros, Toluene impurity effects on CO2 separation using a hollow fiber membrane for natural gas, J Membrane Sci, 369 (2011) 490-498.

[5] J.K. Ward, CROSSLINKABLE MIXED MATRIX MEMBRANES FOR THE PURIFICATION OF NATURAL GAS, PhD Dissertation, in: School of Chemical & Biomolecular Engineering, Georgia Institute of Technology, Atlanta, GA, 2010.

[6] D.Q. Vu, W.J. Koros, S.J. Miller, Effect of condensable impurities in CO2/CH4 gas feeds on carbon molecular sieve hollow-fiber membranes, Ind Eng Chem Res, 42 (2003) 1064-1075.

[7] I.C. Omole, R.T. Adams, S.J. Miller, W.J. Koros, Effects of CO2 on a High Performance Hollow-Fiber Membrane for Natural Gas Purification, Ind Eng Chem Res, 49 (2010) 4887-4896.

[8] W.J. Koros, G.K. Fleming, Membrane-Based Gas Separation, J Membrane Sci, 83 (1993) 1-80.

[9] W.C. Madden, THE PERFORMANCE OF HOLLOW FIBER GAS SEPARATION MEMBRANES IN THE PRESENCE OF AN AGGRESSIVE FEED STREAM, PhD Dissertation, in: Chemical Engineering, Georgia Institute of Technology, Atlanta, GA, 2005.

[10] J.Y. Park, D.R. Paul, Correlation and prediction of gas permeability in glassy polymer membrane materials via a modified free volume based group contribution method, J Membrane Sci, 125 (1997) 23-39.

[11] A.M. Kratochvil, THICKNESS DEPENDENT PHYSICAL AGING AND SUPERCRITICAL CARBON DIOXIDE CONDITIONING EFFECTS ON CROSSLINKABLE POLYIMIDE MEMBRANES FOR NATURAL GAS PURIFICATION, PhD Dissertation, in: School of Chemical & Biomolecular Engineering, Georgia Institute of Technology, Atlanta, GA, 2008.

CHAPTER 7

DEVELOPMENT OF DEFECT-FREE AND DELAMINATION-FREE ESTER-CROSSLINKED COMPOSITE HOLLOW FIBERS

7.1 Introduction

High productivity and CO_2 plasticization resistant ester-crosslinked *monolithic* hollow fibers were developed and characterized under extremely challenging operation conditions, as shown in previous chapters. Despite the high separation performance, the selective PDMC sheath layer polymer is expensive. The dual-layer spinning technique utilizes a low-cost polymer as the supporting core layer and only small amount of PDMC is required for the sheath layer, and the cost of membrane spinning is significantly reduced. This chapter aimed to develop crosslinked *composite* hollow fibers without skin layer defects or sheath/core layer delamination. Specifically, Chapter 7 will address solutions to overcome challenges to achieve desirable open porous morphology, sheath/core layer compatibility and core layer thermal stability during crosslinking. The *composite* hollow fibers will be characterized under aggressive feed conditions, including high partial CO_2 pressures and hydrocarbon contaminants.

7.2 Core layer material selection

The selection of a core layer material is challenging due to the complexity of dual-layer hollow fiber spinning and the further crosslinking required after the spinning process. Crosslinking composite hollow fibers can cause the sheath/core layer delamination or core layer collapse. Therefore, this study will consider a robust supporting layer polymer, which provides good adhesion with PDMC sheath layer and maintains an open porous substructure during crosslinking.

For the proof of concept dual-layer hollow fiber spinning, two core layer polymer candidates were examined in the preliminary campaign: cellulose acetate (CA) and Torlon®. Cellulose acetate has been studied as a core layer material in previous research [1, 2]. Liu showed that cellulose acetate was compatible with 6FDA-DAM:DABA(3:2) in the *uncrosslinked* format of hollow fibers [2]. It is expected that cellulose acetate should be also compatible with PDMC, since there are ester bonds in PDMC, similar to the structure of cellulose acetate. The structures of cellulose acetate and PDMC are shown in Figure 7.1~7.2.

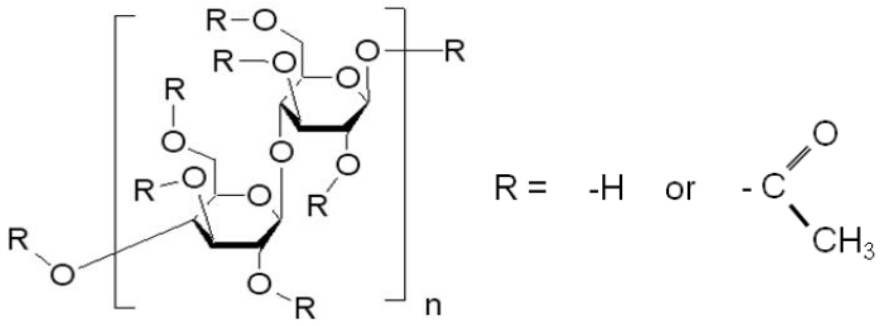

Figure 7.1: Chemical structure of cellulose acetate polymer.

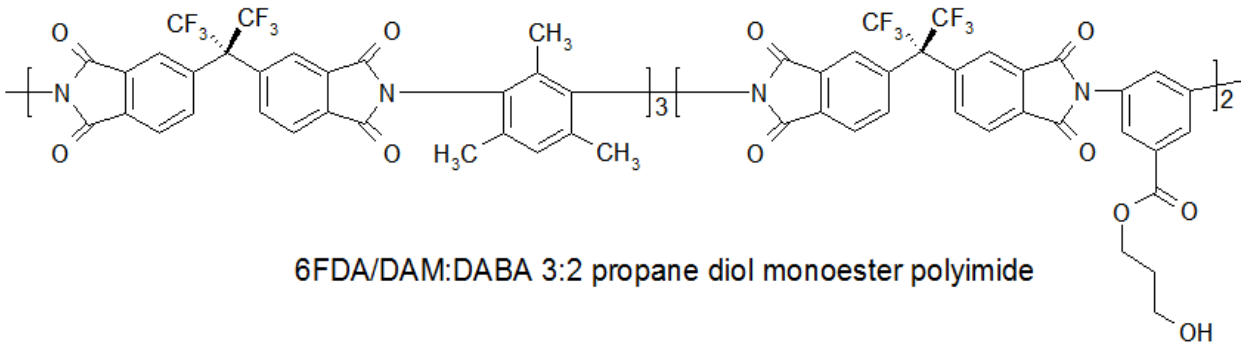

Figure 7.2: Chemical structure of PDMC polymer.

Another polymer material studied in this work was Torlon®. Since the hydrogen in amide bonds of Torlon® have the potential to form hydrogen bonds with -OH groups in PDMC, Torlon® was thought to have the potential to be compatible with PDMC. The chemical structure of Torlon® is shown in Figure 7.3.

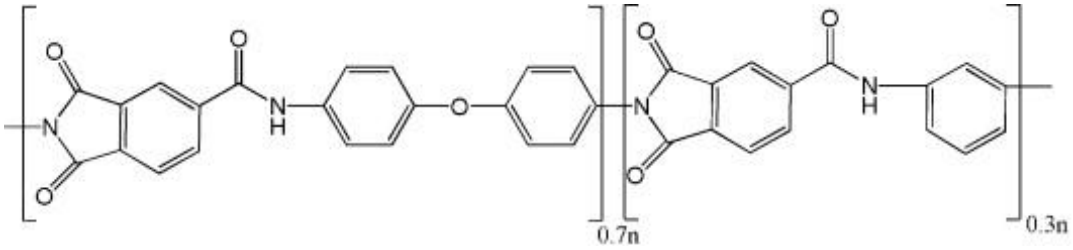

Figure 7.3**:** Chemical structure of Torlon® polymer.

7.3 PDMC/CA dual-layer hollow fiber spinning

Monolithic hollow fiber spinning with cellulose acetate has been studied in previous research [2, 3]. By using nominally the same dope composition described in reference [3], the cellulose acetate core dope was prepared, which consists of 15% CA, 72% NMP and 13% H_2O. The PDMC sheath dope composition was chosen to be the same as the *monolithic* hollow fiber spinning, which contained 30.5% PDMC, 30.5% NMP, 19.5% EtOH, 13.0% THF and 6.5% $LiNO_3$. *Composite* PDMC/CA hollow fibers were spun through a dry-jet/wet-quench hollow fiber spinning system, as shown in Figure 7.4.

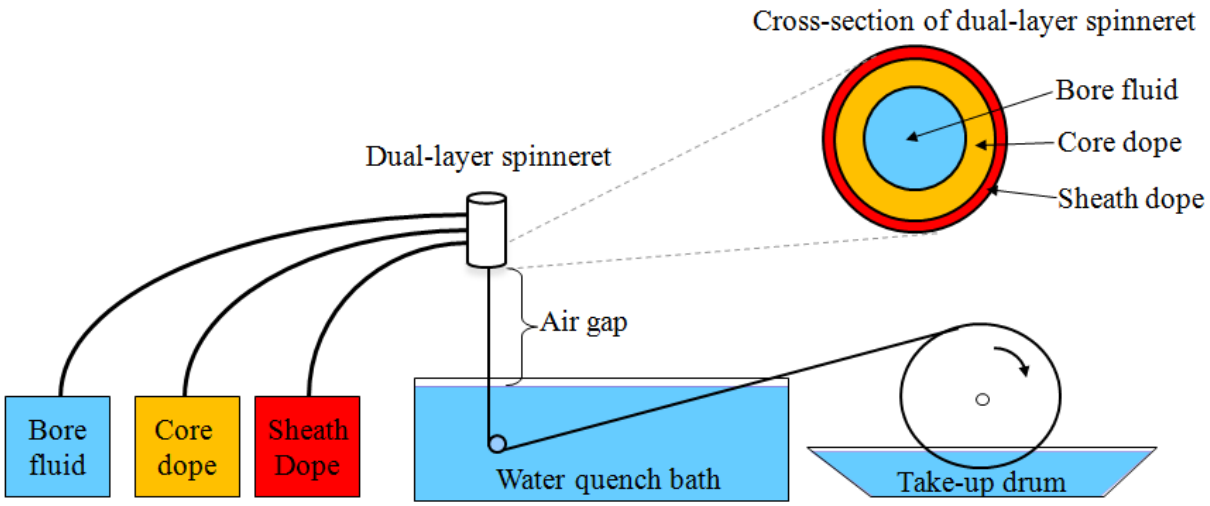

Figure 7.4: Dry-jet/wet-quench dual-layer spinning to form composite hollow fiber membranes.

The sheath dope and core dope are co-extruded with bore fluid through a dual-layer spinneret by using the spinning conditions described in Table 7.1.

Table 7.1: Composite hollow fiber spinning conditions

Spinning conditions	
Sheath dope extrusion rate	30~60 ml/hr
Core dope extrusion rate	120~180 ml/hr
Bore fluid composition	NMP/H_2O 70/30wt%
Bore fluid rate	60 ml/hr
Spinneret temperature	50~70^oC
Air gap	1~5 cm
Quench bath	20~50^oC
Take-up rate	15~50 m/min

The spinning conditions shown in Table 7.1 are primarily based upon previous research [2, 4]. The *uncrosslinked* PDMC/CA dual-layer hollow fibers were characterized by using Scanning Electron Microscope (SEM), as shown in Figure 7.5.

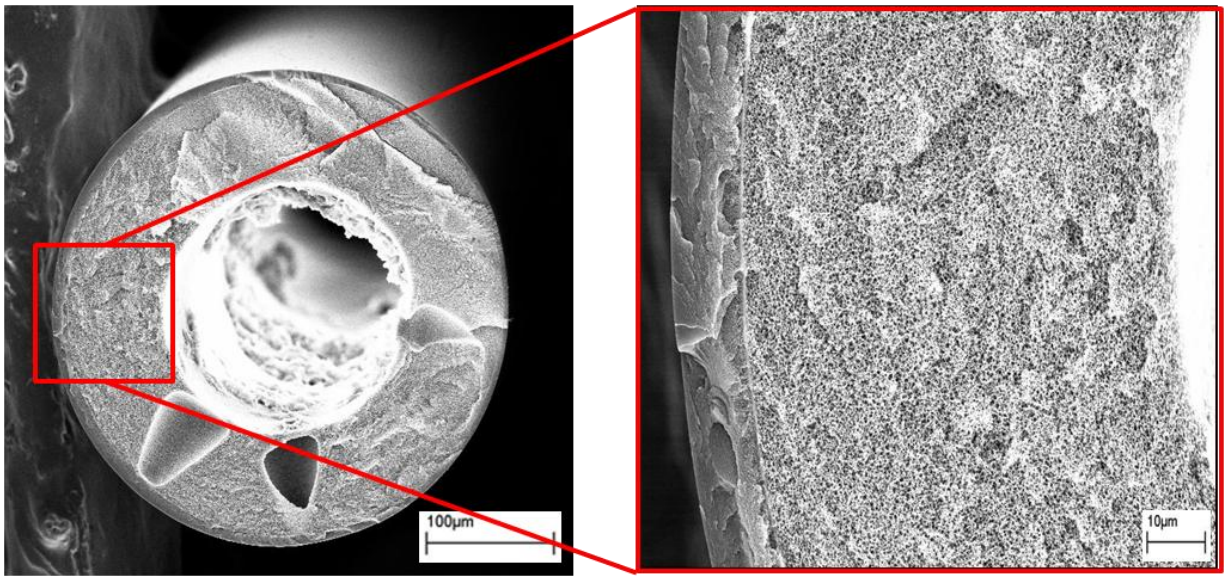

Figure 7.5**:** Scanning electron microscope (SEM) images showing the cross-section of an *uncrosslinked* PDMC/CA composite hollow fiber.

Figure 7.5 shows that cellulose acetate is compatible with PDMC. The PDMC/CA dual-layer fibers also show good continuity of sheath layer and concentricity of the core layer. The PDMC/CA composite hollow fibers were further crosslinked by using 200^{o}C, 2 hrs crosslinking conditions. The SEM of a *crosslinked* PDMC/CA composite hollow fiber is shown in Figure 7.6.

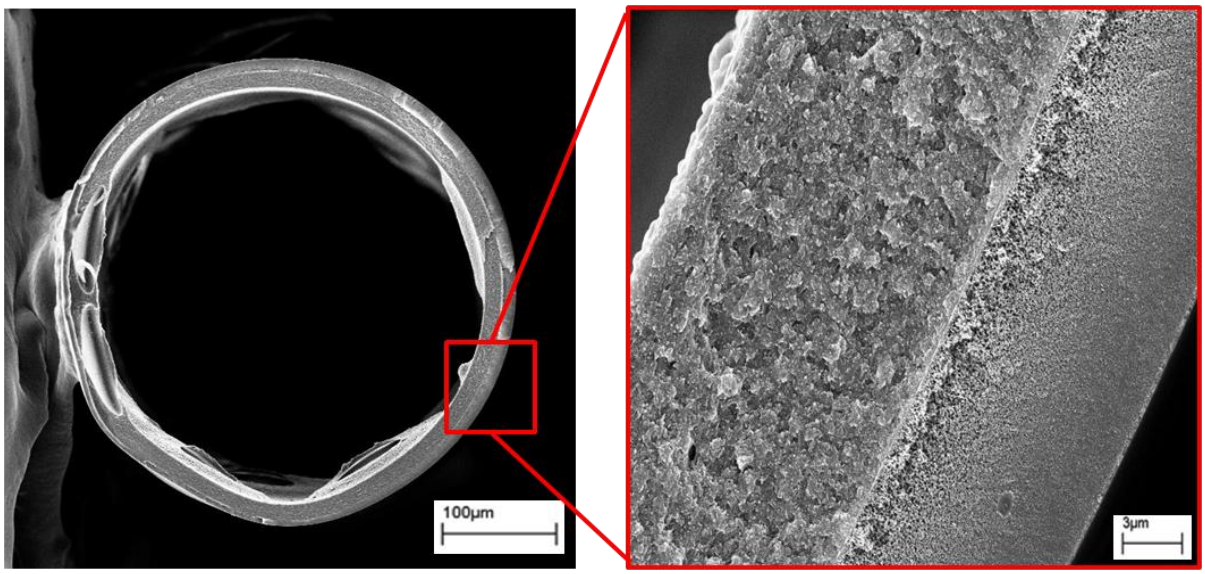

Figure 7.6**:** Scanning electron microscope (SEM) images showing the cross-section of a *crosslinked* PDMC/CA composite hollow fiber.

Figure 7.6 shows that despite the good adhesion with PDMC, the cellulose acetate core layer collapsed during crosslinking. The significant collapse of cellulose acetate core layer is presumably due to the lower glass transition temperature (T_g) of cellulose acetate, which is 180~210^{o}C based on the literature [5]. To develop composite hollow fibers with an open porous substructure during aggressive crosslinking, a polymer with a T_g higher than cellulose acetate should be pursued. This will be discussed in Section 7.4 below.

7.4 PDMC/Torlon® dual-layer hollow fiber spinning

7.4.1 Core layer dope development

The components of the core layer dope were first determined. N-methylpyrrolidone (NMP) can dissolve Torlon® and serves as the primary solvent for the core dope. Typical non-solvents, such as water or ethanol, are chosen due to their relatively low toxicity and easy

processing. Polyvinylpyrrolidone (PVP) or lithium nitrate ($LiNO_3$) can be also added in the dope as a "pore-former", which can help form an open porous substructure in the fibers.

To develop a spinnable dope, the binodal should be constructed to ensure that the dope composition is located in the one-phase region and close to the binodal to allow rapid phase separation. A straightforward technique to determine the approximate binodal location is provided by the so-called "cloud point determination", as described in references [6, 7]. The results of cloud point experiments are summarized and plotted in a ternary phase diagram as shown in Figure 7.7. The ternary phase diagram for PDMC can be found in Section 4.5.1.

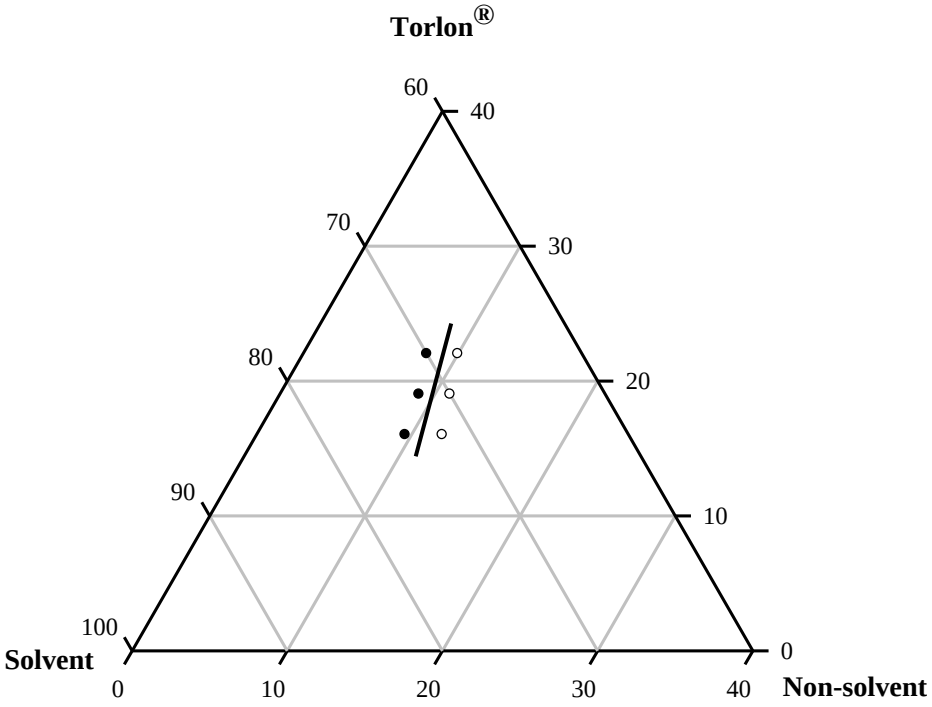

Figure 7.7: Ternary phase diagram showing the binodal (black solid line) of Torlon®/solvent/non-solvent system. Solid dots and open circles represent one-phase dope and two-phase dope, respectively.

In Figure 7.7, the solid dots represent the one-phase samples and open circles represent the two-phase samples for the ternary phase system. The binodal, shown as the black solid line, lies between the one-phase region and two-phase region. For proof of concept dual-layer spinning, the Torlon® core dope composition was determined by using 16.0% Torlon®, 74.4% NMP, 5.57% H_2O and 4.03% PVP (55,000 Mw). PVP was used as a non-solvent to promote the formation of an open porous substructure. On the other hand, the sheath dope composition is the same as *monolithic* spinning in this preliminary campaign, which consists of 30.5% PDMC, 30.5% NMP, 19.5% EtOH, 13.0% THF and 6.5% $LiNO_3$.

7.4.2 Dual-layer hollow fiber spinning

The sheath PDMC dope and core Torlon® dope are co-spun to produce composite hollow fibers by using the spinning conditions summarized in Table 7.2.

Table 7.2: PDMC/Torlon® composite hollow fiber spinning conditions.

Spinning conditions	
Sheath dope extrusion rate	30~60 ml/hr
Core dope extrusion rate	120~180 ml/hr
Bore fluid composition	NMP/H_2O 80/20wt%
Bore fluid rate	60 ml/hr
Spinneret temperature	35~70^oC
Air gap	1~15 cm
Quench bath	20~50^oC
Take-up rate	10~50 m/min

The spinning conditions shown in Table 7.2 are primarily based upon previous research [2, 4]. The complex nature of polymer solutions, sheath/core layer interface, and aggressive crosslinking, suggests that the dual-layer hollow fiber spinning includes considerable trial and error to develop the desirable composite hollow fibers. Further crosslinking and characterization was performed on some of the best spinning states from this preliminary campaign, as shown in sections below.

7.4.3 Crosslinking PDMC/Torlon® composite hollow fibers

As shown in Section 7.3, the crosslinking temperature is critical to develop delamination-free composite hollow fibers and maintain the open porous substructure of the core layer. A crosslinking temperature higher than the glass transition temperature of the core layer polymer will collapse the core layer and reduce the permeance significantly. On the other hand, a lower crosslinking temperature may not be able to stabilize the hollow fibers against CO_2 plasticization due to a lower degree of crosslinking. In the work, the crosslinking temperature was 200^{o}C and the crosslinking time was 2 hrs, primarily based on successful development of crosslinked *monolithic* hollow fibers [1, 8].

Since Torlon® does not dissolve in THF, it is relatively difficult to characterize the crosslinkability of PDMC/Torlon® *composite* hollow fibers by THF dissolution experiment. However, the 200^{o}C, 2 hrs crosslinked *monolithic* PDMC hollow fiber does not dissolve in THF at room temperature. It is expected the crosslinked *composite* hollow fibers have the same crosslinkability as the *monolithic*, since the same PDMC and crosslinking conditions were used in both of these cases.

7.5 Characterization of PDMC/Torlon® composite hollow fibers

7.5.1 Scanning Electron Microscope (SEM)

Scanning Electron Microscope (SEM) is commonly used to observe the cross-sectional structure of asymmetric composite hollow fibers. To prepare a fiber sample for SEM measurement, the fiber is cryogenically fractured in liquid nitrogen to preserve their cross-section structure. As the polymeric fibers are non-conductive, the cross-section of fibers must be coated with a gold layer. SEM images are particularly important to characterize hollow fibers,

especially for checking the adhesion of sheath/core layers. A SEM image of an *uncrosslinked* composite PDMC/Torlon® hollow fiber spun from this work is shown in Figure 7.8.

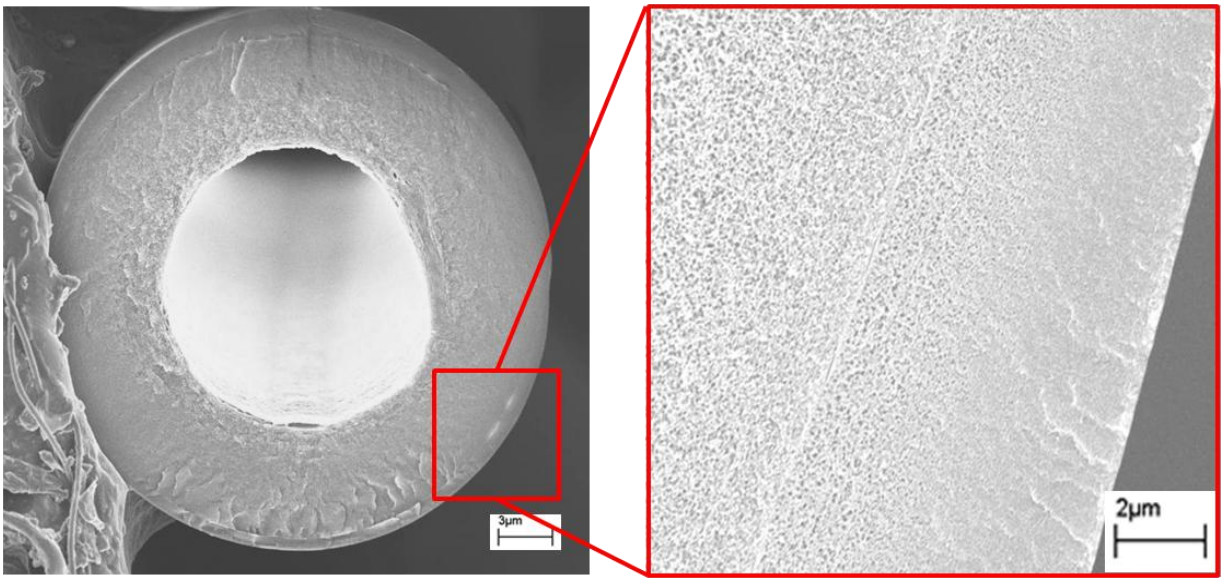

Figure 7.8: Scanning electron micrographs of the cross-section of an *uncrosslinked* PDMC/Torlon® composite hollow fiber, showing the dense skin layer, sheath layer, core layer and the open porous substructure.

Figure 7.8 shows that Torlon® is compatible with PDMC as there is no delamination of sheath/core layer in the fibers during spinning. The skin layer and open porous substructure are apparent in the SEM images. After 200°C, 2 hrs crosslinking, the *crosslinked* PDMC/Torlon® composite hollow fibers were checked by SEM, as shown in Figure 7.9.

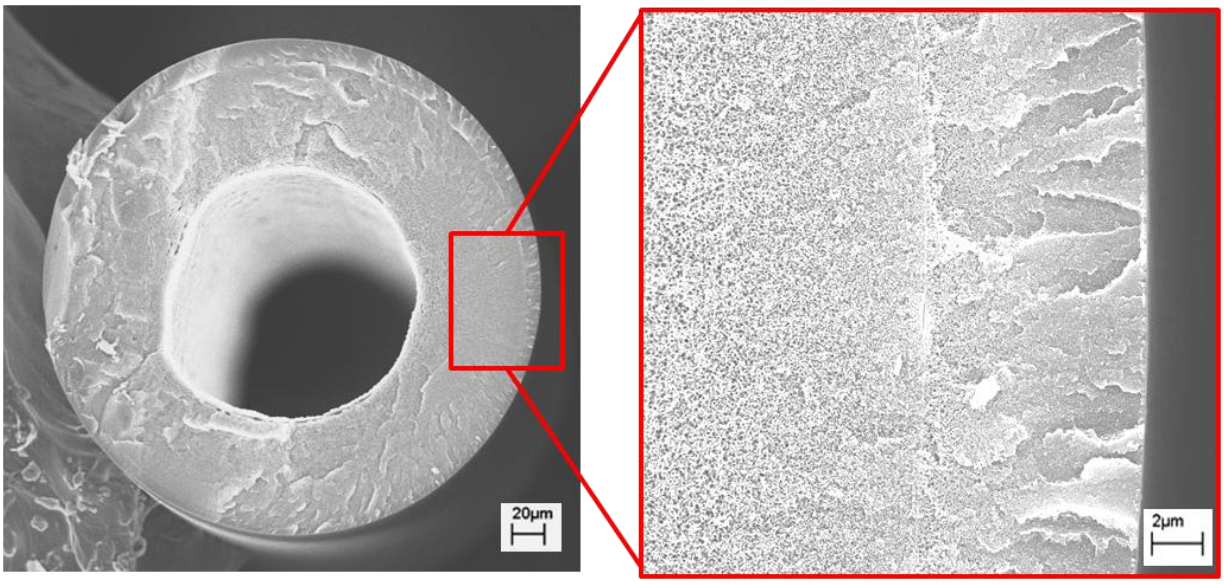

Figure 7.9**:** Scanning electron micrographs of the cross-section of a *crosslinked* PDMC/Torlon® composite hollow fiber, showing the dense skin layer, sheath layer, core layer and the open porous substructure.

Figure 7.9 shows the core layer shows good adhesion with the sheath layer after crosslinking, suggesting that the crosslinking does not cause delamination of the sheath/core layers. Moreover, the open porous substructure of Torlon® core layer did not collapse after crosslinking, indicative of a strong thermal stability of the Torlon® core layer during crosslinking. The morphologies shown in the SEM images suggest that Torlon® provides the desirable open porous morphology, compatibility with PDMC and thermal stability after crosslinking. Further mixed gas permeation was performed to explore the natural gas separation performance of the composite hollow fibers.

7.5.2 Natural gas separation performance

The composite PDMC/Torlon® hollow fibers were further evaluated by using a 50/50 CO_2/CH_4 mixed gas at a total feed pressure up to 300 psi. Figure 7.10~7.11 show the mixed gas permeation results on *uncrosslinked* and 200°C, 2 hrs *crosslinked* PDMC/Torlon® composite hollow fibers.

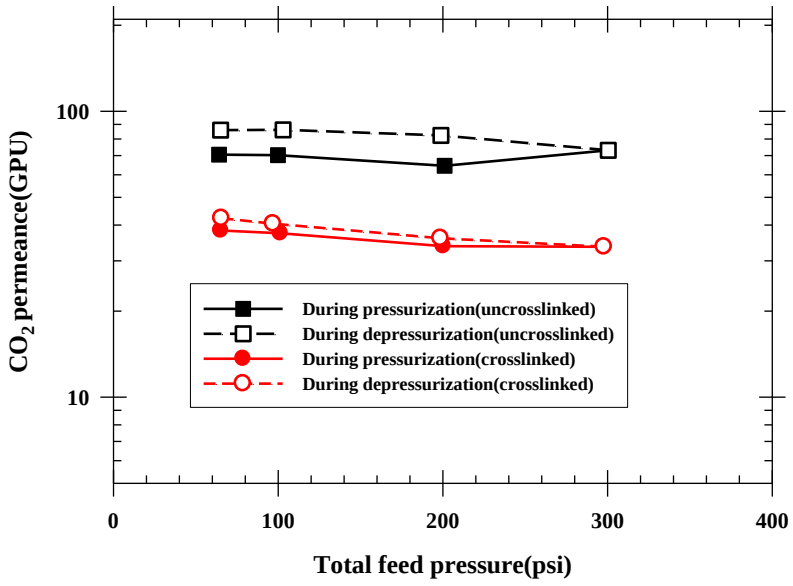

Figure 7.10: CO_2 permeance of *uncrosslinked* and *crosslinked* PDMC/Torlon® composite hollow fiber membranes at elevated feed pressures. Permeances calculated by using fugacity. Test conditions: 50/50 CO_2/CH_4, 35°C.

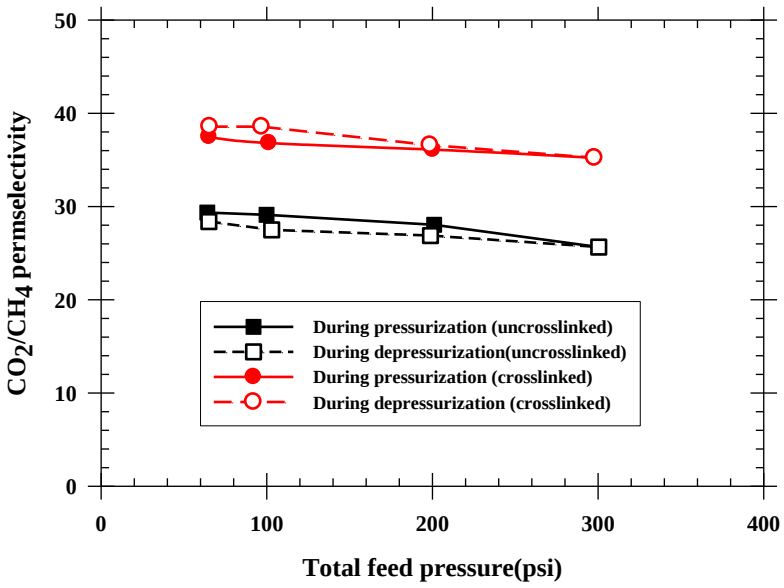

Figure 7.11: CO_2/CH_4 selectivity of *uncrosslinked* and *crosslinked* PDMC/Torlon® composite hollow fiber membranes at elevated feed pressures from this work. Permeance calculated by using fugacity. Test conditions: 50/50 CO_2/CH_4, 35°C.

Figure 7.10 indicate that the *uncrosslinked* PDMC/Torlon® composite hollow fibers show a slight CO_2 permeance upswing at 200 psi feed pressure, indicative of the onset of possible CO_2 plasticization. The plasticization of *uncrosslinked* monolithic hollow fibers was also found in reference [9]. However, no apparent CO_2 permeance upswing was found in the *crosslinked* composite hollow fibers, an indication of absence of CO_2 plasticization. The gas separation performance was re-checked by depressurization experiments. Figure 7.10 shows that the *uncrosslinked* fibers demonstrated a larger extend of swelling after depressurization than the *crosslinked* fibers, suggesting the crosslinking can stabilize hollow fibers against CO_2 induced polymer swelling. Although crosslinking causes a significant loss of permeance due to the densification of transition layer after crosslinking, the CO_2 permeance achieved was 40 GPU at 100 psi, 35°C. Nevertheless, the CO_2 permeance of those initial proof of concept *crosslinked*

composite hollow fibers is lower vs. the *monolithic* developed in this study, as shown in Chapter 5 (above 100 GPU).

On the other hand, Figure 7.11 shows that the crosslinking improved the CO_2/CH_4 selectivity from 29 (*uncrosslinked*) to 38 (*crosslinked*) at 100 psi feed pressure, 35°C. It also shows that the *crosslinked* composite hollow fibers have a CO_2/CH_4 selectivity of 36 at 200 psi, which is close to the intrinsic (dense film $\alpha_{CO2/CH4}$=43.8), suggesting the delamination-free *crosslinked* PDMC/Torlon® composite hollow fibers are defect-free. The high performing *crosslinked* PDMC/Torlon® composite hollow fibers were further characterized in the presence of high-level toluene impurity to simulate realistic feed conditions, as shown in the section below.

7.5.3 Characterization of composite hollow fibers with contaminants

As shown in Section 7.5.2, the *crosslinked* PDMC/Torlon® composite hollow fibers show excellent separation performance in a model natural gas feed consisting of only CO_2 and CH_4. However, since typical raw natural gas feeds contain undesirable hydrocarbon impurities, it is important to explore those fibers with contaminants to probe their performance under extremely challenging feed streams. In this study, the *crosslinked* PDMC/Torlon® composite hollow fibers were tested by using a toluene content from 30~1000 ppm in a 50/50 CO_2/CH_4 mixture at 35°C. The permeation results are summarized in Figure 7.12~13.

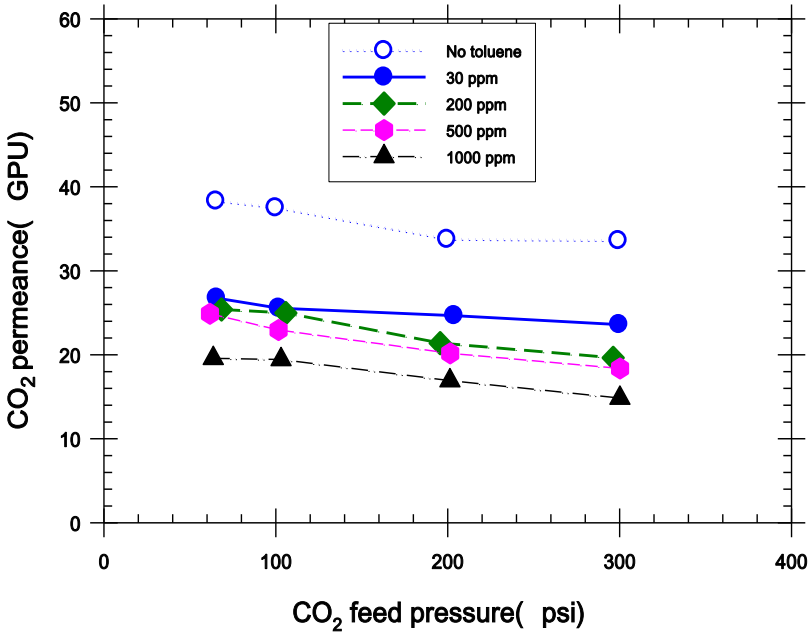

Figure 7.12: CO_2 permeance of *crosslinked* PDMC/Torlon® composite hollow fiber membranes at different toluene levels. Permeances calculated by using fugacity. Test conditions: 50/50 CO_2/CH_4, 35°C.

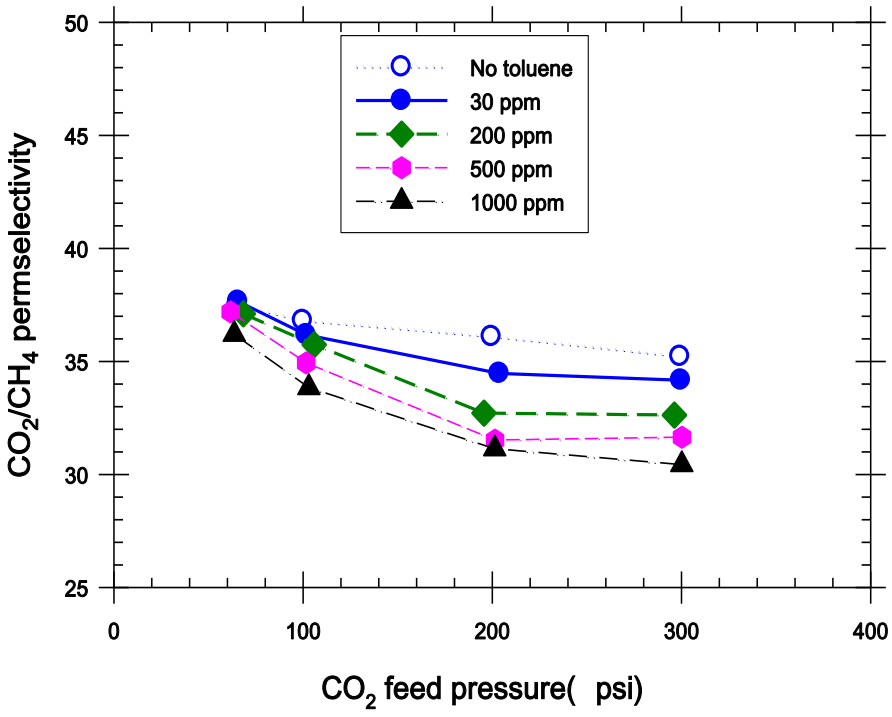

Figure 7.13**:** CO_2/CH_4 selectivity of *crosslinked* PDMC/Torlon® composite hollow fiber membranes at different toluene levels. Permeances calculated by using fugacity. Test conditions: 50/50 CO_2/CH_4, 35°C.

For proof of concept composite hollow fibers, a total feed pressure above 400 psi was found to cause failure of some of fibers; therefore, a total feed pressure up to 300 psi was used to avoid damaging the composite hollow fibers. Figure 7.12 shows that the increasing of the toluene level reduces both the CO_2 permeance and CO_2/CH_4 selectivity, which is primarily due to the antiplasticization effect induced by toluene. Antiplasticization occurs when an antiplasticizer reduces the fractional free volume (*FFV*) and increases the stiffness of polymer by lowering the glass transition temperature [10, 11]. The presence of toluene will, therefore, hinder the diffusion of each penetrant and reduce the permeance significantly.

To show the depression of CO_2 permeance in the presence to toluene, the separation performance of crosslinked *composite* hollow fibers were compared with *monolithic* fibers. They were tested with 200 psi 50/50 CO_2/CH_4 mixed gas with a toluene level from 30~1000 ppm. The permeation results on crosslinked *composite* and *monolithic* hollow fibers are shown in Figure 7.14~7.15.

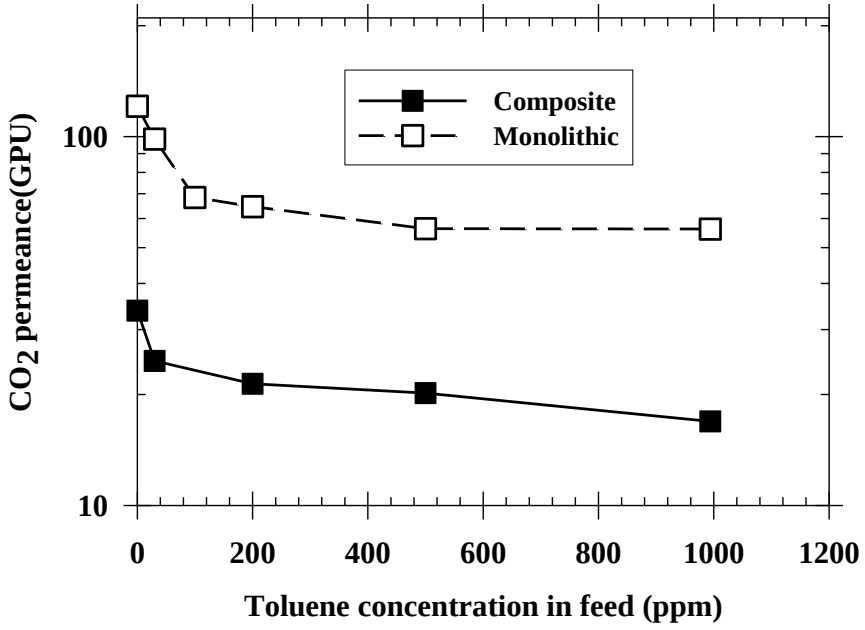

Figure 7.14**:** CO_2 permeance of crosslinked PDMC/Torlon® *composite* hollow fibers and *monolithic* hollow fibers at different toluene levels. Permeances calculated by using fugacity. Test conditions: 200 psi, 50/50 CO_2/CH_4, 35°C.

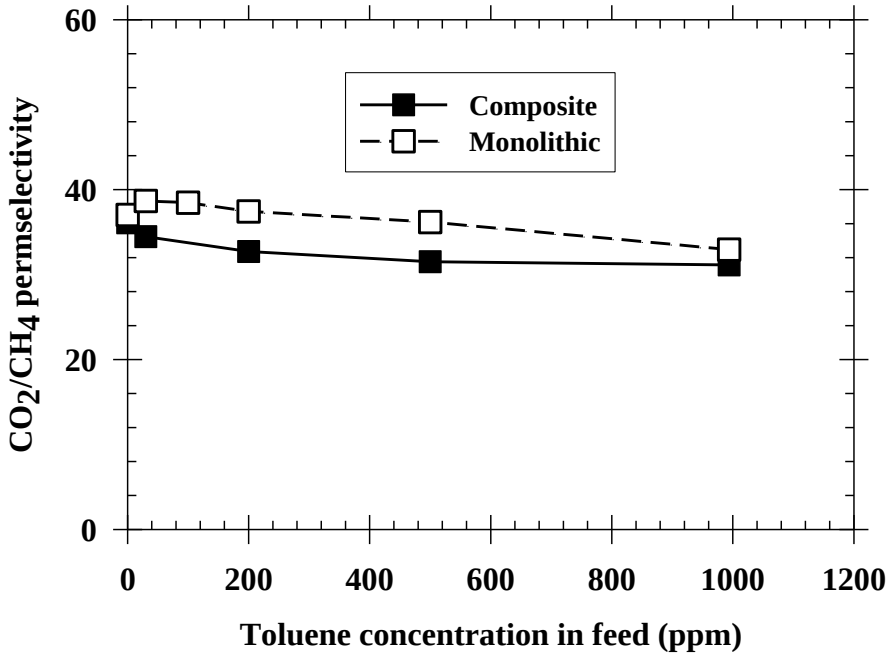

Figure 7.15**:** CO_2/CH_4 selectivity of crosslinked PDMC/Torlon® *composite* hollow fibers and *monolithic* hollow fibers at different toluene levels. Permeances calculated by using fugacity. Test conditions: 200 psi, 50/50 CO_2/CH_4, 35°C.

As shown in Figure 7.14, the CO_2 permeance of crosslinked *composite* hollow fibers under toluene impurity is lower vs. the *monolithic* hollow fibers. Despite the reduction of permeance induced by toluene, the crosslinked *composite* hollow fibers maintained a CO_2 permeance over 15 GPU in the presence of 1000 ppm toluene, which is 50% higher than the crosslinked *monolithic* hollow fibers reported in literatures [1, 12]. Figure 7.14 also shows that the CO_2 permeance of crosslinked *composite* hollow fibers dropped ~50% vs. ~54% for the crosslinked *monolithic* in the presence of 500 ppm toluene. On the other hand, the CO_2/CH_4 selectivity of the *composite* hollow fibers is slightly lower than the *monolithic* but the difference is within 13%. Although toluene somehow reduces the CO_2/CH_4 selectivity, the *composite*

hollow fibers show an attractive CO_2/CH_4 selectivity higher than 30 at all testing toluene levels. The high separation performance in the presence of high-level toluene contaminants suggests that the *crosslinked* PDMC/Torlon® composite hollow fibers are also viable under very challenging feed conditions.

7.6 Summary and conclusions

Dual-layer hollow fiber spinning and ester-crosslinking showed that ester-crosslinking can cause collapse of cellulose acetate core layer and damage the open porous substructure. To overcome the collapse of core layer, Torlon® was studied and found to be compatible with PDMC. Torlon® also demonstrates excellent compatibility with crosslinked PDMC sheath layer. Moreover, Torlon® shows strong thermal stability and maintains the open porous substructure during crosslinking, which is critical for preserving the high permeance and selectivity of *composite* hollow fibers. *Composite* PDMC/Torlon® hollow fibers were successfully developed without skin layer defects or delamination of sheath/core layers.

Mixed gas permeation shows that the crosslinked *composite* hollow fibers demonstrate attractively high separation performance and CO_2 plasticization resistance under a CO_2 feed pressure up to 300 psi. A total feed pressure over 400 psi may cause failure of fibers. The *crosslinked* composite hollow fibers also show excellent separation performance under a hydrocarbon level of 1000 ppm, suggesting the crosslinked *composite* hollow fibers are viable under challenging feed conditions.

The advanced dual-layer spinning technique can significantly cut the cost of hollow fiber formation and achieve the high separation performance under aggressive feed conditions. The desirably high natural gas separation performance and significantly reduced cost of hollow fiber

membrane formation provides a significant advance in the state of the art for natural gas separations.

7.7 References

[1] I.C. Omole, Crosslinked Polyimide Hollow Fiber Membranes for Aggressive Natural Gas Feed Streams, Ph.D. Dissertation, in: Chemical and Biomolecular Engineering, Georgia Institute of Technology, Atlanta, GA, 2008.

[2] J. Liu, DEVELOPMENT OF NEXT GENERATION MIXED MATRIX HOLLOW FIBER MEMBRANES FOR BUTANE ISOMER SEPARATION, PhD Dissertation, in: School of Chemical & Biomolecular Engineering, Georgia Institute of Technology, Atlanta, GA, 2010.

[3] N. Bessho, ADVANCED PRESSURE SWING ADSORPTION SYSTEM WITH FIBER SORBENTS FOR HYDROGEN RECOVERY, PhD Dissertation, in: School of Chemical & Biomolecular Engineering, Georgia Institute of Technology, Atlanta, GA, 2010.

[4] S. Husain, MIXED MATRIX DUAL LAYER HOLLOW FIBER MEMBRANES FOR NATURAL GAS SEPARATION, PhD Dissertation, in: School of Chemical & Biomolecular Engineering, Georgia Institute of Technology, Atlanta, GA, 2006.

[5] D. Bhandari, HOLLOW FIBER SORBENTS FOR THE DESULFURIZATION OF PIPELINE NATURAL GAS, in: School of Chemical & Biomolecular Engineering, Georgia Institute of Technology, Atlanta, GA, 2010.

[6] R.M. Boom, T. Vandenboomgaard, J.W.A. Vandenberg, C.A. Smolders, Linearized Cloudpoint Curve Correlation for Ternary-Systems Consisting of One Polymer, One Solvent and One Nonsolvent, Polymer, 34 (1993) 2348-2356.

[7] D.W. Wallace, Crosslinked Hollow Fiber Membranes for Natural Gas Purification and Their Manufacture from Novel Polymers, Ph.D. Dissertation, in: Chemical Engineering, The University of Texas at Austin, Austin, TX, 2004.

[8] C. Ma, OPTIMIZATION OF ASYMMETRIC HOLLOW FIBER MEMBRANES FOR NATURAL GAS SEPARATION, MS THESIS, in: School of Chemical and Biomolecular Engineering, Georgia Institute of Technology, Atlanta, GA, 2011.

[9] I.C. Omole, R.T. Adams, S.J. Miller, W.J. Koros, Effects of CO2 on a High Performance Hollow-Fiber Membrane for Natural Gas Purification, Ind Eng Chem Res, 49 (2010) 4887-4896.

[10] W.J. Koros, G.K. Fleming, Membrane-Based Gas Separation, J Membrane Sci, 83 (1993) 1-80.

[11] W.C. Madden, THE PERFORMANCE OF HOLLOW FIBER GAS SEPARATION MEMBRANES IN THE PRESENCE OF AN AGGRESSIVE FEED STREAM, PhD Dissertation, in: Chemical Engineering, Georgia Institute of Technology, Atlanta, GA, 2005.

[12] I.C. Omole, D.A. Bhandari, S.J. Miller, W.J. Koros, Toluene impurity effects on CO2 separation using a hollow fiber membrane for natural gas, J Membrane Sci, 369 (2011) 490-498.

CHAPTER 8

CONCLUSIONS AND RECOMMENDATIONS

8.1 Overview

This research addresses the solutions of challenges in developing high-performance low-cost crosslinked composite hollow fiber membranes for aggressive natural gas separations. The final chapter summarizes the study and provides recommendations for further work.

8.2 Conclusions

8.2.1 Formation of defect-free thin-skinned uncrosslinked hollow fibers

Defect-free selective crosslinkable hollow fibers with a skin layer thinner than 0.1 μm were successfully developed through simultaneous optimization of the polymer solution and spinning process variables. The defect-free *uncrosslinked* hollow fibers exhibit ideal morphology. The skin layer thickness of hollow fiber is reduced to the order of 0.1 μm without skin layer defects or substructure resistance.

8.2.2 Development of thin-skinned high-performance crosslinked hollow fibers

Extensive study on the dope reformulation and spinning optimization were performed to develop most productive ester-crosslinked hollow fibers. Key spinning parameters in determining the skin layer formation and separation productivity were identified and optimized. The ester-crosslinked hollow fibers demonstrated not only a CO_2 plasticization resistance up to 800 psi of 50/50 CO_2/CH_4 but also strong stability under high feed pressure for extended time. Thinner skin layer hollow fibers show a faster physical aging rate. However, active CO_2 feed can significantly reduce the rate of physical aging of crosslinked hollow fibers.

8.2.3 Significantly improved separation performance under high-level contaminants

The ester-crosslinked hollow fibers were characterized in the presence of high-level impurities to probe their separation performance under extremely challenging feed conditions. The intrinsic permeability of PDMC polymer and skin layer thickness of hollow fibers was found to affect the toluene sensitivity of membranes. Despite the depression of CO_2 permeance caused by antiplasticization, the ester-crosslinked hollow fibers demonstrated high CO_2 permeance even at an impurity level up to 1000 ppm at 800 psi. Moreover, in Chapter 6, those fibers showed stable and reversible high separation performance after removal of contaminates (including toluene, heptane and water impurities), suggesting the fibers are viable under extremely challenging feed conditions. The water contaminant level was tested only in the presence of nitrogen, so future studies should consider actual simulated natural gas with trace water contaminant. Our current system did not allow this more complex feed to be tested.

8.2.4 Development of defect-free and delamination-free crosslinked composite hollow fibers

Cellulose acetate and Torlon® were studied as the core layer materials in this work. Torlon® demonstrated excellent compatibility with PDMC sheath layer and maintained the open porous substructure of Torlon® core layer during crosslinking. PDMC/Torlon® *Composite* hollow fibers were successfully developed without skin layer defects or delamination of sheath/core layers. The ester-crosslinked PDMC/Torlon® *Composite* hollow fibers showed attractive separation performance under high feed pressures with contaminants. This advanced dual-layer spinning technique can significantly cut the cost of hollow fiber formation and achieve high separation performance under aggressive feed conditions.

8.3 Recommendations for future work

8.3.1 Fundamental understanding the toluene sensitivity

As shown in this study, membranes with different permeabilities or skin layer thickness showed significantly different sensitivities to toluene impurity. The Fractional Free Volume (FFV) of polymer samples is hypothesized as the key factor in affecting the toluene sensitivity of membranes. Further analysis of the FFV, such as using density column, high resolution gas sorption and/or positron annihilation lifetime spectroscopy (PALS), will facilitate a better understanding of the different toluene sensitivities.

8.3.2 Aggressive feed conditions

The high performance ester-crosslinked hollow fibers in this work were characterized by using with a 50/50 CO_2/CH_4 mixed gas with or without contaminants. Further mixed gas permeation can be done with a high CO_2 content over 70% in the feed to probe plasticization resistance under an even higher CO_2 partial pressure. Moreover, other impurities, such as H_2S, may exist in the gas streams in practical feeding. The separation performance of crosslinked hollow fibers under those aggressive feed conditions should be also explored.

8.3.3 Catalyst-assisted crosslinking

Catalysts are believed to lower the crosslinking temperature by reducing the activation energy of ester-crosslinking reaction. Attempts of using catalysts were done on crosslinked hollow fibers. However, the significant loss of CO_2 permeance or CO_2/CH_4 selectivity during catalyst-assisted crosslinking suggests that further optimization work should be pursued. This involves the methods of adding catalysts in the fibers and the optimization of crosslinking conditions (such as crosslinking temperature, crosslinking time and catalyst concentration).

8.3.4 Skin layer optimization for ester-crosslinked composite hollow fibers

The ester-crosslinked PDMC/Torlon® *composite* hollow fibers provide proof of concept success in achieving low-cost high-performance hollow fibers for aggressive natural gas separations. The separation productivity of crosslinked *composite* hollow fibers is relatively lower than the optimum crosslinked *monolithic* hollow fibers. This clearly suggests that there is plenty of room to reduce the skin layer thickness of crosslinked *composite* hollow fibers to achieve even higher separation performance. The skin layer thickness can be reduced through the optimization of dope composition and spinning process variables. Other polymers, such as P84, can also be studied as a high-performing core layer material.

8.3.5 Extension of ester-crosslinking application

Ester-crosslinked hollow fibers can be further used in developing high-performance carbon molecular sieves (CMS) membranes. CMS membranes show significant permeance loss during pyrolysis vs. polymeric precursor membranes. The interconnected structure formed during crosslinking may resist the serious collapse of polymeric membranes during aggressive pyrolysis process; thereby increasing the separation productivity. The resultant CMS membranes may be capable of separating olefin/paraffin and offer improved performance than CMS derived from conventional polymers.

APPENDIX A: MONOESTERIFICATION

The 6FDA-DAM: DABA (3: 2) precursor is monoesterified with 1, 3-propane diol. The reaction mechanism is shown in Figure A.1.

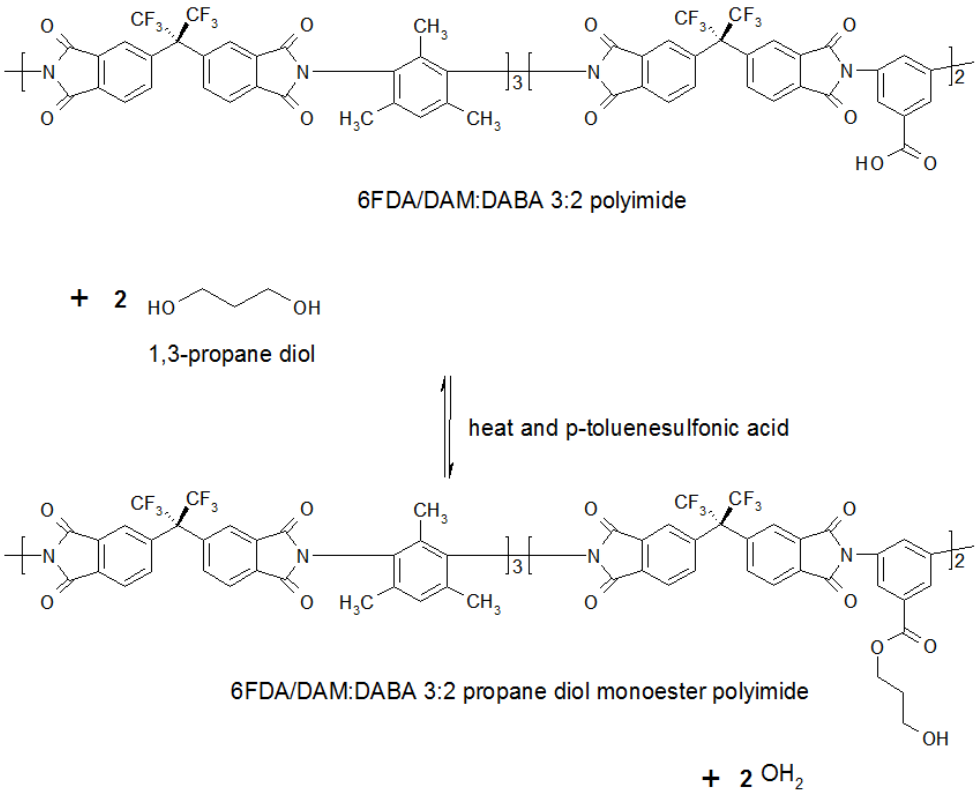

Figure A.1: Monoesterification reaction of 6FDA-DAM: DABA (3:2) polyimide with 1, 3-propane diol [1].

The monoesterification reaction is conducted by the following procedures:

1) Dry molecular sieves to dry NMP, dehydrating agents and 1, 3-propane diol.
2) Clean and dry glassware.
3) Needle-transfer NMP to dry round-bottom with molecular sieves.

4) Transfer ortho-dichlorobenzene (ODCB) or toluene to dry round-bottom with molecular sieves.

5) Transfer 1, 3-propane diol to dry round-bottom with molecular sieves.

6) Assemble glassware in fume hood, as shown in Figure A.2.

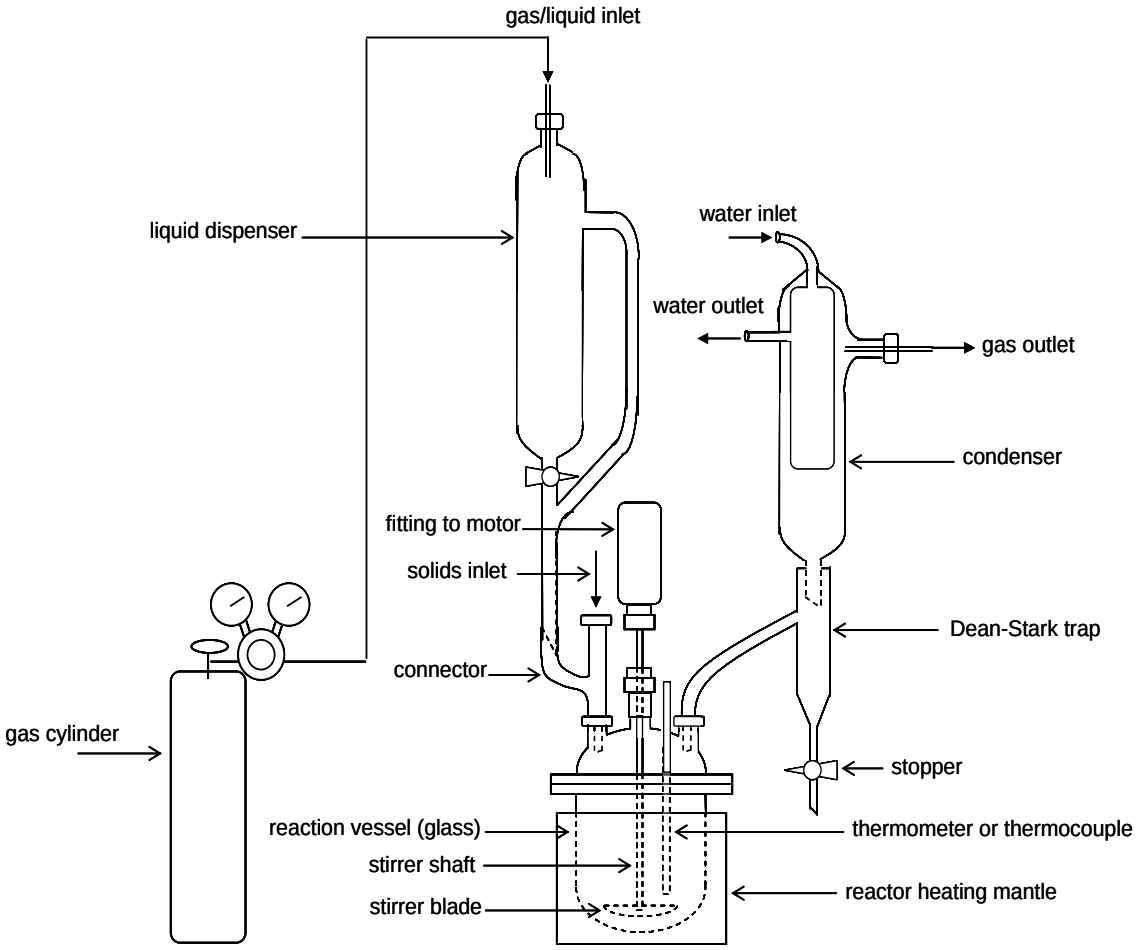

Figure A.2: Schematic showing the set-up for monoesterification reaction [2].

7) Weight the 6FDA-DAM: DABA (3:2) polyimide precisely.

8) Dissolve the 6FDA-DAM: DABA (3:2) polyimide in NMP with a polymer content of ~20 wt % in the flask.

9) Heat up solution to ~140^{o}C and keep purging the reaction with N_2.

10) Add ~2.5 ml of ortho-dichlorobenzene (ODCB) or toluene per gram polyimide to reaction solution.
11) Add ~2.5 mg of para-toluenesulfonic acid per gram polyimide to reaction solution.
12) Add 40-70 times the stoichiometric amount of 1, 3-propanediol slowly enough to avoid large precipitates formed in reactor.
13) React for ~ 24 hrs at ~ 140^{o}C while collecting water produced. Keep reaction always purged with N_2.
14) Cool reaction solution to less than ~ 70^{o}C, and then precipitate solution by pouring it slowly into methanol solvent.
15) Blend polymer, wash several times with methanol, filter, and then dry in hood overnight.
16) Dry polymer in vacuum oven at 70^{o}C for 24 hrs to prevent crosslinking of the polymer.
17) The monoesterified polymer is ready for characterization and further membrane formation.

References

[1] C. Ma, OPTIMIZATION OF ASYMMETRIC HOLLOW FIBER MEMBRANES FOR NATURAL GAS SEPARATION, MS THESIS, in: School of Chemical and Biomolecular Engineering, Georgia Institute of Technology, Atlanta, GA, 2011.

[2] I.C. Omole, Crosslinked Polyimide Hollow Fiber Membranes for Aggressive Natural Gas Feed Streams, Ph.D. Dissertation, in: Chemical and Biomolecular Engineering, Georgia Institute of Technology, Atlanta, GA, 2008.